

Wright State University

CORE Scholar

---

[Browse all Theses and Dissertations](#)

[Theses and Dissertations](#)

---

2015

## Distinguishing Melanocytic Nevi from Melanoma by DNA Copy Number Changes: Array-Comparative Genomic Hybridization as a Research Tool

Ahmed Ibrahim Mahas  
*Wright State University*

Follow this and additional works at: [https://corescholar.libraries.wright.edu/etd\\_all](https://corescholar.libraries.wright.edu/etd_all)



Part of the [Molecular Biology Commons](#)

---

### Repository Citation

Mahas, Ahmed Ibrahim, "Distinguishing Melanocytic Nevi from Melanoma by DNA Copy Number Changes: Array-Comparative Genomic Hybridization as a Research Tool" (2015). *Browse all Theses and Dissertations*. 1313.

[https://corescholar.libraries.wright.edu/etd\\_all/1313](https://corescholar.libraries.wright.edu/etd_all/1313)

This Thesis is brought to you for free and open access by the Theses and Dissertations at CORE Scholar. It has been accepted for inclusion in Browse all Theses and Dissertations by an authorized administrator of CORE Scholar. For more information, please contact [library-corescholar@wright.edu](mailto:library-corescholar@wright.edu).

Distinguishing Melanocytic Nevi From Melanoma by DNA Copy Number Changes:  
Array-Comparative Genomic Hybridization As a Research Tool

A thesis submitted in partial fulfillment of the  
requirements for the degree of  
Master of Science

By

AHMED IBRAHIM MAHAS  
B.S., King Khalid University, 2010

2015

Wright State University

WRIGHT STATE UNIVERSITY  
GRADUATE SCHOOL

July 6, 2015

I HEREBY RECOMMEND THAT THE THESIS PREPARED UNDER MY SUPERVISION BY  
Ahmed Ibrahim Mahas ENTITLED Distinguishing Melanocytic Nevi From Melanoma by DNA  
Copy Number Changes: Array-Comparative Genomic Hybridization As a Research Tool. BE  
ACCEPTED IN PARTIAL FULFILLMENT OF THE REQUIREMENTS FOR THE DEGREE  
OF Master of Science.

Committee on Final Examination

---

Michael Markey, Ph.D.

Assistant Professor of  
Biochemistry & Molecular Biology

---

Michael L. Raymer, Ph.D.

Professor of Computer Science and  
Engineering

---

Weiwen Long, Ph.D.

Assistant Professor of  
Biochemistry & Molecular Biology

---

Robert E.W. Fyffe, Ph.D.

Vice President for Research and  
Dean of the Graduate School

---

Michael Markey, Ph.D.

Thesis Director

---

Madhavi P. Kadakia, PhD.

Chair, Department of Biochemistry and  
Molecular Biology

## **ABSTRACT**

Mahas, Ahmed Ibrahim. M.S. Department of Biochemistry and Molecular Biology, Wright State University, 2015. Distinguishing Melanocytic Nevi From Melanoma by DNA Copy Number Changes: Array-Comparative Genomic Hybridization As a Research Tool.

Skin melanocytes can give rise to different benign and malignant neoplasms. Discrimination of an early melanoma from an unusual/atypical benign nevus can represent a significant challenge. However, previous studies have shown that in contrast to benign nevi, melanoma demonstrates pervasive chromosomal aberrations. This substantial difference between melanoma and benign nevi formed the idea of exploiting this difference to discriminate between melanoma and benign nevi. Array-comparative genomic hybridization (aCGH) is an approach that can be used on DNA extracted from formalin-fixed paraffin-embedded (FFPE) tissues to assess the entire genome for the presence of changes in DNA copy number. In this study, high resolution, genome-wide single-nucleotide polymorphism (SNP) arrays were utilized to perform comprehensive and detailed analyses of recurrent copy number aberrations in 42 melanoma samples in comparison with 21 benign nevi. We found statistically significant copy number gains and losses within melanoma samples. Some of the identified aberrations are previously implicated in melanoma. Moreover, novel regions of copy number alterations were identified, revealing new candidate genes potentially involved in melanoma pathogenesis. Taken together, these findings can

help improve the melanoma diagnosis and introduce novel melanoma therapeutic targets.

## **HYPOTHESIS**

The hypothesis of this study was that melanoma differs from melanocytic nevi by the presence of changes in DNA copy number. Finding these differences will be exploited diagnostically to classify melanocytic tumors that are ambiguous based on histopathologic assessment. In addition to potential diagnostic applications, detailed analyses of recurrent aberrations will lead to the identification of genes associated with melanocytic tumors.

## **PROJECT AIMS**

1. Extract DNA from FFPE specimens with sufficient quantity and quality to be hybridized to SNP6.0 microarrays.
2. Utilize the high resolution SNP6.0 microarrays to identify regions of copy number variations between melanoma and benign nevi samples.
3. Utilize the high resolution SNP6.0 microarrays to reveal novel somatic copy number changes with potential novel therapeutic targets.

## TABLE OF CONTENTS

I. INTRODUCTION .....	1
Melanoma Prevalence .....	1
Diagnostic Difficulties .....	2
Current Diagnostic Techniques .....	2
Copy Number Variations in Melanoma versus Benign Nevi.....	3
Array-Comparative Genomic Hybridization for more detailed analysis .....	4
Difficulties of DNA Extraction from FFPE tissues .....	5
Utilization of GISTIC to Detect Copy Number Aberrations .....	5
Summary of the Findings In This Study .....	6
II. MATERIAL AND METHODS .....	7
Specimen Collection and Preparation .....	7
DNA Isolation from FFPE Tissues.....	8
Qiagen Extraction Method .....	8
Adaptive Focused Acoustics (AFA)-Based Extraction Method .....	16
Phenol-Chloroform-Isoamyl Alcohol Extraction Method .....	21

Quality Control .....	25
Array Comparative Genomic Hybridization to SNP6.0 Microarrays.....	26
Data Analysis .....	28
Affymetrix SNP6.0 Copy Number Inference Pipeline .....	29
View the Segmented Copy Number Data By Using IGV .....	34
Genomic Identification of Significant targets in Cancer (GISTIC2.0).....	35
 III. RESULTS AND DISSCUSSION .....	 44
Specimen Collection and Preparation .....	44
Improving the Quality of DNA Extracted from FFPE Specimens .....	48
RAPD-PCR, A Predictor for aCGH Success of FFPE Samples .....	54
Processing the Qualified DNA Through SNP 6.0 Protocol .....	56
Validating the Recurrent Copy Number Changes in Melanoma .....	60
Genomic Identification of Significant Targets in Melanoma .....	66
GISTIC Analysis Reveals Novel Genes Potentially Involved in Melanoma .	96
 III. CONCLUSION.....	 98
 IIII. REFERENCES.....	 99

## LIST OF FIGURES

1. Workflow recommended for processing 48 samples through SNP6.0 protocol....	27
2. GISTIC Methodology .....	36
3. H&E Staining for Sections Taken from Melanoma Sample .....	48
4. Genomic DNA size range of samples extracted by three different methods .....	50
5. RAPD-PCR profile for 4 samples extracted by three different methods .....	53
6. RAPD-PCR profile for 12 different samples .....	55
7. Example of SNP6.0 PCR product of 4 different samples run on 2% agarose gel ..	57
8. Examples of Enzymatic fragmentation performances run on 4% agarose gel.....	58
9. APT analysis of Nsp1 and Sty1 Fragments .....	60
10. IGV copy number scale.....	61
11. A comprehensive overview of the segmented copy number data .....	62
12. Copy number change of known amplified genes in melanoma .....	64
13. Copy number change of known deleted genes in melanoma.....	66
14. Row segmented copy number data obtained from SNP6 microarray analysis ..	68



15. A driver mutation should occur in multiple tumors more often than would be expected by chance.....	69
16. Statistically significant genomic amplifications identified by GISTIC.....	70
17. Statistically significant genomic deletions identified by GISTIC analysis.....	77

## LIST OF TABLES

1. Details of specimens used in this study.....	44
2. Details of specimens used in the quest of improving DNA quality.....	49
3. Summary of the QC metrics for the methods comparisons. ....	51
4. Description of the statistically significant amplified regions identified by GISTIC.....	71
5. Description of the statistically significant deleted regions Identified by GISTIC..	78
6. Summary of somatic copy number alterations containing novel genes.....	97

## **I. INTRODUCTION AND BACKGROUND:**

In the United States, skin cancer is the most common of all cancers [1]. Most cases of skin cancer are non-melanoma skin cancer. In fact, melanoma accounts for less than 2% of skin cancer [1]. Melanoma is a cancer that arises from the malignant transformation of epidermal melanocytes, pigment-synthesizing cells of the skin. When melanoma escapes early detection, it becomes one of the most aggressive and highly lethal forms of cancers. Although it accounts for the minority of skin cancers, a large majority (75%) of skin cancer related-deaths are due to melanoma [1, 2]. The incidence and mortality of melanoma have increased dramatically in the last few decades [3]. The American Cancer Society estimates that about 73,870 people in United States will be diagnosed with melanoma in 2015 and about 9,940 people are expected to die from the disease. Importantly, the 5-year survival rate of melanoma depends on the stage of the disease when it is diagnosed. It can be as high as 98% when the melanoma is detected early before it spreads to the lymph nodes or other organs. When melanoma reaches the lymph nodes, the 5-year survival rate goes down to 62%, and to 15% when melanoma spreads to other organs [2]. Different factors are responsible for the increased risk of melanoma development. These factors include physical characteristics such as red hair, blue eyes, light complexion and presence of pigmented lesions. Moreover, environmental factors such as sun exposure are associated with the increase risk of melanoma. Yet, the genetic factor and families with strong history of the disease are the most important factors contributing to the increased risk of melanoma [4, 5].

The pigment-producing cells, melanocytes, can give rise to different benign (melanocytic nevi) and malignant (melanoma) neoplasms. Early diagnosis of melanoma is still the most effective way for long term survival and saving melanoma patients' lives from the disease [6]. In the majority of the cases, dermatopathologists can correctly diagnose and differentiate a melanocytic nevus from a malignant melanoma. However, dermatopathologists are aware of the diagnostic difficulties of a subset of melanocytic tumors that cannot be easily classified as benign or melanoma. These tumors have ambiguous histopathological features that overlap between melanocytic nevi and melanoma, where some benign melanocytic nevi, due to secondary changes, show unusual attributes that are more associated with melanoma diagnosis. Therefore, the pathology of melanocytic neoplasms remains as one of the most challenging and controversial areas in diagnostic histopathology [7]. The uncertainty and discordance among expert dermatopathologists in diagnosing melanocytic neoplasms have been shown in several studies [8-14]. The diagnostic uncertainty and the ambiguity of some melanocytic tumors results in melanoma misdiagnosis, which in turn can lead to melanoma overdiagnosis accompanied with increase in medical costs and unnecessary surgeries and stress. Conversely, melanoma underdiagnoses results in negligence of a lethal disease [6] that would have been imminently curable if resected earlier.

Histopathological examination of hematoxylin and eosin (H&E)-stained tissue sections remains the main approach for evaluating melanocytic tumors. However, due to the histopathological ambiguity of some melanocytic neoplasms, molecular diagnostic techniques have emerged in the field of dermatopathology as ancillary tests that can help in the diagnosis of melanoma. These molecular tests have shown promise in improving the differential diagnosis of melanoma. One of these molecular

diagnostic techniques that has been used intensively in melanoma diagnosis is immunohistochemical staining for melanocytic markers such as Melan-A (A103), S-100 and HMB-45 [15-17]. More recently, cytogenetic analysis have been developed and become popular method in the area of distinguishing melanoma from benign nevi. For instance, using fluorescence *in situ* hybridization (FISH) assays as an adjunctive test in the diagnosis of ambiguous melanocytic tumors have been increasingly utilized in dermatopathology laboratories. Several studies have shown the potential of the FISH assay as a successful discriminatory test that can distinguish between problematic melanocytic lesions [7, 18-20]. Currently, the most commonly used FISH assay employs a 4-probe panel targeting 4 loci (RREB1, MYB, centromere 6, and CCND1) on 2 different chromosomes. The 4-probes FISH has shown a sensitivity and specificity of 86.7% and 95.4% respectively [18]. Recent study has shown an improvement of the FISH assay by incorporating new probes that target 4 different chromosomes (CDKN2A on 9p21, RREB1 on 6p25, MYC on 8q24 and CCND1 on 11q13) with increased sensitivity and specificity to 94% and 98% respectively [7].

Although the FISH assay was introduced as a diagnostic tool in the field of differential diagnosis of melanoma fairly recently, the principle of developing this assay was based on findings that existed over a decade ago. After the emersion of comparative genomic hybridization as a novel technique that can screen the entire genome for copy number changes in one experiments in 1992 [21], several studies (by Bastian and others) have revealed that the majority of melanomas differ from benign nevi in their genetic makeup. These studies demonstrated gain or loss of specific chromosomal segments and showed that the majority of melanomas harbor recurrent chromosomal copy number aberrations. With some exceptions such as in Spitz nevi,

these chromosomal rearrangements are rarely detected in melanocytic nevi [22-25]. Frequent genomic alterations known to occur in melanoma include gains at 1q, 6p, 7p, 7q, 8q, 17q and 20q in conjunction with deletions at 6q, 8p, 9p, 9q, 10p, 10q, 11q and 21q[22-24]. These fundamental differences in the pattern of genetic alterations between melanomas and benign nevi established the idea that copy number variations can be diagnostically valuable for histopathologically ambiguous melanocytic neoplasms. Therefore, developing diagnostic assays targeting these genetic differences, such as FISH assays, would help improve the differential diagnosis and prognosis of melanoma.

Utilizing CGH as a research tool has been decidedly a huge advancement in the cancer research field. As previously mentioned, the use of CGH has enhanced our knowledge of the genetic alterations occurring in the melanocytic tumors. However, in melanoma, these genetic alterations tend to be broad copy number events spanning large genomic regions. Rationally, the frequent existence of changes in these genomic regions in melanoma, but not in the benign nevi, indicates the presence of critical melanoma-related genes within these regions. The task of uncovering such genes remains a challenge. Yet, significant progress in CGH technology and the development of newer, high-density, genome-wide single-nucleotide polymorphism (SNP) arrays have simplified this task and make it achievable. The high-resolution microarrays allow for detection of more precise and smaller regions of specific copy number changes. The effectiveness of using these arrays in accurate identification of copy number alterations has been shown in various cancer studies [26-30]. Applying this high-resolution technique in melanoma has shown more detailed and recurrent amplifications and deletions of genomic regions containing important cancer genes. Among these genes are CDKN2A and PTEN in the statistically significant deleted

regions; BRAF, EGFR and CCND as the most frequently amplified genes [4, 31, 32]. Furthermore, good examples of the ability of these high-resolution microarrays in revealing potential cancer genes were demonstrated in identifying the current melanoma biomarker MITF gene [33] and the melanoma metastatic gene NEDD9 as well [34]. Therefore, these advances in array CGH technology have provided great opportunities to detect novel and previously unrecognized key driver genes that can help improve melanoma prognosis, diagnosis, and even developing targeted therapies.

However, aCGH presents its own set of unique challenges. DNA is required of sufficient quantity and quality to hybridize to arrays and provide meaningful results. The reliability and accuracy of this molecular test depends on our ability to obtain quality DNA from the same biomaterials that that are provided by pathologists. This is especially difficult for DNA from formalin-fixed paraffin-embedded (FFPE) tissues. Consequently, it is important to use efficient methods for the extraction of quality nucleic acids, especially when the available tissue sections are small and irreplaceable. In the course of this project, we compared DNA extracted from the same specimens by three different methods and found that the extraction method can significantly affect the quality and quantity of DNA obtained from a given specimen.

Here, we report our investigation for chromosomal aberrations that can help in the identification of genomic targets for melanoma diagnosis and therapy. To detect genome-wide statistically significant copy number events, we analyzed high-density single-nucleotide polymorphism (SNP) array data of 42 melanoma samples compared with 21 benign nevi. We utilized a statistical method called genomic identification of significant targets in cancer (GISTIC) that allows of detection of genomic regions that have high probability to contain driver cancer genes [35, 36]. GISTIC has been

actively used in different cancer studies and has helped in the detection of different amplified and deleted genes [37-41].

The 42 melanoma samples analyzed by GISTIC show 8 statistically significant amplifications and 32 deletions. Some of the identified aberrations are previously known in melanoma and being used in some of the diagnostic techniques to differentiate between melanoma and benign nevi. Furthermore, GISTIC analysis revealed novel regions of aberration harboring potential candidate genes involved in melanoma pathogenesis.



## II. MATERIAL AND METHODS:

### *Specimen Collection and preparation:*

Following IRB review, melanocytic tumor specimens (melanoma and benign nevi) were selected from a large archive of FFPE skin biopsies collected at a national dermatopathology laboratory (Dermatopathology Laboratory of Central States, DLCS, Dayton, OH). De-identified retrospective clinical data were obtained from clinical databases and patient health records software (Intellipath) at DLCS. Patients ranged in age from 14 to 90 years. The biopsy specimens were collected between 2001 and 2013, making their age range between 2 and 14 years. Specimens were stored in a temperature-controlled environment.

For all experiments, 10  $\mu$ m thick sections were taken for each sample from paraffin blocks by using a microtome with disposable blades. Care was taken to avoid contamination between the specimens by changing gloves when handling the blocks, cleaning the microtome after cutting a block, and using fresh blades for each specimen. The sections were placed in a warm water bath to help mounting them on slides. Then, tissues were incubated overnight at room temperature to be air dried. The first and last sections from each block were stained with H&E staining to verify that the region of interest (consisting of cellular material) still presents and had not been exhausted. For DNA extraction, tissues were scraped from slides using either sterile scalpel blades into 1.5 mL microcentrifuge tubes in case of Qiagen and

phenol-chloroform extraction methods; or by using Covaris SectionPicks into Screw-Cap microTUBES for the adaptive focused acoustics-based extraction method. The number of sections taken per sample varies between methods, as described below.

***DNA isolation from FFPE tissues:***

To optimize the DNA quality and acquire DNA of sufficient length, purity, and “amplifiability for aCGH analysis, DNA isolation was carried out by comparing three different extraction methods for extracting quality DNA from FFPE tissues; Qiagen QIAamp DNA FFPE tissue kit, phenol-chloroform isoamyl alcohol extraction and Adaptive Focused Acoustics (AFA) - based extraction using the Covaris truXTRAC FFPE DNA kit. Metrics of quantity and quality were considered for each method. However, only the DNA extracted by column-based methods (Qiagen QIAamp DNA FFPE tissue kit and Adaptive Focused Acoustics (AFA) - based extraction using the Covaris truXTRAC FFPE DNA kit) was used for aCGH.

***Qiagen extraction method:***

The original protocol of the Qiagen QIAamp DNA FFPE tissue kit (QIAGEN GmbH, D-40724 Hilden) is as follows:

1. Using a scalpel, trim excess paraffin off the sample block.
2. Cut up to 8 sections 5–10  $\mu\text{m}$  thick .If the sample surface has been exposed to air, discard the first 2–3 sections.
3. Immediately place the sections in a 1.5 or 2 ml micro centrifuge tube and add 1 ml xylene to the sample. Close the lid and vortex vigorously for 10 sec.
4. Centrifuge at full speed for 2 min at room temperature (15–25°C).

5. Remove the supernatant by pipetting. Do not remove any of the pellet.
6. Add 1 ml ethanol (96–100%) to the pellet, and mix by vortexing.  
The ethanol extracts residual xylene from the sample.
7. Centrifuge at full speed for 2 min at room temperature.
8. Remove the supernatant by pipetting. Do not remove any of the pellet. Carefully remove any residual ethanol using a fine pipet tip.
9. Open the tube and incubate at room temperature or up to 37°C.  
Incubate for 10min or until all residual ethanol has evaporated.
10. Resuspend the pellet in 180 µl Buffer ATL. Add 20 µl proteinase K, and mix by vortexing.
11. Incubate at 56°C for 1 h (or until the sample has been completely lysed).
12. Incubate at 90°C for 1 h. The incubation at 90°C in Buffer ATL partially reverses formaldehyde modification of nucleic acids. Longer incubation times or higher incubation temperatures may result in more fragmented DNA. If using only one heating block, leave the sample at room temperature after the 56°C incubation until the heating block has reached 90°C.
13. Briefly centrifuge the 1.5 ml tube to remove drops from the inside of the lid. If RNA-free genomic DNA is required, add 2 µl RNase A (100 mg/ml) and incubate for 2 min at room temperature before continuing with step 14. Allow the sample to cool to room temperature before adding RNase A.

14. Add 200  $\mu$ l Buffer AL to the sample, and mix thoroughly by vortexing. Then add 200  $\mu$ l ethanol (96–100%), and mix again thoroughly by vortexing. It is essential that the sample, Buffer AL, and ethanol are mixed immediately and thoroughly by vortexing or pipetting to yield a homogeneous solution. Buffer AL and ethanol can be premixed and added together in one step to save time when processing multiple samples. A white precipitate may form on addition of Buffer AL and ethanol. This precipitate does not interfere with the QIAamp procedure.
15. Briefly centrifuge the 1.5 ml tube to remove drops from the inside of the lid.
16. Carefully transfer the entire lysate to the QIAamp MinElute column (in a 2 ml collection tube) without wetting the rim, close the lid, and centrifuge at 6000 x g (8000rpm) for 1min. Place the QIAamp MinElute column in a clean 2ml collection tube, and discard the collection tube containing the flow-through. If the lysate has not completely passed through the membrane after centrifugation, centrifuge again at a higher speed until the QIAamp MinElute column is empty.
17. Carefully open the QIAamp MinElute column and add 500  $\mu$ l Buffer AW1 without wetting the rim. Close the lid and centrifuge at 6000 x g (8000 rpm) for 1 min. Place the QIAamp MinElute column in a clean 2ml collection tube, and discard the collection tube containing the flow-through.

18. Carefully open the QIAamp MinElute column and add 500  $\mu$ l Buffer AW2 without wetting the rim. Close the lid and centrifuge at 6000 x g (8000 rpm) for 1 min. Place the QIAamp MinElute column in a clean 2ml collection tube, and discard the collection tube containing the flow-through. Contact between the QIAamp MinElute column and the flow-through should be avoided. Some centrifuge rotors may vibrate upon deceleration, resulting in the flow-through, which contains ethanol, coming into contact with the QIAamp MinElute column. Take care when removing the QIAamp MinElute column and collection tube from the rotor, so that low-through does not come into contact with the QIAamp MinElute column.
19. Centrifuge at full speed (20,000 x g; 14,000 rpm) for 3 min to dry the membrane completely. This step is necessary, since ethanol carryover into the elute may interfere with some downstream applications.
20. Place the QIAamp MinElute column in a clean 1.5 ml microcentrifuge tube (not provided), and discard the collection tube containing the flow-through. Carefully open the lid of the QIAamp MinElute column and apply 20–100  $\mu$ l Buffer ATE to the center of the membrane.

Important: Ensure that Buffer ATE is equilibrated to room temperature. If using small elution volumes (<50  $\mu$ l), dispense Buffer ATE onto the center of the membrane to ensure complete elution of

bound DNA. QIAamp MinElute columns provide flexibility in the choice of elution volume. Choose a volume according to the requirements of the downstream application. The volume of elute will be up to 5 µl less than the volume of elution solution applied to the column.

21. Close the lid and incubate at room temperature for 1 min. Centrifuge at full speed (20,000 x g; 14,000 rpm) for 1 min, incubating the QIAamp MinElute column loaded with Buffer ATE for 5min at room temperature before centrifugation generally increases DNA yield.

A previous lab member had modified this original protocol of the Qiagen FFPE DNA Tissue kit in order to optimize the results. The modifications for the original protocols included: 1) Increasing the number of 10 µm sections from 10 to 20-24 sections, 2) mounting the sections on glass slides first to be air dried, instead of placing the ribbon of FFPE sections directly from the microtome into the microcentrifuge tubes, 3) increasing the volumes of the lysis buffer and proteinase K, and 4) increasing the digestion time with proteinase K from 1 hour to overnight incubation (up to 16 hours). The modified protocol was as follows:

1. Take 20-24 10µm thickness sections off the glass slides into microcentrifuge tubes and incubate tissue at 60°C in water bath for 30 minutes.

2. Add 1 ml of 100% xylene, Vortex and centrifuge at 20,000xg for 5 minutes. Remove supernatant.
3. Wash tissues with 500µl of 100% ethanol, vortex and centrifuge at 20,000xg for 3 minutes then remove supernatant.
4. Wash tissues for the second time with 500µl of 75% ethanol, vortex and centrifuge at 20,000xg for 3 minutes then remove supernatant.
5. Wash tissues for third time with 500µl of 50% ethanol, vortex and centrifuge at 20,000xg for 3 minutes and then remove supernatant.
6. Allow tissue to dry before processing.
7. Add 300µl buffer ATL to dried tissue.
8. Add 100µl proteinase K and mix by vortexing.
9. Incubate overnight (8-12 hours, never longer than 16 hours) at 56°C.
10. Add 400µl buffer AL to the sample and mix by inversion.
11. Incubate at 70°C for 10 minutes.
12. Add 400µl ethanol to the sample and mix by inversion.
13. Pipet mixture into DNeasy Mini Spin Column then centrifuge at 6000xg for 1 minute. Discard the flow through.
14. Add 500µl wash buffer AW1, then centrifuge at 6000xg for 1 minute. Discard the flow through.
15. Add 500µl wash buffer AW2 then centrifuge at 6000xg for 1 minute. Discard the flow through.
16. Add 500µl wash buffer AW2 again, then centrifuge at 6000xg for 1 minute. Discard the flow through.

17. Replace flow through tube with clean tube, then centrifuge at 20,000xg for 3 minutes to remove any residual ethanol from the spin column.
18. Replace flow through tube with clean micro centrifuge tubes.
19. Add 100µl buffer ATE, incubate at room temperature for 5 minutes.
20. Centrifuge at 20,000xg for 1 minute.

When we used this modified protocol, we noticed that the DNA yield still low, and that mainly was because that some tissues (during the suggested digestion time) are not completely digested. Therefore, we have optimized the protocol by extending the digestion time from 16 hours to 72 hours. Moreover, instead of adding 100 µl of proteinase K at one time, the proteinase K was added partially by adding 40 µl first, then 30 µl at 24 hours, and another 30 µl at 48 hours. The current modified and optimized protocol of the Qiagen FFPE DNA Tissue kit is as follows:

1. Cut 24 FFPE sections of 10 µm thickness for each DNA extraction and mount them on glass slides .
2. After scraping the tissues from the slides into microcentrifuge tubes, incubate tissue samples in water bath at 60°C for 30 minutes.
3. Wash tissues in microcentrifuge tube twice in 1 mL xylene, vortex and centrifuge at 20,000xg for 3 minutes each time.



4. Wash tissues in a descending concentration of ethanol (100, 75%, and then 50%). For each time, vortex and centrifuge at 20,000xg for 3 minutes and then remove supernatant .
5. Allow tissues to dry in the microcentrifuge tubes completely before proceeding to next step.
6. Add 300  $\mu$ l Qiagen buffer ATL plus 40  $\mu$ l proteinase K (20mg/mL, 5 PRIME Inc., Gaithersburg, MD, USA) to dried tissue and mix by vortexing, incubate at 56 °C for 72 hours.
7. Add an additional 30  $\mu$ l proteinase K at 24 hours and another 30  $\mu$ l at 48 hours of incubation.
8. After 72 hours digestion, add 400 $\mu$ l buffer AL to the sample, mix by inversion (never vortex after the incubation, which can degrade the DNA).
9. Incubate at 70°C for 10 minutes.
10. Add 400 $\mu$ l ethanol to the sample and mix by inversion.
11. Pipet sample mixture into Qiagen DNeasy Mini Spin Columns, then centrifuge at 6000xg for 1 minute. Discard the flow through.
12. Add 500 $\mu$ l wash buffer AW1, centrifuge at 6000g for 1 minute and discard the flow through .
13. Add 500 $\mu$ l wash buffer AW2, centrifuge at 6000g for 1 minute and discard the flow through .
14. Add 500 $\mu$ l wash buffer AW2 again, then centrifuge at 6000xg for 1 minute. Discard the flow through.

15. Replace flow through tube with clean tube, then centrifuge at 20,000xg for 3 minutes to remove any residual ethanol from the spin column.
16. Replace flow through tube with clean microcentrifuge tube.
17. Add 100µl buffer ATE, incubate at room temperature for 5 minutes.
18. Centrifuge at 20,000xg for 1 minute.

*Adaptive Focused Acoustics (AFA)-based extraction method:*

One of the advantages of using this method is that it requires less input material (8-10 sections) compared to the other two methods. Here, the Slides are warmed up on a heat block at 37 °C for 30 seconds to facilitate scraping the tissues. FFPE tissues are then scraped from the slides, trying to avoid paraffin, using Covaris SectionPicks into Screw-Cap microTUBES provided by Covaris. The DNA extraction was performed Per manufacturer's instructions following the protocol suggested by Covaris (Woburn, MA, USA) in the truXTRAC FFPE DNA kit ("protocol C") on a Covaris M220 Focused-Ultrasonicator. The protocol is as follows:

1. Open microTUBE Screw-Cap, add 100 µl Tissue SDS Buffer into microTUBE and load FFPE tissue (section or core). Affix Screw-Cap back in place.
2. Process the sample using the settings provided in the protocol to dissociate the paraffin while simultaneously rehydrating the

tissue. During the AFA process it is normal for the solution to turn milky white as the paraffin is emulsified.

- Paraffin removal and tissue rehydration settings

System	Duty Factor	Peak Incident Power	Cycles per burst	Treatment Time	Temperature (Instrument)
S220 or E220	10%	175 Watts	200	300 sec	20 °C
S2 or E210	10%	5 (Intensity)	200	300 sec	20 °C
M220	20%	75 Watts	200	300 sec	20 °C
LE220	30%	450 Watts <sup>(1)</sup>	200	300 sec	20 °C

3. Open Screw-Cap microTUBE, add 20 µl of Proteinase K solution to the sample and affix Screw-Cap back in place.
4. Process the sample using the settings provided to properly mix Proteinase K with the sample.

- Proteinase K mixing settings

System	Duty Factor	Peak Incident Power	Cycles per burst	Time	Temperature (Instrument)
S220 or E220	10%	175 Watts	200	10 sec	20 °C
S2 or E210	10%	5 (Intensity)	200	10 sec	20 °C
M220	20%	75 Watts	200	10 sec	20 °C
LE220	30%	450 Watts <sup>(1)</sup>	200	10 Sec	20 °C

5. Protein digestion at 56°C. Insert the required number of Heat Block microTUBE Adapters into a Heat Block and set the temperature to 56°C.
6. Load the microTUBE into the adapter once the heat block has reached its set point.
7. An incubation time of 1 hour at 56°C is sufficient for sections 10 µm or less in thickness; 12-hour (i.e. overnight) incubation should be used for larger samples, such as 25 µm sections and cores. If the digestion is incomplete after 12 hours, add 20 µl of Proteinase K solution, mix, and incubate for 1 more hour. Here,

the homogenized tissue was digested for 2 hours instead of 1 hour in proteinase K provided by Covaris kit.

8. Incubate the samples at 80°C for 1 hour to reverse formaldehyde crosslinks.
9. Insert the required number of Heat Block microTUBE Adapters into a Heat Block and set the temperature to 80°C. Load the microTUBE into the adapter once the heat block has reached its set point.
10. If using the same heat block for both the 56°C & 80°C incubations, the microTUBE should be stored at room temperature until the heat block reaches 80°C.
11. Transfer the sample to a clean 1.5 ml microcentrifuge tube.
12. Optional: The sample can be treated with RNase A to remove RNA before DNA purification. Add 5µl of RNase A solution and incubate for 5 minutes at room temperature.

-Then DNA purification:

Set heat block to 70°C and preheat the required volume of Buffer BE in a 1.5mL microfuge tube: (number of samples x 100 µl x 1.1)

1. Add 140 µl Buffer B1 to your sample and vortex thoroughly.
2. Add 160 µl ethanol (>96%) to the sample and vortex thoroughly.
3. Centrifuge at 10,000 x g for 2 minutes at room temperature. After centrifugation much of the paraffin will have formed a white layer, floating on top of the liquid.
4. Place a Purification Column into a provided Collection Tube.

5. While holding the sample tube at about the same angle as in the rotor, use a pipette to slowly recover the liquid layer, and transfer to the column. Transfer of a small amount of paraffin particles to the column is acceptable and will not interfere with the DNA purification.
6. Spin the assembly at 11,000 x g for 1 minute.
7. Discard the flow-through and place the Column back in the Collection Tube.
8. 1st wash: Add 500 µl Buffer BW. Spin the assembly at 11,000 x g for 1 minute.
9. Discard the flow-through and place the Column back in the Collection Tube.
10. 2nd wash: Add 600 µl Buffer B5. Spin the assembly at 11,000 x g for 1 minute.
11. Discard the flow-through and place the column in a new Collection Tube
12. Dry column: Spin the assembly at 11,000 x g for 1 minute.
13. Elute DNA - 1st step: Place the Purification Column into a new 1.5 ml microcentrifuge tube and add 50 µl pre-warmed Buffer BE (70 °C) to the center of the column. Incubate at room temperature for 3 minutes. Spin the assembly at 11,000 x g for 1 minute.
14. Elute DNA – 2nd step: Add a second aliquot of 50 µl pre-warmed Buffer BE. Incubate again at room temperature for 3 minutes. Spin the assembly at 11,000 x g for 1 minute.

15. DNA is eluted in 100 µl Buffer BE.

In order to get enough concentration for the SNP 6.0 protocol, some of the samples were concentrated by speed vac . For each Sty and Nsp restriction enzyme digestion, an amount of genomic DNA input of 500 ng in a volume of 10 µl is required. Therefore, DNA samples with low concentrations (<50 ng/µl) need to be concentrated in order to get the required amount of DNA (500 ng) in 10 µl. The Speed vac protocol used to concentrate the DNA is as follows:

1. For samples with low DNA concentration, calculate the amount of DNA (µl) required to obtain 500 ng of DNA . For example, sample with DNA concentration of 10 ng/µl, 50 µl from that sample is needed to make 500 ng of DNA ( $10 \text{ ng} \times 50 \text{ µl} = 500 \text{ ng}$  of DNA).
2. Put DNA from each sample in a separate micro centrifuge tube for speed vac.
3. Equalize the volume in all speed vac tubes by bringing the volume up with nuclease-free water to have a similar volume in all tubes.
4. Make a separate tube with 10 µl of water to be used as a control .
5. Speed vac the DNA on low drying rate until it is close to 10 µl (compare to the control tube).
6. Each tube now should have approximately 500 ng in 10 µl volume.

*Phenol-chloroform-isoamyl alcohol extraction method:*

The Phenol-chloroform-isoamyl alcohol extraction is a well-known nucleic acids extraction method that, differently than the previously described two extraction methods, is a non-column based extraction method. It depends mainly on using some chemicals such as phenol-chloroform-isoamyl alcohol to separate the nucleic acids from other cellular components after lysing the tissues, and then precipitating the DNA with ethanol. We used this protocol as was described by Isola et al [42] with including some modifications. The protocol described by Isola et al. is as follows:

1. 20 to 30 5µm sections were de-paraffinized in Eppendorf tubes (2 x 1 ml xylene for 10 minutes each and 2 x 1 ml 100% ethanol for 10 minutes each).
2. After air drying at room temperature, samples were suspended in 1 ml DNA extraction buffer (0.3 mg/ml proteinase K (Sigma, St. Louis, MO), 100 mmol/L NaCl, 10 mmol/L Tris-HCl pH 8, 25 mmol/L EDTA pH 8, and 0.5% sodium dodecyl sulfate) and were incubated with shaking at 55°C overnight.
3. Additional proteinase K (10µl from 20 mg/ml stock solution) was added 24 hours and 48 hours later for a total incubation time of 72 hours.
4. A 500µl of the digested sample were mixed with 500 µl phenol – chloroform-isoamyl alcohol 25:24:1 (Fisher Scientific, Fair Lawn, New Jersey, USA) and incubated at room temperature for 10 minutes and then centrifuged.

5. DNA in the top (aqueous ) layer was collected and precipitated with 250 µl of 7.5 mol/L ammonium acetate and 1 ml of ice-cold 100% ethanol.
6. DNA was pelleted by centrifugation (14,000 rpm for 20 minutes).
7. Glycogen (0.1 mg/ml; Sigma) was added before centrifugation as a carrier to increase the volume of the pellet.
8. DNA was dissolved overnight in 20 to 40 µl of TE buffer (10 mmol/L Tris, 1 mmol/L EDTA)

We used the same protocol but with some modifications. The modified protocol is as follows:

1. 24 sections of 10 µm thickness were used from each FFPE sample. FFPE sections were scraped from the air-dried slides using sterile scalpel blades into 1.5 mL microcentrifuge tubes.
2. Add 1 ml of xylene to each tube, vortex vigorously and incubate for 10 min, centrifuge for 5 min at 20,000 x g. Discard the supernatant.
3. Repeat step 2 again.
4. Washing the xylene by Add 1 ml of 100% ethanol, vortex, incubate for 10 min, centrifuge for 3 min at 20,000 x g. Discard the supernatant.
5. Repeat step 4 again.



6. Add 1 ml of 75% ethanol, vortex, incubate for 10 min, centrifuge for 3 min at 20,000 x g. Discard the supernatant.
7. Air dry the tubes at room temperature by inverting them on a clean tissue.
8. Add 985 µl of DNA extraction buffer (described above) and 15 µl of 20 mg/ml stock solution of proteinase k.
9. Incubate tubes on water bath shaking incubator at 57°C and adjust the speed of shaking to 3-3½ rpm.
10. Keep checking the water level in the shaker regularly (the water level will decrease over time due to evaporation).
11. Add additional 10 µl proteinase k to each tube after 24 hours and mix by vortex very lightly.
12. Add another 10 µl of proteinase k to each tube after 48 hours and mix by flipping the tubes (to avoid DNA degradation, do not vortex the samples at this point).
13. After 72 hours, incubate the samples at 95°C for 40 min to reverse formaldehyde crosslinks. Then, cool the samples down to room temperature before proceeding.
14. Mix 500 µl of the digested sample with 500 µl of the phenol-chloroform-isoamyl alcohol 25:24:1, then mix by shaking the tubes.
15. 2 layers will form in each tube; incubate the tubes for 5 min at room temperature.
16. Centrifuge at 20,000 rcf for 10 min at 4°C.

17. Transfer the top aqueous layer (which has the DNA) to a new tube.
18. Add an equal amount of chloroform to the DNA in the new tube (for example: 100  $\mu$ l of aqueous layer with 100  $\mu$ l of chloroform), mix by flipping the tubes, incubate for 5 min at room temperature and centrifuge at 20,000 rcf for 10 min (the chloroform will wash the residual phenol).
19. Transfer the top layer into a new tube. Discard the organic solvent by disposing them in the chemical waste container.
20. Add 1 ml of ice cold 100% ethanol to each tube.
21. Add 250  $\mu$ l of ammonium acetate and mix by flipping the tubes for few times.
22. Incubate the tubes in  $-80^{\circ}\text{C}$  for 35 min or in  $-20^{\circ}\text{C}$  overnight, then centrifuge at 14,000 rpm for 20 min at  $4^{\circ}\text{C}$ .
23. Discard the supernatant carefully without breaking the pellet.
24. Wash the pellet by adding 500  $\mu$ l 70% ethanol, invert several times without breaking the pellet, and spin at maximum speed at  $4^{\circ}\text{C}$  for 5 min.
25. Aspirate the supernatant carefully without breaking the pellet.
26. Dry the pellet completely by leaving the tubes open at room temperature for 5-10 min. It is important to make sure that there is no ethanol in the tube before dissolving the pellet.
27. Add 40  $\mu$ l of TE buffer (Tris 10Mm, EDTA 1Mm pH8.0) and incubate at room temperature for overnight.

### *Quality control*

#### DNA quantification:

A Nanodrop spectrophotometer was used to quantify DNA concentration as well as determine the  $A^{260}/A^{230}$  and  $A^{260}/A^{280}$  ratios. For a more accurate quantitation, the Qubit® dsDNA BR Assay Kit (Thermo Fisher Scientific, Waltham, MA) was used to check the concentrations of dsDNA for all samples.

#### DNA fragment sizes:

After DNA extraction and quantification, genomic DNA fragment sizes were first estimated by agarose gel electrophoresis of 250 ng DNA using 1% agarose gels (90 mM Tris –borate, 2 mM EDTA, 1% agarose). Samples with visible DNA fragments as large as 23,000 base pairs (bp) were used.

#### Randomly Amplified Polymorphic DNA PCR (RAPD-PCR):

RAPD-PCR was used as a quality control step to directly assess the ability of each sample to produce high molecular weight amplicons (“amplifiability”) and be ideal for SNP6.0 protocol (SNP6.0 success indicator). RAPD-PCR was performed as was described by Siwoski A et al [43]. RAPD-PCR reactions were carried out in a 20 µL volume containing 25 ng DNA and using 10µl of GoTaq 2X Green Master Mix (Promega, Madison, WI USA). PCR was performed in 0.2 mL tubes in a GeneAmp PCR System 9700 thermocycler (Life Technologies, Carlsbad, CA, USA). Two

different sets of primers were used for RAPD-PCR and were generated by Eurofins MWG Operon Inc (Huntsville, AL, USA). Sequences for the primer pairs and cycling parameters were as follows: 5'-AATCGGGCTG-3' and 5'-GAAACGGGTG-3', 94°C for 2.5 minutes, then 45 cycles of 1 minute 94°C, 1 minute 55°C and 2 minutes 72°C, then 7 minutes 72°C and holding at 4°C; or 5'- TGTGCCCAGTGAAGACTCAG-3' and 5'- GAGTGAGCGGAGAGGGAAGT-3', 45 cycles of 94° C for 1 minute, 35° C for 1 minute, and 72° C for 2 minute. PCR products were resolved on 3% TBE agarose plus SYBR Safe dye (Life Technologies). Gels were visualized with a GE ImageQuant LAS-3000 camera (GE Healthcare Life Sciences, Piscataway, NJ, USA).

***Array Comparative Genomic Hybridization to SNP6.0 Microarrays:***

Samples with good quality and quantity were processed and hybridized to the SNP6.0 microarrays through SNP6.0 protocol to generate data for copy number analysis. A diagram of the main steps of the SNP6.0 protocol is shown in (Figure 1).

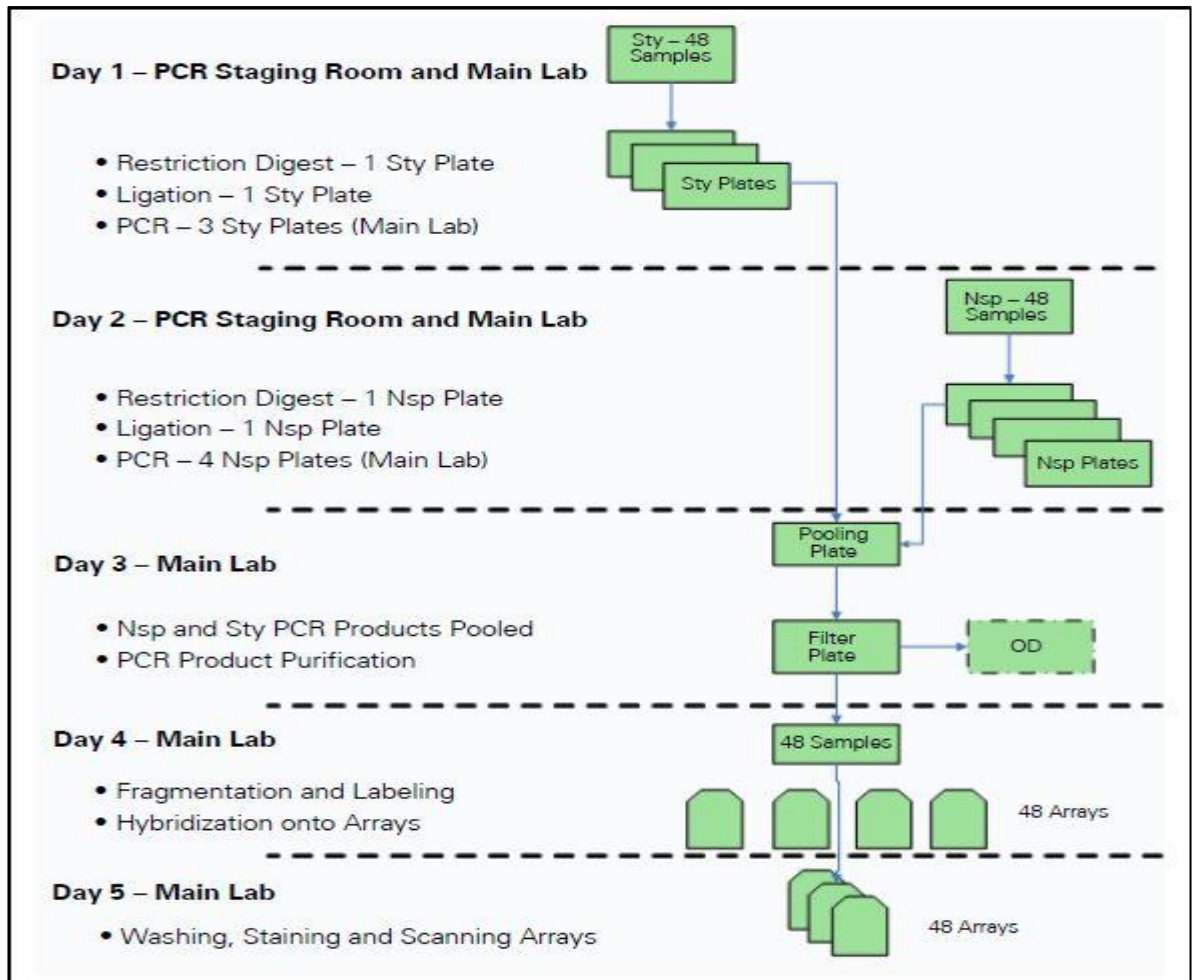


**Figure 1: ) Workflow recommended for processing 48 samples through SNP6.0 protocol.**

The detailed SNP6.0 protocol is described in Affymetrix Genome-Wide Human SNP Nsp/Sty 6.0 User Guide. The SNP6.0 protocol was performed as suggested in the original protocol, but a few modifications were included in order to optimize the results. These modifications included:

1. Increase in the input amount of DNA from 250 ng per restriction enzyme (Nsp1 and Sty1) to 500 ng each.
2. The number of PCR reactions was doubled from the suggested three for Sty1 and four for Nsp1 to six for Sty1 and eight for Nsp1. It is important

to note that the number of reactions was increased; the number of cycles in each reaction remained the same. The additional PCR reactions were combined as in the standard protocol.

3. PCR cleanup was performed using isopropanol extraction (refer to Affymetrix User Bulletin 2: Improvements to step 7 of the SNP Assay 6.0, PCR cleanup, using an isopropanol precipitation method, P/N 702968 Rev. 1).

The Hybridization and scanning of the arrays followed the manufacturer's protocol.

#### ***Data analysis:***

After washing, staining, and scanning the microarrays, CEL files and other files such as CHP and ARR files will be generated. CEL files are the files used for copy number analysis through GenePattern. CEL files contain the raw intensity values of the individual probes on the arrays. These intensity values are normalized and then compared to intensity of the same probes of control samples (should have diploid normal copy number) to produce positive and negative values indicating copy number gain or loss at a specific genomic region. To find differences between melanoma and benign nevi in copy number changes, data generated from a set of 42 melanoma samples were compared to data generated from 21 benign nevi samples. The analysis tools used for analyzing the data and detecting copy number variations are described below.

GenePattern Workflow:

*I. Affymetrix SNP6 Copy Number Inference Pipeline.*

The Copy Number Inference Pipeline is a method in GenePattern from the Broad Institute (Massachusetts Institute of Technology, Cambridge, MA) that takes Affymetrix SNP6 CEL files and process them in a pipeline consists of different modules for data processing and analysis to generate segmented copy number calls for each sample [44, 45]. DNA copy number was estimated probe set-wise by comparing the normalized signal from 42 melanoma samples to data generated from 21 benign samples that were used as a reference. The pipeline first uses *SNPFileCreator\_SNP6* module to normalize all of the SNP arrays by adjusting the raw intensity values from the SNP6 array so that they can be compared with other arrays. The second step is to convert intensity measurements into copy number calls by using the *CopyNumberInference* module. Then the copy number noise was calculated and then the copy number calls were de-noised with the *RemoveCopyNumberOutliers* module that removes probes that are outliers, which have radically different copy number calls than their hg19-adjacent neighbors. The *Tangent normalization algorithm* then reduced the noise further by subtracting out variation seen in a pre-defined set of a panel of more than 3000 blood normals from the Cancer Genome Atlas (TCGA). This exclusion of the germline CNVs is particularly important for algorithms that identify somatic alterations that are statistically significant such as GISTIC. The copy number data then were segmented by using the CBS (Circular Binary segmentation) algorithm that identifies regions in the genome that, in spite of noise, probably have a uniform underlying copy number. It compresses the values from a set of adjacent probes into a

single value for that interval [46]. The output of this pipeline (the segmented copy number calls) can then be used to run GISTIC to find the statistically significant copy number variations, as will be described further in this section.

Here are step-by-step instructions for running copy number analysis through the *CopyNumberInferencePipeline* in GenePattern:

1. An account is needed to use the GenePattern public sever, which is available at <http://genepattern.broadinstitute.org/gp/pages/login.jsf>.
2. Register an account, and then sign in.
3. After signing in, in the Modules panel on the left side of the screen, search and locate the *CopyNumberInferencePipeline* and select it. One easy way to do this: type the first few characters of the name into the search box and click on *CopyNumberInferencePipeline* when it appears in the list of matching analyses.
4. GenePattern will display the *CopyNumberInferencePipeline* parameters.
5. For the *SNP6 cel files* parameter, click the Upload File button and load the *SNP6 cel files* file (step 6 below explains the preparation of the *SNP6 cel files* file).
6. How to prepare the "*SNP6 cel files*" file:
  - Compress (or zip) all of the cel files that are going to be analyzed (the tumor (melanoma) and the control samples (benign nevi) ) in one zip file.
  - Name the file as "snp6\_sample\_data".



- The zip file should only have the cel files that are being analyzed and match the sample information in the *Sample Info File* (see step 7). Having any file other than the cel files in the zip file will cause an error when running the pipeline.

7. For the *Sample Info File* parameter, click the Upload File button and load the *Sample Info File* (step 8 below explains the preparation of the *Sample Info File* file).

8. How to prepare the "*Sample Info File*" :

This is a text file containing information about the samples. This information includes the array names, the gender of the patients, specification of the samples as either tumor or normal (control), and an indication that the normal (benign nevi) are diploid or not.

- Use Microsoft Excel to prepare this file.
- Four columns are required in this file. Name the first column as "Array", the second column as "Gender", the third column as "Tumor/Normal" and the fourth column as "Birdseed\_normals".
- In the first column (Array), list all of the array names that are being analyzed. The array names are the cel file names. Make sure to delete the ".CEL" extension from the name. For example: if the array name is "20111201\_A8\_M27\_(GenomeWideSNP\_6).CEL" it should be listed in the excel file as "20111201\_A8\_M27\_(GenomeWideSNP\_6)".
- In the second column (Gender), indicate the samples gender as "M" for male, and "F" for female. The samples gender can be acquired from the samples clinical data from the clinical databases and patient health records software (Intellipath) at DLCS.

- In the third column (Tumor/Normal), all of the sample that are used as a control should be indicated as "Normal" and other (test) samples should be indicated as "Tumor". The samples that are indicated as Normal will be used as a baseline to which the tumor samples will be compared. In this study, the benign nevi samples were used as a control samples to form a baseline, and the melanoma samples were compared to these benign nevi samples. The pipeline requires minimum of ten normal samples to perform the analysis.
  - In the fourth column (Birdseed-normal), put Y (for Yes) for all of the normal "control" samples, and leave it blank (for No) for all of the tumor samples.
  - Make sure that there is no space in the array names, because that can cause an error when running the pipeline.
  - Save the file as a text file. To do so, in Excel, click on File, then Save As, then name the file as "*snp6\_sample\_data.sif*", then click on Save as type, then locate and select the type "Text (Tab delimited)", then click Save.
9. For the *Include CNVs* parameter, select output without CNVs. This selection helps the algorithm to subtract out variation seen in a pre-defined set of a panel of more than 3000 blood normals from the Cancer Genome Atlas (TCGA) along with the normals that are in the current batch. This exclusion of the germline CNVs is particularly important for algorithms that identify "somatic" alterations that are statistically significant such as in GISTIC.

10. For the *genome annotation* parameter, select hg19 (human genome build 19).
11. Lastly, click run to start the analysis.

GenePattern sends the analysis job to the GenePattern server and displays the Job Status page. The running time depends on the number of samples being analyze (it can take days to run the analysis).

Once the job is completed, GenePattern will display the results page, where many different output files will be shown. There are two important output files:

1. "cbsResult.seg" file. It is the segmentation file that has the segmented copy number data for all of the samples identified by the CBS segmentation algorithm. It is a six-column, tab-delimited (text) file; the 6 columns are identified as: Sample, Chromosome, Start, End, Num\_Probes, and Segment-Mean.
2. "snp6\_sample\_data.pip3avg.log mdQUAD" file. It is a CN file that contains sorted SNPs and raw copy number value per probe. It also identifies the probe names and positions in the original dataset before segmentation. The first three columns of this file are identified as: Marker, Chromosome, and physical position. The rest of the columns have the array names. This file will be used to create the *Markersfile* for GISTIC, as will be described later.

### *Viewing the segmented copy number data:*

The segmented data that are generated from the segmentation algorithm (CBS) and stored in the *cbsResult.seg* file can be viewed and explored by using the Integrative Genomics Viewer (IGV). IGV is a high-performance visualization tool for interactive exploration of large, integrated genomic datasets [47, 48]. Using IGV to visualize the segmented data is useful for examining a genomic region of interest or specific genes to see if they are affected by copy number change. The steps to visualize the data in the IGV are:

1. IGV needs to be downloaded first. Go to the IGV downloads page:  
<http://www.broadinstitute.org/igv/download>.
2. When prompted, register or log in as requested. You must register to download IGV.
3. After logging in, in the downloads page, under the Java Web Start option, Click the launch icon for the option that is suitable for your system (Mac or Windows, the size of the memory).
4. Save the IGV application.
5. Go to the IGV application that was downloaded and start it. If the system displays messages about trusting the application, confirm that you trust the application and click Run.
6. In IGV interface, go to File and then select "Load from File".
7. Load the *cbsResult.seg* file. The IGV will display the segmented data for all of the cel files (samples) that were analyzed by the *CopyNumberInferencePipeline*.

8. Now, the segmented data can be explored either by choosing the chromosome of interest or searching for a specific gene by typing the gene name in the search box.

## *II. Genomic Identification of Significant targets in Cancer (GISTIC2.0).*

GISTIC is a statistical method (also from GenePattern) that identifies likely driver somatic copy number alterations that drive cancer pathogenesis; and that by evaluating the frequency and amplitude of observed copy number events that are more frequent than would be expected by chance [35, 36]. GISTIC identifies significant alterations by two steps (Figure 2). First, GISTIC computes a statistic G score that considers the frequency F of the occurrence and the average amplitude A of the aberration (for example: the number of genomic region copies that are amplified or deleted) with higher score given to homozygous deletions or high level gene copy number amplification because they are less likely to take place by chance. Therefore, a genomic significant score ( $G^{\text{AMP}}$  and  $G^{\text{DEL}}$ ) represents the frequency of a genetic aberration (amplifications or deletions) seen at that locus across a set of samples, multiplied by the average (increase or decrease) in the log2 ratio in the region of aberration;  $G = F \times A$ . GISTIC G-score, can be defined as :

$$G_i = \frac{1}{N} \sum_{a_{ij} > \theta} a_{ij}$$

for marker  $i$ , sample log<sub>2</sub> copy ratios  $a_{ij}$ , and copy-ratio threshold  $\theta$ , is equivalent to multiplying the frequency of alteration by the mean amplitude in altered samples. Second, GISTIC determines the statistical significance of each computed metric G by comparing it to a background score metric (represents the results that would be expected by chance-null hypothesis) using a permutation test that is based on the

overall pattern of aberrations seen across the entire genome. A peak region is reported at each statistically significant genomic region of aberration and known genes located at that region are listed. GISTIC performs false discovery rate control where G-scores are compared against a null model, and regions with q-values below 0.25 are considered statistically significant.

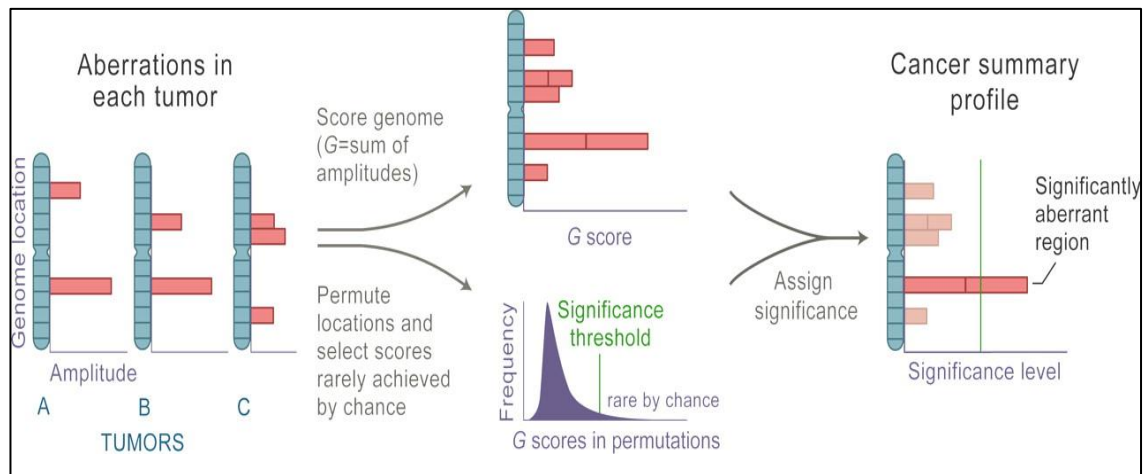



**Figure 2: GISTIC methodology.** After identifying the locations and magnitudes (as log2 signal intensity ratios) of chromosomal aberrations in multiple tumors (Left), GISTIC assigns each genomic marker with a G score that is proportional to the total magnitude of aberrations at each location (Upper Center). Additionally, by permuting the locations in each tumor, GISTIC identifies the frequency with which a given score would be obtained if the events were due to chance and therefore randomly distributed (Lower Center). A significance threshold (green line) is determined such that significant scores are unlikely to occur by chance alone. Alterations are considered significant if they occur in regions that surpass this threshold (Right).

GISTIC can be run on GenePattern with similar steps of running the *CopyNumberInferencePipeline*, but with more parameters to take into account:

1. Sign in to GenePattern at <http://genepattern.broadinstitute.org/gp/pages/login.jsf>.
2. After signing in, in the Modules panel on the left side of the screen, search and locate the *GISTIC2.0* and select it. One easy way to do this:

type the first few characters of the name into the search box and click on *GISTIC\_2.0* when it appears in the list of matching analyses.

3. GenePattern will display the GISTIC2.0 parameters.
4. For the *refgene file* parameter, select hg19 (human genome build 19).
5. For the *seg file* parameter, click the Upload File button and load the *cbsResult.seg* file (step 6 below explains the preparation of *cbsResult.seg* for GISTIC).
6. How to prepare the "*cbsResult.seg*" for GISTIC:

 This *cbsResult.seg* file is the same file that was generated by the *CopyNumberInferencePipeline*, and it is the same file that is uploaded to IGV. This file has segmented data for both the control (benign nevi) and tumor (melanoma) samples. But for GISTIC to find the statistical significant copy number changes in the melanoma samples, only the segmented data of the tumor (melanoma) samples are needed. Therefore, the segmented data of the control (benign nevi) need to be removed from the *cbsResult.seg* before loading it to GISTIC. To remove the segmented data of the control samples:

- Open the *cbsResult.seg* file and copy all of the data in the file (click CTRL+A to highlight all of the data and then click CTRL+C to copy them).
- Open a new Microsoft Excel file and paste all of the data in it (the data should form 6 columns identified as Sample, Chromosome, Start, End, Num\_Probes, and Segment\_Mean respectively).
- Locate the control (benign nevi) sample names, which are listed in the first column (Sample).

- For each control (benign nevi) sample, there will more than a hundred of rows (starting from chromosome 1 to chromosome X as shown in the second column (Chromosome)).
  - Deleted all of the rows for all of the control samples.
  - Make sure to leave only the tumor (melanoma) samples in the Excel file without any space or empty rows between them.
  - Make sure not to delete any row that belongs to the tumor (melanoma) samples, where that can cause an error when running GISTIC.
  - Save the file as a text file. To do so, in Excel, click on File, then Save As, then name the file as " *cbsResult.seg* ", then click on Save as type, then locate and select the type "Text(Tab delimited)", then click Save.
7. For the *markers file* parameter, click the Upload File button and load the *markersfile* file (step 8 below explains the preparation of *markersfile* for GISTIC).
8. How to prepare the " *markersfile* ":

This is a text file that identifies the marker names and positions in the original dataset before segmentation. It should contain three columns identified as: Marker, Chromosome, and physical position. The data in these three columns can be taken from the CN

"*snp6\_sample\_data.pip3avg.log\_mdQUAD*" file (see the two important output files of the *CopyNumberInferencePipelin* above). To create the *markersfile*:

- Open the *snp6\_sample\_data.pip3avg.log\_mdQUAD* file. Note that this is a very large text file, so a large file text editor is needed to edit this file (EmEditor software was used to deal with this file).



- Copy only the first three columns (Marker, Chromosome, and Physical position).
  - Open a Microsoft Excel file and paste the copied three columns in it.
  - Make sure to copy all of the data in the three columns without missing any number (especially in the physical position column), where that can cause an error when running GISTIC.
  - Save the file as a text file. To do so, in Excel, click on File, then Save As, then name the file as "*markersfile*", then click on Save as type, then locate and select the type "Text(Tab delimited)", then click Save.
9. The *array list file* and *cnv file* parameters, these are optional parameters and they can be ignored.
  10. For *gene gistic* parameter, Yes was selected (the default). This means the gene GISTIC algorithm should be used to calculate the significance of deletions at a gene level instead of a marker level.
  11. The *amplification* and *deletion thresholds*, these are thresholds that indicate the minimal copy-number variation sufficient to contribute to significance calculations. These parameters are used as cutoffs to exclude the noise from the analysis, where the copy number events that are not really significant (with low log<sub>2</sub> ratios) are not considered in the analysis. The default is to use 0.1 for both the amplification and deletion, where log<sub>2</sub> ratios of the amplification copy number events above 0.1 will contribute to the significant calculation ( log<sub>2</sub> ratio above 0.1 of a certain genomic locus indicates that the locus has more than the normal copy number, which is 2. For example, the log<sub>2</sub> ratio of a locus with three copy numbers =  $\log_2(3/2) = 0.58 > 0.1$ ). Similarly, log<sub>2</sub> ratios for

deletion copy number events below -0.1 will contribute to the significant calculation ( $\log_2$  ratio below -0.1 of a certain genomic locus indicates that the locus has less than the normal copy number, which is 2. For example, the  $\log_2$  ratio of a locus with 1 copy number =  $\log_2(1/2) = -1 < -0.1$ ). Here, 0.1 was used for the *amplification threshold* and 0.3 was used for the *deletion threshold* (in our data, the deletions seem to be noisy, so 0.3 was used to exclude the bulk of the noise and just consider the significant deletions that have  $\log_2$  ratios below -0.3). Using these low-level cutoffs (0.1 and 0.3) allow of finding significant variation of all types; both broad low-level alterations and focal high level alterations.

12. The *join segment size* parameter, this parameter indicates the smallest number of markers to allow in segments from the segmented data. Segments that contain a number of markers less than or equal to this number are joined to the neighboring segment that is closest in copy number. When the default threshold (4) was used, the amplification peaks looked good, but the deletion peaks looked so noisy. Therefore, looking in literature and at studies that used GISTIC, I noticed that some studies have set the parameter to 10, which means segments that contain a number of markers less than or equal to 10 are joined to the neighboring segment that is closest in copy number. So two GISTIC runs were performed, one with the parameter set to 4, and just the amplification results were considered, and the other run was done with the parameter set to 10, and only the deletion results were considered.
13. The *qv thresh* parameter, this is a significance threshold for q-values. The q-values are obtained by correcting the resulting p-values for

multiple-hypothesis testing using Benjamini-Hochberg false discovery rate method [35]. These q-values represent an upper bound on the expected fraction of false positives in the resulting list. 0.25 (default) was used and regions with q-values below 0.25 are considered significant and are reported.

14. The *remove X* parameter, which indicates whether to remove data from the X-chromosome before analysis. The default (Yes) was used.
15. The *cap val* parameter, which indicates the minimum and maximum cap values on the analyzed data. The GISTIC runs were performed with cap values (in log2 ratio) of -2 and 2, where any values above 2 (8 copies) were replaced by 2 and values below -2 (0.5 copies) were replaced with -2. These cap values were used to limit problems of hyper-segmentation that occur particularly in regions with extreme values due different attenuation curves of adjacent probes.
16. The *confidence level* parameter, which indicates the confidence level used to calculate the region containing a driver. 0.99 was used.
17. The *run broad analysis* parameter, which indicates whether an additional broad-level analysis should be performed. The default (No) was used.
18. The *broad length cutoff* parameter, which is used to distinguish broad from focal events, given in units of fraction of chromosome arm. 0.98 (the default) was used, which means that copy number events spanning more than 98% of a chromosome arm are replaced with more narrowed peak. Yet, these narrowed peak still represent the broad copy number event when looking at the size of the genomic region.

19. The *max sample segs* parameter. This parameter sets the maximum number of segments allowed for a sample in the input data. Samples with more segments than this threshold are excluded from the analysis. The default (2500) was used in this analysis.
20. The *arm peel* parameter, which indicates whether to perform arm level peel off or not. This helps separate peaks to clean up noise. The noise could be as a results of some samples showing disconnected (choppy) amplifications or deletions, which (in fact) seem to be individual significant regions for different parts of the same chromosomal alteration, this can cause GISTIC to report them as individual significant peaks, which causes the noise. This parameter was used (YES) to avoid these false peaks.
21. After adjusting all of the parameters, click run to start the analysis.

GISTIC sends the analysis job to the GenePattern server and displays the Job Status page. The running time depends on the number of samples being analyze (it can take days to run the analysis).

Once the job is completed, GenePattern will display the results page, where many different output files will be shown. The important output files are:

1. *cbsResult.seg.all\_lesions.conf\_99*. This is the all lesions file, which summarizes the results from the GISTIC run. It contains data about the significant regions of amplification and deletion as well as which samples are amplified or deleted in each of these regions. The identified

regions are listed down the first column, and the samples are listed across the first row, starting in column 10.

2. *cbsResult.seg.amp\_genes.conf\_99* file. This is a table of amplification peaks, followed by the genes contained in them, organized in "ragged columns." The amp genes file contains one column for each amplification peak identified in the GISTIC analysis. The first four rows are: cytoband , q-value, residual q-value, and wide peak boundaries. The remaining rows list the genes contained in each wide peak. For peaks that contain no genes, the nearest gene is listed in brackets.
3. *cbsResult.seg.del\_genes.conf\_99*. Similar to the *cbsResult.seg.amp\_genes.conf\_99* file, but this is for the deletion peaks.
4. *cbsResult.seg.amp\_qplot*. This is the Amplification GISTIC plot (in both PDF and PNG format) shows the G-scores (top) and q-values (bottom) with respect to amplifications for all markers over the entire region analyzed.
5. *cbsResult.seg.del\_qplot*. Similar to the *cbsResult.seg.amp\_qplot*, but with respect to deletions for all markers over the entire region analyzed.
6. *cbsResult.seg.raw\_copy\_number*. This is the segmented copy number file (both PDF and PNG) . It is a heat map image of the segmented copy number profiles in the input data.

### III. RESULTS AND DISCUSSION:

#### *Specimen collection and preparation:*

To Compare between the genetic-makeup of melanoma tumors and benign melanocytic nevi, total of sixty-three melanocytic biopsy specimens (42 melanomas + 21 benign melanocytic nevi) were identified in the archives of the Dermatopathology Lab of Central States (Dayton, OH). These specimens (Table 1) were preserved in FFPE and stored at room temperature. Specimens represent biopsies from a variety of locations on the skin. All were found to be large enough to take a sufficient number of slides for the DNA extraction.

**Table 1: Details of specimens used in this study.**

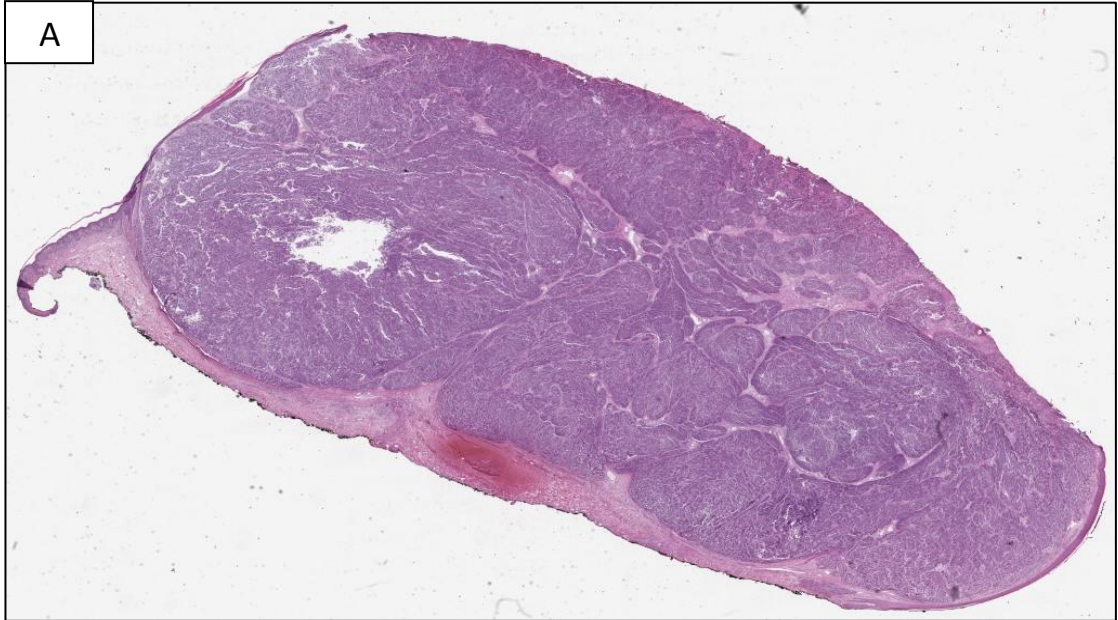
#	Sample	Age at Diagnosis	Year of the sample	Sex	Location	Clark's level	Type
1	M07	77	2008	Male	Right Arm	IV	SUPERFICIAL SPREADING TYPE
2	T10	-	2005	Male	-	-	MALIGNANT MELANOMA
3	T12	80	2005	Male	Forehead	IV	DESMOPLASTIC TYPE
4	T15	75	2005	Female	Upper Back	IV/V	SUPERFICIAL SPREADING TYPE
5	T17	-	2006	Male	-	-	MALIGNANT MELANOMA
6	M18	40	2007	Male	Back	IV	MALIGNANT MELANOMA
7	T19	60	2007	Female	Left Leg	IV	NODULAR SPITZOID TYPE
8	T20	-	2007	Female	Elbow	IV	SUPERFICIAL SPREADING TYPE
9	T23	81	2008	Male	Left Auricular	IV	SUPERFICIAL SPREADING TYPE
10	M27	93	2001	Male	Right Groin	IV	NODULAR MALIGNANT MELANOMA

11	M28	60	2007	Female	Left Leg	IV	NODULAR SPITZOID TYPE
12	M30	-	2011	Male	-	-	MALIGNANT MELANOMA
13	M31	63	2008	Female	Right Forearm	IV	SUPERFICIAL SPREADING TYPE
14	M33	76	2008	Female	Right Cheek	IV	SUPERFICIAL SPREADING TYPE
15	M50	57	2010	Male	Left Arm	IV	SUPERFICIAL SPREADING TYPE
16	M54	45	2012	Female	Left Back	IV	ULCERATED NODULAR MALIGNANT MELANOMA
17	M56	60	2012	Male	Left Shin	IV	SPITZOID TYPE
18	M58	66	2011	Male	Right Cheek		POORLY-DIFFERENTIATED CARCINOMA !!!
19	M59	77	2011	Male	Right Elbow	IV	INVASIVE MALIGNANT MELANOMA
20	M64	27	2011	Female	Right Neck	IV	POSTERIOR INVASIVE POLYPOID MALIGNANT MELANOMA
21	M74	69	2010	Male	Left Temple	IV	SUPERFICIAL SPREADING TYPE
22	M75	74	2010	Male	Left Neck	IV	SUPERFICIAL SPREADING TYPE
23	M76	67	2010	Female	Right Back	IV	Malignant Melanoma with verticle Growth
24	M77	53	2010	Male	Right Arm	IV	NODULAR MALIGNANT MELANOMA
25	M84	-	-	Female	-	-	MALIGNANT MELANOMA
26	M86	54	2009	Female	Anterior Thigh	IV	SUPERFICIAL SPREADING TYPE
27	M98	72	2005	Male	Right Shoulder	III	SUPERFICIAL SPREADING TYPE
28	M107	80	2005	Male	Forehead	IV	DESMOPLASTIC TYPE
29	M111	48	2005	Female	Right Forearm	V	NODULAR VARIANT
30	M113	40	2007	Male	Back	IV	Malignant melanoma
31	M116	74	2007	Female	Right Arm	II	SUPERFICIAL SPREADING TYPE
32	M130	63	2001	Male	Back	IV	SUPERFICIAL SPREADING TYPE
33	M131	45	2001	Female	Left Arm	III	SUPERFICIAL SPREADING TYPE
34	M132	75	2001	Male	Right Chest	III-IV	DESMOPLASTIC TYPE
35	M136	40	2001	Female	Upper Back	III-IV	NODULAR TYPE
36	M137	85	2001	Female	Right Cheek	IV/V	Malignant melanoma
37	M139	87	2001	Male	Right Cheek	V	CONSISTENT WITH THE LENTIGO MALIGNA MELANOMA SUBTYPE
38	M147	90	2002	Male	Left Back	IV	SUPERFICIAL SPREADING TYPE
39	M148	55	2002	Female	Middle Back	II/III	SUPERFICIAL SPREADING TYPE
40	M173	28	2008	Female	Left Shoulder	III	INVASIVE SPITZOID MALIGNANT MELANOMA
41	M174	42	2008	Male	Right Pretibial	III	SUPERFICIAL SPREADING TYPE

<b>42</b>	M191	75	2001	Male	Left Back	IV	MELANOMA WITH REGRESSION
<b>43</b>	NT06	34	2010	Male	Right Arm	-	DERMAL NEVUS
<b>44</b>	NT07	44	2010	Female	Right Buttock	-	DERMAL NEVUS
<b>45</b>	NT12	-	-	Male	-	-	DERMAL NEVUS
<b>46</b>	B15	19	2010	Female	Left Back	-	DERMAL NEVUS
<b>47</b>	B27	39	2011	Male	Left Neck	-	DERMAL NEVUS
<b>48</b>	B29	35	2011	Male	Left Flank	-	DERMAL NEVUS
<b>49</b>	B30	34	2011	Female	Right Neck	-	DERMAL NEVUS
<b>50</b>	B31	44	2011	Male	Right Groin	-	DERMAL NEVUS
<b>51</b>	B47	27	2011	Female	Right Back	-	DERMAL NEVUS
<b>52</b>	B51	62	2011	Female	Right Eyebrow	-	DERMAL NEVUS
<b>53</b>	B52	48	2011	Female	Left Neck	-	DERMAL NEVUS
<b>54</b>	B53_3	75	2011	Female	Left Shoulder	-	DERMAL NEVUS
<b>55</b>	B254	34	2007	Female	Left Deltoid	-	DERMAL NEVUS
<b>56</b>	B267	33	2013	Female	Right Back	-	DERMAL NEVUS
<b>57</b>	B272	38	2013	Female	-	-	DERMAL NEVUS
<b>58</b>	B279	52	2013	Female	Right Back	-	DERMAL NEVUS
<b>59</b>	B282	41	2013	Female	Right Neck	-	DERMAL NEVUS
<b>60</b>	B283	14	2013	Female	Right Shoulder	-	DERMAL NEVUS
<b>61</b>	B285	16	2013	Female	-	-	DERMAL NEVUS
<b>62</b>	B286	21	2013	Male	Right Back	-	DERMAL NEVUS
<b>63</b>	B287	60	2013	Female	Right Neck	-	DERMAL NEVUS

The first slide and the last slide taken from each specimen were examined by staining with hemotoxylin and eosin (H&E) to verify the presence of cellular material in all sections (Figure 3). This is particularly important for the test sensitivity, where melanocytes should represent the majority of the entire tissue (> 60%) used for DNA extraction in order to avoid false-negative aCGH results [49]. Therefore, some of the melanoma samples' sections underwent microdissection to remove part of tissues that did not contain melanocytes.





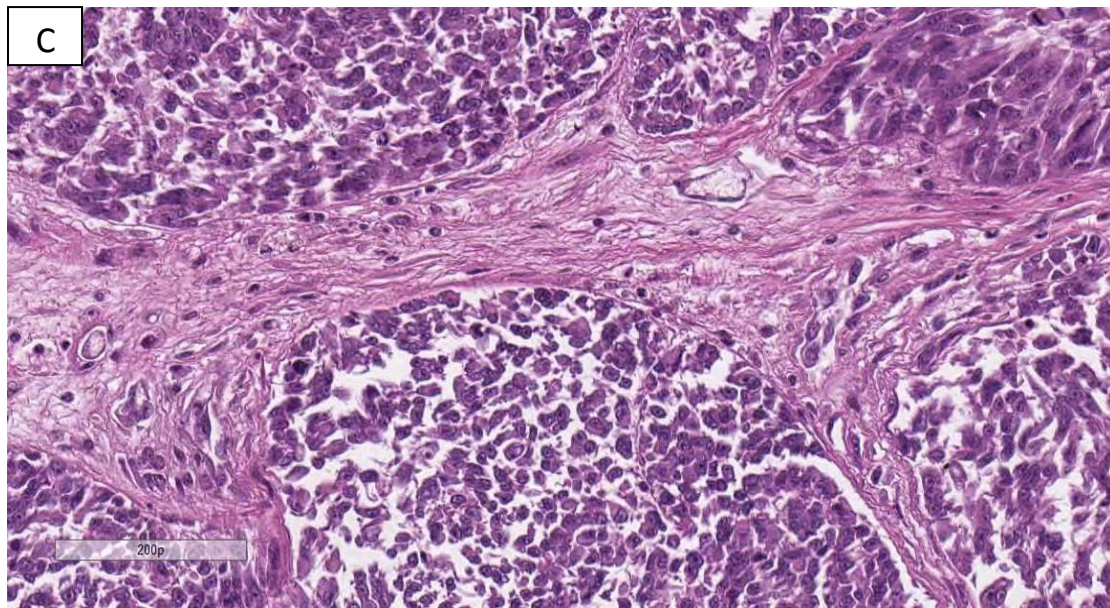


**Figure 3: H&E staining for sections taken from melanoma sample. A) The first section taken from the sample showing melanoma cells (purple). B) The last section taken from the same sample showing that melanoma cells still present. C) The H&E staining showing atypical, pleomorphic cells of malignant melanoma.**

#### ***Improving the quality of DNA extracted from FFPE specimens:***

FFPE tissues represent a great wealth of human biospecimens that exists in the archives of many hospitals, tissue banks, and pathology laboratories. They are some of the most readily available biomaterials for researchers, due in part to their long shelf life and accreditation requirements for their storage. Despite the availability of archived specimens, the process of fixation complicates the use of nucleic acids from these tissue blocks [50]. Formalin treatment cross-links biological molecules such as DNA and proteins [51]. Additionally, longer nucleic acids like DNA and RNA, in particular, are fragmented in the preservation process, leading to poor performance in downstream analyses [52, 53]. Array CGH performs best with long, intact chromosomes. This is one of the fundamental challenges of FFPE tissues. During aCGH, genomic DNA is first digested with restriction enzymes and then these fragments are amplified from adapters ligated to these restriction sites. Therefore, if a

region between restriction sites is broken in our input, that region will not be represented in the material hybridized to the array. To optimize utility of nucleic acids from FFPE specimens for aCGH, we must reverse these cross links and avoid further degradation during the DNA or RNA extraction process. Therefore, we sought to improve the quality of the DNA by comparing DNA extracted from the same specimens by three different methods, phenol- chloroform-isoamyl alcohol, Qiagen columns, or adaptive focused acoustics (AFA), with consideration of metrics of quantity and quality for each method.

Twenty-seven benign melanocytic biopsy specimens were identified in the archives of the Dermatopathology Lab of Central States (Dayton, OH) and used in this quest (Table 2).

**Table 2: Details of specimens used in this quest.**

Sample number	Patient age	Sex	Specimen age (years)	Clinical notes
1	30	F	8	Biopsy, nose, left side dermal nevus
2	25	M	8	Biopsy, scalp, right post dermal nevus
3	16	M	8	Biopsy, abdomen left dermal nevus
4	35	F	8	Biopsy, back, left center dermal nevus
5	38	M	8	Biopsy, scalp dermal nevus
6	21	M	8	Biopsy, back right middle dermal nevus
7	26	M	8	Biopsy, abdomen dermal nevus
8	32	F	8	Biopsy, cheek, right dermal nevus
9	31	M	8	Biopsy, axilla, right dermal nevus
10	69	F	8	Biopsy, back, right upper dermal nevus
11	40	F	8	Biopsy, axillary area. Anterior nevus lipomatosus superficialis
12	44	F	8	Biopsy, calf, left post dermal nevus
13	22	F	8	Biopsy, chest, left lateral neurotized dermal nevus
14	56	M	8	Biopsy, cheek, left intradermal melanocytic nevus
15	47	F	8	Biopsy, axilla, left dermal nevus
16	35	F	8	Biopsy, chest dermal nevus
17	29	F	8	Biopsy, back, midline lower neurotized dermal nevus
18	34	F	8	Biopsy, deltoid left anterior dermal nevus
19	44	F	8	Biopsy, lip, left upper dermal nevus

<b>20</b>	75	F	8	Biopsy, knee, left medial dermal nevus
<b>21</b>	36	M	8	Biopsy, axilla right dermal nevus
<b>22</b>	60	F	11	Biopsy, back dermal nevus
<b>23</b>	16	F	11	Biopsy, back, left upper dermal nevus
<b>24</b>	41	F	11	Biopsy, forehead, right neurotized dermal nevus
<b>25</b>	16	F	11	Biopsy, back, inferior lower dermal nevus
<b>26</b>	35	M	11	Excision, malar, left dermal nevus
<b>27</b>	74	F	11	Biopsy, back, left upper dermal nevus
<b>Average:</b>	38.04		8.67	

After extracting DNA from the same 27 samples using phenol- chloroform-isoamyl alcohol, Qiagen columns, or adaptive focused acoustics (AFA), the DNA was separated by electrophoresis to determine the genomic DNA size range. Four representative samples are shown in (Figure 4) by each method.

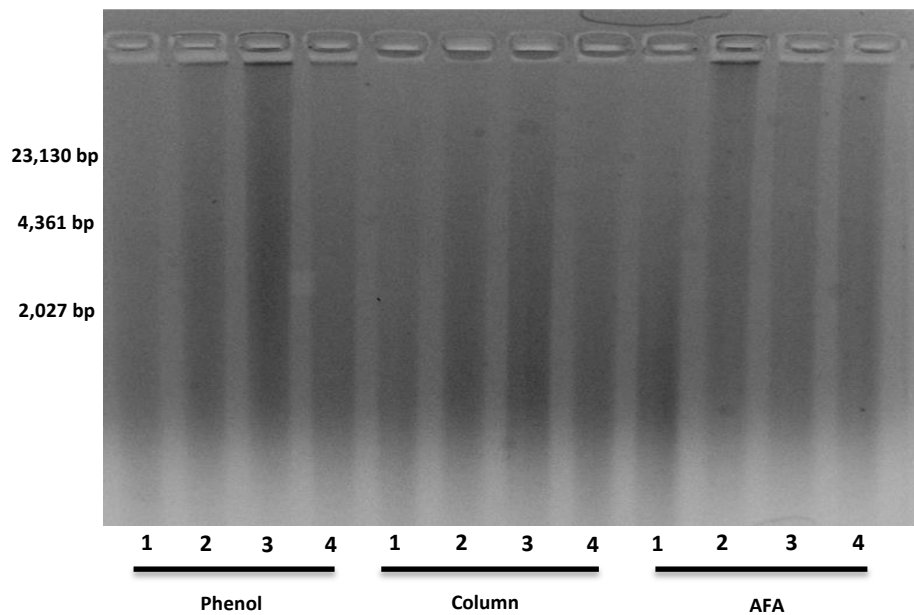


**Figure 4: ) Genomic DNA size range of samples extracted by three different methods . Genomic DNA was extracted from four specimens (numbered 1-4) by three different methods, Phenol chloroform isoamyl alcohol (“Phenol”), commercial column-based extraction kit (“Column”) and adaptive focused acoustics (“AFA”). Total extracted DNA was separated by electrophoresis on 1% agarose.**

Samples with visible DNA fragments as large as 23,000 base pairs (bp) are considered eligible for further processes. Here, DNA extracted by AFA showed slightly higher size distributions, but these results were mostly equivocal, suggesting that any method worked about as well as the other.

The quantity and quality of the extracted DNA was compared across all samples. Interestingly, there was a significant difference in the DNA yield per section between methods. This controlled for the number of slides used in each extraction as well as the elution volumes used for each method. A variety of incubation times have been suggested in the literature for deparaffinization and proteinase K digestion [42, 54-56]. Increasing the proteinase K digestion time from one hour to overnight or even 72 hours has been shown to increase the amount of retrieved DNA in some studies [42, 54]; therefore, in this study a prolonged proteinase K digestion time was afforded to both the phenol-chloroform and column methods to compare best performance against the newer AFA method. Here there was a clear difference between the column-based method and the other two methods. The commonly used column-based kit (Qiagen) retrieved approximately twice as much DNA per section as phenol-chloroform or AFA. Table 3 shows the quantification of recovered DNA by both a fluorometric method (Qubit) and a spectrophotometric method (Nanodrop).

**Table 3: Summary of the QC metrics for the methods comparisons.**

<b>Quality Metrics</b>	<b>Phenol</b>	<b>Column</b>	<b>AFA</b>
<b>DNA (ng)/section (Qubit)</b>	106.2 ± 33.1	264.3 ± 35.4	134.6 ± 18.1
<b>DNA (ng)/section (Nanodrop)</b>	702.1 ± 200.2	716.0 ± 116.1	453.8 ± 53.9
<b>A260/A280</b>	1.94 ± 0.02	2.04 ± 0.03	1.90 ± 0.02
<b>A260/A230</b>	1.71 ± 0.18	1.71 ± 0.12	1.75 ± 0.43
<b>Max. amplicon (bp)</b>	346.7 ± 24.1	347.4 ± 21.4	401.9 ± 10.2
<b>PCR failure rate</b>	25.93%	22.22%	3.70%



Importantly, purity of the DNA is critical for most applications. Inhibitors of PCR can be carried over from the purification process and become apparent first by spectroscopy as lower  $A^{260}/A^{230}$  ratios. Therefore, the purity of the extracted DNA was compared by spectrophotometry to measure absorbance at 260 and 230 nanometers. All three methods produced samples that would typically be called pure with an  $A^{260}/A^{230}$  ratio of approximately 1.7, which is sufficient for most applications (Table 3).

In order to measure the performance of the DNA in downstream PCR, RAPD-PCR was performed for each sample across all three extraction methods. The ability of the DNA to be amplified by PCR is a measure of its purity, as common contaminants (such as alcohols, xylene, and salts) often inhibit the PCR reaction (the utilization of RAPD-PCR as a quality control step is discussed further in the "RAPD-PCR, a predictor for aCGH success of FFPE samples ) section. Here, DNA produced by AFA showed amplicons of greater length than DNA extracted by other means (Table 3). Furthermore, more products of a larger size were able to be amplified from DNA obtained by AFA than by other methods (Figure 5).

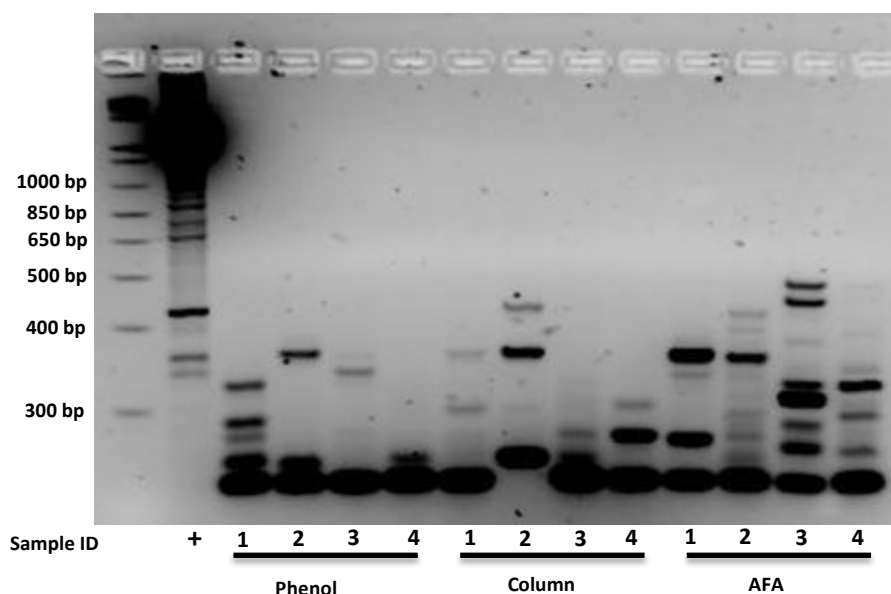


**Figure 5: ) RAPD-PCR profile of 4 samples extracted by three different methods. Extracted DNA was used for randomly amplified polymorphic DNA (RAPD) PCR to produce a variety of amplicons. The same four samples (1-4) isolated by three different methods were compared side-by-side. +, positive control Jurkat genomic DNA. More products of a larger size were obtained from DNA extracted by AFA.**

Additionally, the PCR failure was calculated to observe the performance of the DNA extracted from each method in the RAPD-PCR. We defined PCR failure as a RAPD-PCR resulting in amplicons less than 300 bp in length; we do not proceed to use these samples as this predicts poor performance in downstream PCR [43]. The rate of these failures was over 25% by phenol-chloroform and over 22% by columns. However, only one of 27 samples (3.7%) failed by AFA (Table 3). An alternative explanation for failure to produce larger amplicons is that each method varies in its ability to extract intact DNA molecules of sufficient length. This is suggested by a greater proportion of gDNA below 2,000 bp in Figure 3 for phenol-chloroform and column methods. One possibility is that the reduced processing times involved in AFA reduces the likelihood that any longer DNA molecules present in the FFPE sample will be fragmented during the extraction.

when determining what method to use, these gains must be weighed against the increased purity, greater amenability to PCR, lower PCR failure rates, and recovery of larger chromosomal fragments when DNA is obtained by AFA. These findings support AFA as an improvement over previous DNA extraction methods for FFPE tissues [57]. For aCGH analysis, none of the samples prepared by phenol-chloroform performed well in the PCR amplification step of the SNP6 protocol. Even when sufficient amplicon length was observed, the total DNA yield was insufficient to move forward with hybridization to arrays. Therefore, only DNA extracted by column-based extraction methods (Qiagen columns, or adaptive focused acoustics (AFA)) was used in the copy number analysis.

***RAPD-PCR, A predictor for aCGH success of FFPE samples.***

Most applications using gDNA from clinical specimens will begin with PCR amplification. SNP genotyping, copy number analysis, comparative genomic hybridization, and other methods all depend on the “amplifiability” of the gDNA. For array CGH in particular, longer amplicons leads directly to greater fragment representation in the final analysis. Randomly Amplified Polymorphic DNA (RAPD) PCR is useful for predicting the suitability of a DNA sample for downstream PCR [43]. While RAPD-PCR does not reliably produce the same specific bands on a gel, we have found RAPD-PCR to be a rapid method to screen many amplicons using a single PCR reaction, and that these results are generally a good measure of performance in downstream applications (specifically aCGH). Therefore, we have included the RAPD-PCR as a quality control step, by which we can screen the DNA ability to be amplified, and identify which samples to be ideal for SNP 6.0 work.



The size range of RAPD products reflect the degree of DNA degradation, where samples that produce a RAPD profile with more than 300 bp fragments are considered eligible to be used in aCGH analysis. On the other hand, samples that produce a RAPD PCR profile with less than 300 bp fragments are considered low-quality DNA and not used for aCGH analysis (Figure 6).

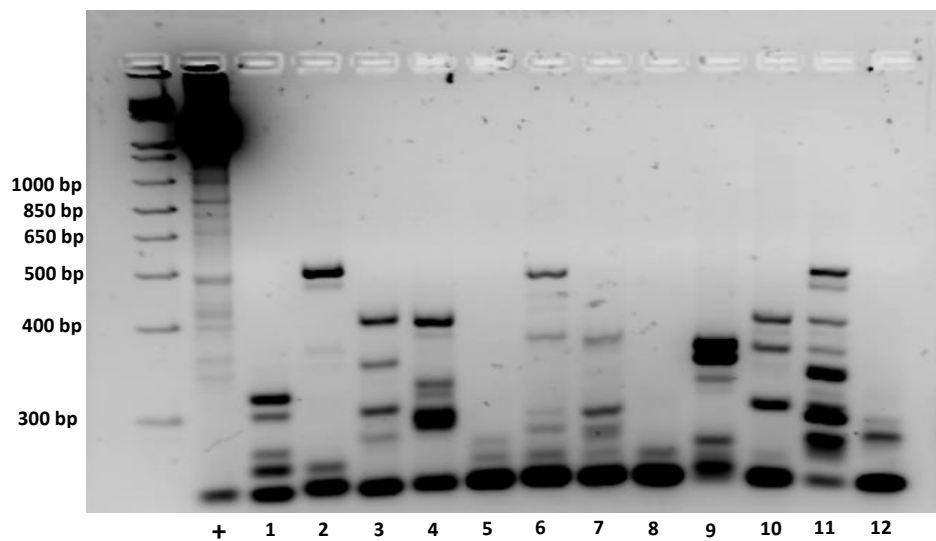


**Figure 6: ) RAPD-PCR profiles for 12 different samples. +, positive control Jurkat genomic DNA. Samples # 5, 8, and 12 showed RAPD PCR product of less than 300 bp fragments, which indicates the low quality of the DNA from these samples. The other samples showed RAPD PCR products of fragments between 300-500 bp, which indicate the higher quality of the DNA from these samples.**

Using the RAPD-PCR as a prescreening technique allows as to avoid using samples with low-quality DNA in the aCGH analysis, thus increasing the reliability and accuracy of the analysis.

***Processing the qualified DNA through SNP 6.0 protocol.***

Array-based genotyping platforms, such as the Affymetrix SNP6.0 microarrays have been validated to be a reliable method for obtaining high resolution copy number information [53, 58, 59]. Unlike other cytogenetic techniques such as FISH, these high-density single-nucleotide polymorphism (SNP) arrays allow for detailed and genome-wide identification of copy-number alterations in one experiment, which make it a powerful discovery tool. The principle of these arrays depends on the hybridization of fragmented single-stranded DNA to arrays containing hundreds of thousands of unique nucleotide probe sequences; each probe is designed to bind to a target DNA subsequence. The high-density SNP6.0 microarrays contain over 940,000 probes for interrogating copy number variations in the entire genome [60].

In order to analyze copy number variation of DNA samples, the DNA needs to be processed through different enzymatic reactions and prepared for hybridization to the microarrays. The DNA first is digested by restriction enzymes (Sty I and Nsp I) to produce different size DNA fragments. This step is highly sensitive to the level of the DNA degradation in the starting material, where the higher the DNA is degraded, the lower the number of restriction sites still present and therefore the less-efficient is the PCR amplification step [61]. The digested DNA fragments are then ligated to adaptors that recognize the sticky ends of the restriction sites. These adaptors-ligated DNA fragments are then amplified to reduce the genome complexity. The PCR conditions were optimized to amplify DNA fragments in the size range of 200-1100 bp and yield a final PCR product concentration (for a typical sample) 4.0 to 6.5 µg/µl. However, because the DNA from FFPE samples is partially degraded, this causes less-efficient amplification and lower PCR yield. Samples that yielded less than the desired PCR product concentration were excluded from moving forward with

hybridization to the arrays (such as in case of samples extracted by the phenol-chloroform method). Therefore, the PCR amplification step was modified to optimize the range of the product size and the yield concentration. The number of PCR reactions was doubled from the suggested three for Sty1 and four for Nsp1 to six for Sty1 and eight for Nsp1. It is important to note that the number of reactions was increased; the number of cycles in each reaction remained the same. Also, the input DNA was increased from 250 ng to 500 ng. These modifications improved the amplification performance and helped yielding an optimal PCR product concentration and average product distribution between 200-1100 bp (Figure 7).

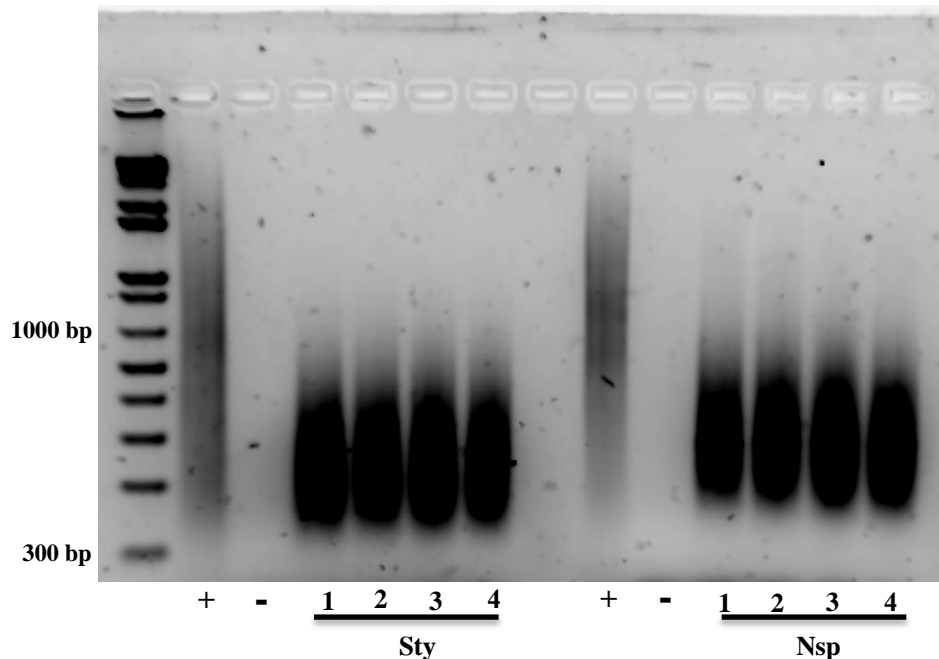


**Figure 7: ) Example of SNP6.0 PCR product of 4 different samples run on 2% agarose gel. +, positive control Jurkat genomic DNA. -, negative control, a mock reaction with no template DNA. The same 4 samples were digested first with Sty I and Nsp I restriction enzymes, and then ligated to adaptors. The adaptors-ligated fragments were PCR-amplified. All samples showed average product distribution between 200 and 1000 bp.**

The PCR product of Sty and Nsp will be combined and then purified. After purification, the DNA undergoes an important step, which is fragmentation. DNase I enzyme is used to unspecifically fragments the PCR product into small fragments. In order for these fragments to successfully hybridized to the SNP6.0 microarrays, they must be around 200 bp (Figure 8).

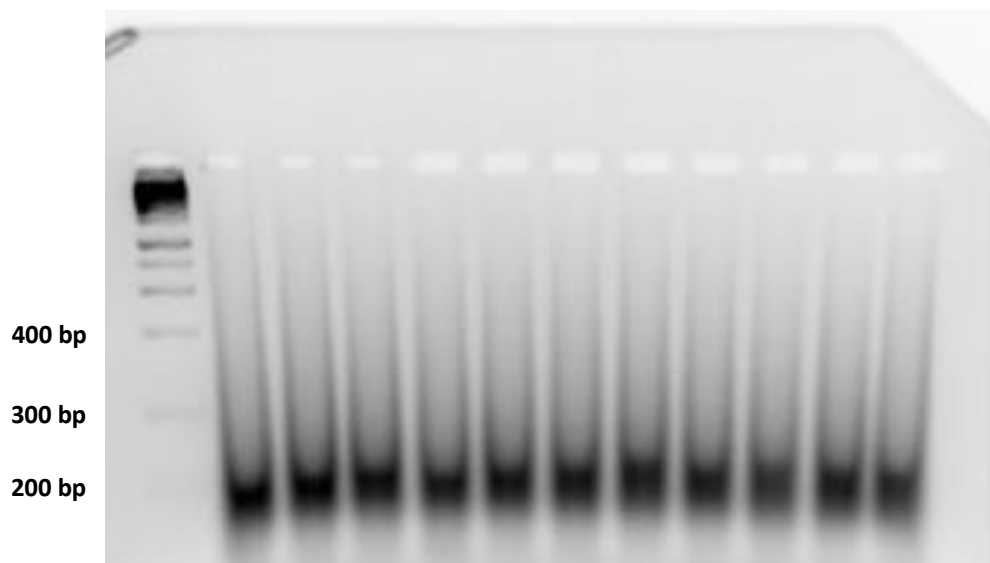


**Figure 8: ) Examples of Enzymatic fragmentation performances run on 4% agarose gel. The fragmentation resulted in all samples showing product of around 200 bp fragments.**

The fragmented DNA is then labeled with a DNA labeling reagent. After that, the fragmented and labeled DNA will be prepared for the hybridization step, where the DNA is denatured on a thermal cycler. After denaturation, each sample will be loaded onto the Genome-Wide Human SNP array 6.0 (one sample per array) and placed in a hybridization oven for 16-18 hours for hybridization.

As a QC step, a program called Affymetrix Power Tools (APT) can be used to evaluate the microarrays and determine which restriction-PCR products had successfully hybridized to the microarrays. The APT program analyzes the probe sets and then assigns a call rate to each of the restriction fragment length depending on how successfully they were hybridized to the microarrays. A contrast QC of at least 0.4 indicates a successful hybridization of DNA fragments to the arrays. The expected restriction fragments are binned by size and graphed versus their abundance on hybridized arrays. Since the DNA in the starting material is partially degraded, we do not expect the hybridization efficiency to be ideal (200bp-1400bp). Yet, we were able to get hybridization efficiency of DNA CQC > 0.5 for DNA fragments 500-600 bp long (Figure 9). The representation of restriction fragments on the microarrays generally agrees with the results of our RAPD-PCR results.

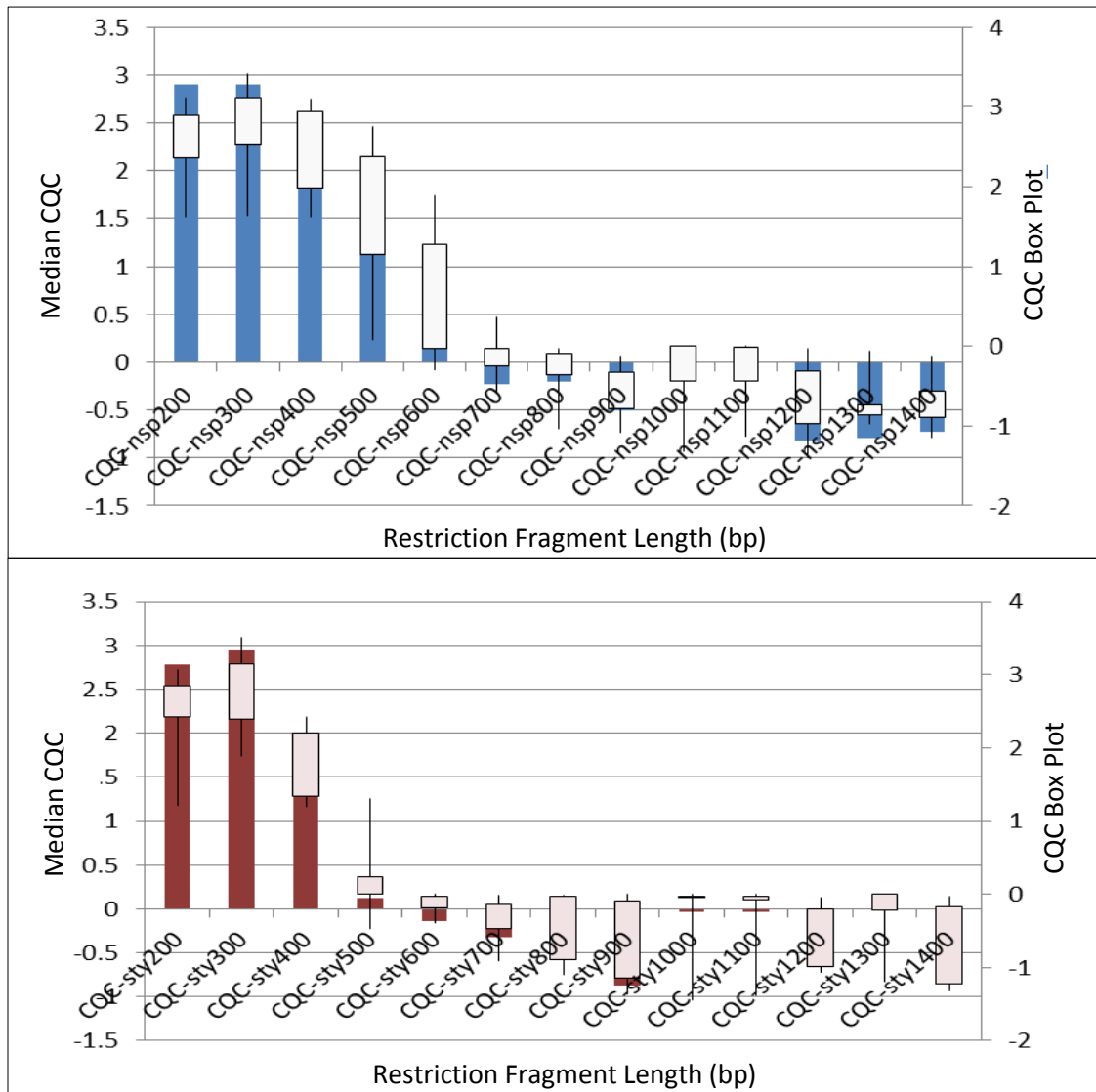


**Figure 9: ) APT analysis of Nsp1 (blue) and Sty1 (red) . Contrast QC, the ability to resolve between alleles on the arrays, was calculated for each probe and plotted against the length of the restriction fragment containing that target. Restriction for these arrays is performed with the enzyme Sty1 (Red) or Nsp1 (Blue). Fragment length was divided into 100 bp bins (x-axis). Median CQC is shown in the bar graph (left y-axis). Distribution of the data is shown by the superimposed box plot (right y-axis).The two graphs show that the probes in the arrays have bound to the DNA fragments at different sizes (200bp – 600bp).**

### ***Validating the recurrent copy number changes in melanoma.***

Upon hybridizing all of the melanoma and benign samples, and having the data ready to be analyzed, we started the copy number analysis by validating copy number

alterations that have been reported in literature. Different melanoma studies have shown some genes that are frequently amplified or deleted in melanoma samples. By applying the Integrative Genomic Viewer (IGV) on the segmented copy number data generated by the *CopyNumberInferencePipeline*, we can search through the segmented data and inspect the known melanoma genes. IGV shows the copy number segmented data as a heatmap ranging between log2 ratios -1.5 to 1.5, where genomic regions with blue color have relatively lower copy number than the normal copy number (2). On the other hand, genomic regions with red color indicate gain in the copy number (Figure 10). This scale is applied on all of the copy number analysis in this study.



**Figure 10: ) IGV copy number scale. Blue color represent deletion, red color represent amplification, and white color represent normal copy number. The different shades of the color represent magnitudes as log2 signal intensity ratios. Log2 ratio of 1.5 represents high amplification (5.6 copies); and log2 ratio of -1.5 represent high deletion (0.7 copies).**

The validation began by looking at a comprehensive overview of the segmented data of the entire genome. We found that most of the melanoma samples exhibit intense copy number changes. In contrast, benign nevi samples show normal copy number throughout their entire genome (Figure 11). This difference in copy number alteration pattern between melanoma and benign nevi has been shown to be a distinguishing characteristic of melanoma and has been exploited to discriminate between melanoma and benign nevi [22, 25, 62-64].

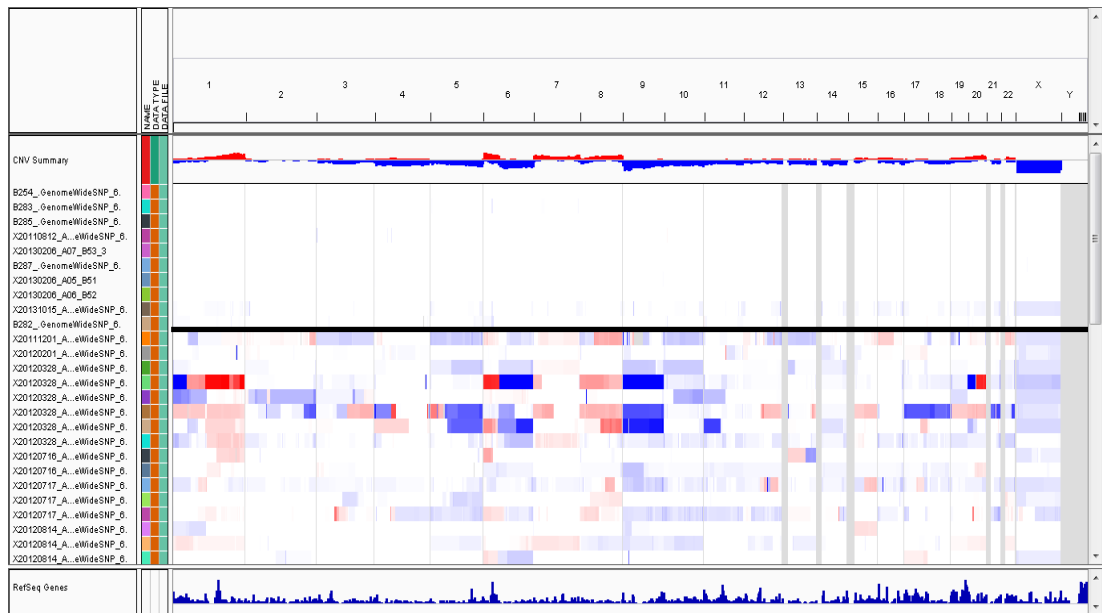
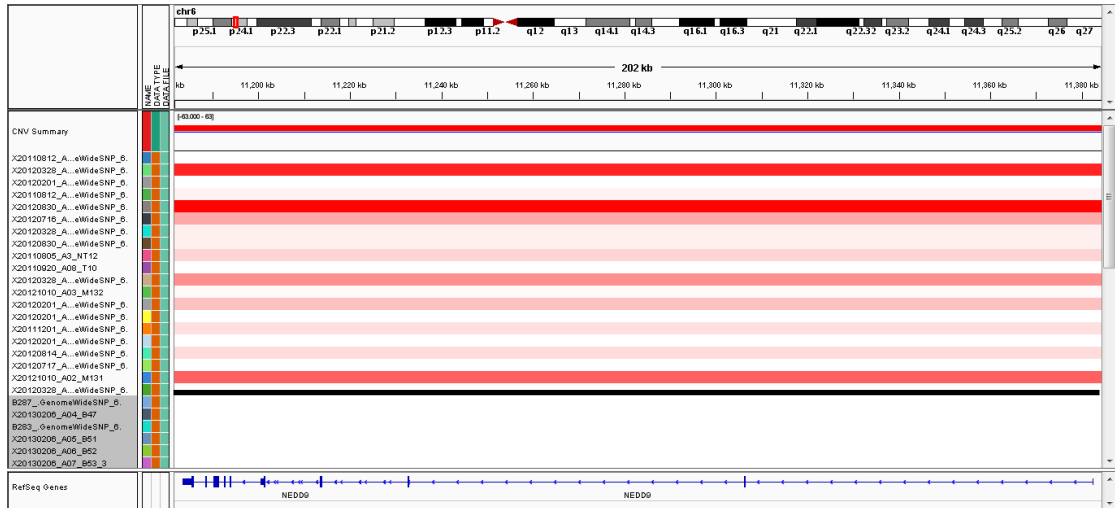


**Figure 11: ) A comprehensive overview of the segmented copy number data of the analyzed melanoma and benign nevi genome. The horizontal axis represents the genome from Chromosome 1 to Y. The vertical axis represents the samples. Blue color indicates a deletion in that region of the genome and red color indicates an amplification. Samples above the black horizontal line are benign nevi sample, and samples below the line are melanoma samples.**

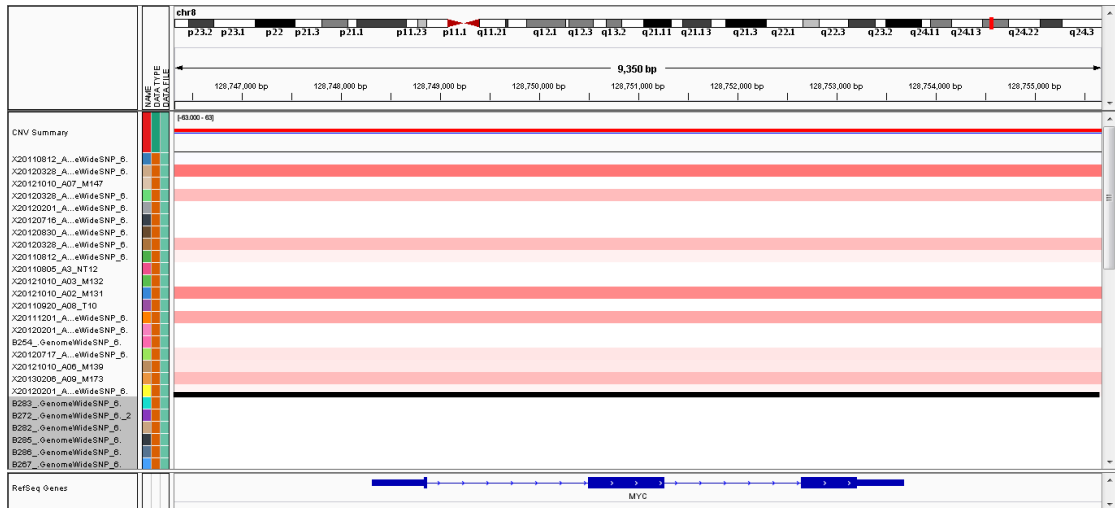
We then sought to inspect the known copy number changes associated with melanoma. Several studies have reported frequent amplification and deletion of some genes in melanoma, but not in benign nevi specimens. Among the highly amplified genes associated with melanoma tumorigenesis are the melanoma metastasis gene NEDD9 [34], the proto-oncogene transcription factor MYC [65], and also AKT3 [66, 67]. We found that most of the melanoma samples show different level of amplification of these genes in comparison with the benign nevi samples (Figure 12 A, B and C).



(A)



(B)



(C)

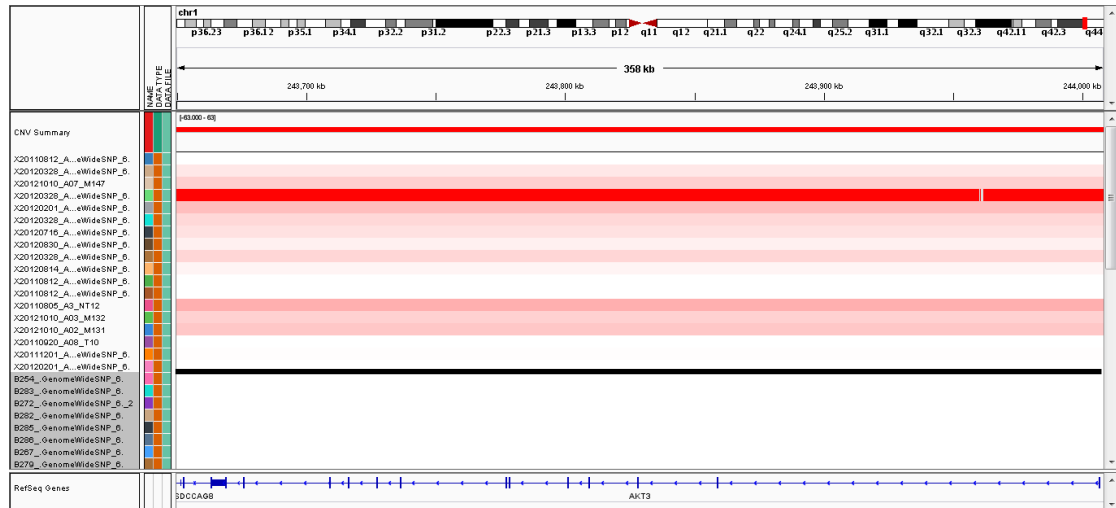
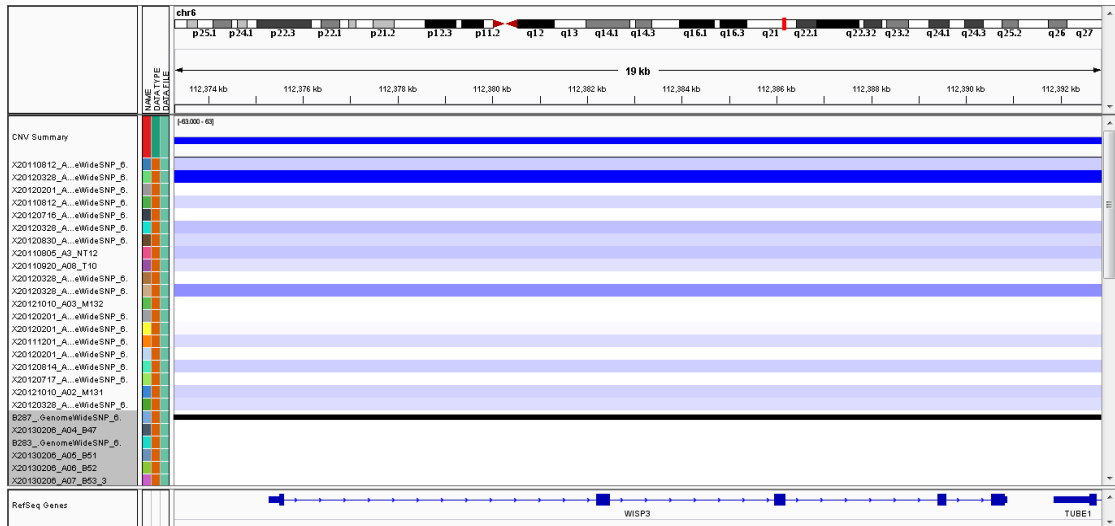


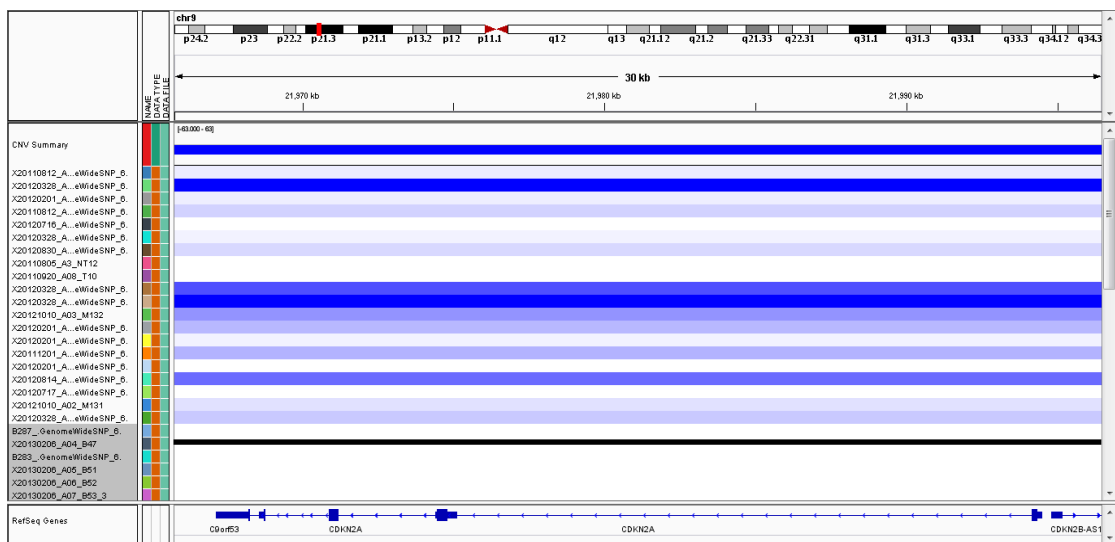
**Figure 12: ) Copy number change of known amplified genes in melanoma. The vertical axis represents the samples. Samples above the black horizontal line are melanoma sample, and samples below the line are benign nevi samples. The gene name is indicated below the heatmap in each figure. The CNV summary on the left above the sample names indicates the overall copy number change in the selected gene. A) Amplification of NEDD9. B) Amplification of MYC. C) Amplification of AKT3.**

Similarly, several studies have reported a frequent deletion of some genes in melanoma. Among the highly deleted genes in melanoma are the Wnt1 Inducible Signaling Pathway protein 3 (WISP3) [68], the tumor suppressor and the melanoma susceptibility gene CDKN2A [69, 70], and the tumor suppressor gene PTEN [71]. Examining these genes in our analysis showed that most of the melanoma samples carry deletions within these genes, while benign nevi samples show no aberration at these genes (Figure 13 A, B, and C).

(A)



(B)



(C)

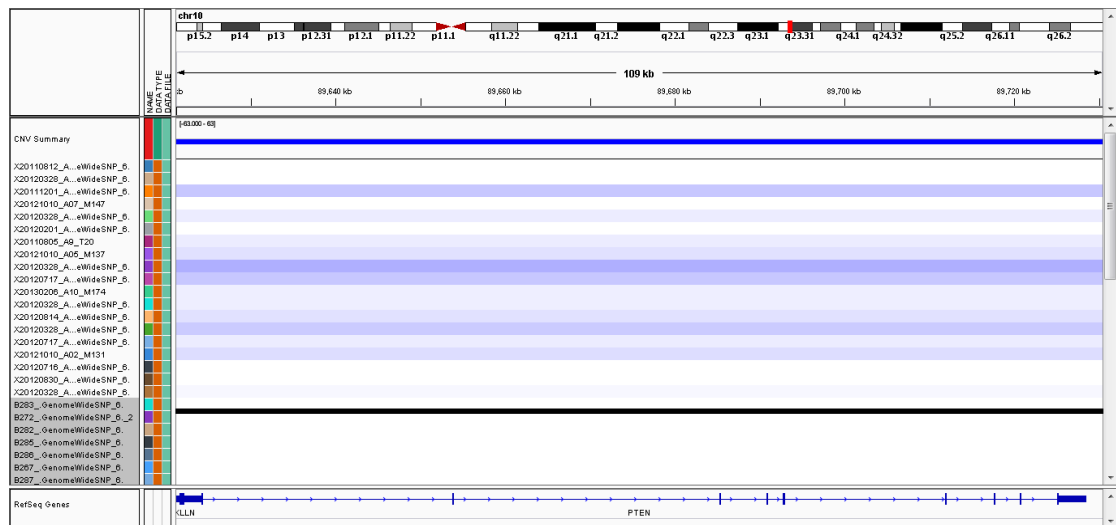


**Figure 13: ) Copy number change of known deleted genes in melanoma. The vertical axis represents the samples. Samples above the black horizontal line are melanoma sample, and samples below the line are benign nevi samples. The gene name is indicated below the heatmap in each figure. The CNV summary on the left above the sample names indicates the overall copy number change in the selected gene. A) Deletion of WISP3. B) Deletion of CDKN2A. C) Deletion of PTEN.**

These initial data indicates regions of amplifications and deletions that are conserved within the samples. These results are consistent with the conserved amplification and deletions reported in literature, which indicate the reliability of our analysis. These 'proof of principle' results lend confidence of any novel copy number changes that may arise from this study.

### ***Genomic identification of significant targets in melanoma.***

Somatic copy number variations play a fundamental role in cancer development and progression [37, 72]. These genetic variations can contribute in activation or inactivation of cancer genes, such as oncogenes and tumor suppressor genes [73]. Knowing and understanding of such genetic alterations have dramatically advanced cancer diagnosis and therapeutics [74-76]. However, copy number changes can affect

broad genomic regions spanning a large number of genes. Nevertheless, one or few of these genes (drivers) are more likely to be responsible for the tumorigenesis [35]. In melanoma, copy number studies have reported a variety of different recurrent genetic alterations affecting large chromosomal segments, without (or with few) target genes identified. Therefore, there still a great demand to identify novel melanoma drivers targeted by such somatic copy number changes, which will help improve the melanoma diagnosis, assessing prognosis, and developing targeted therapies.

The task of revealing new cancer genes being targeted by somatic copy number changes is not simple. The difficulty lies in distinguishing the driver alterations (cancer driver genes) that contribute to tumorigenesis from the random somatic passengers [36, 77]. The great advancement in the technology of microarrays helps yielding precise and detailed DNA copy number profiles corresponding to gains or losses of DNA segments in tumor samples. These DNA copy number profiles are useful in looking at specific genomic region of interest and examining them (see "Validating the recurrent copy number changes in melanoma" above). Nonetheless, finding driver events in these noisy, detailed, row copy number data acquired from the microarrays analysis represents a difficult challenge (Figure 14).

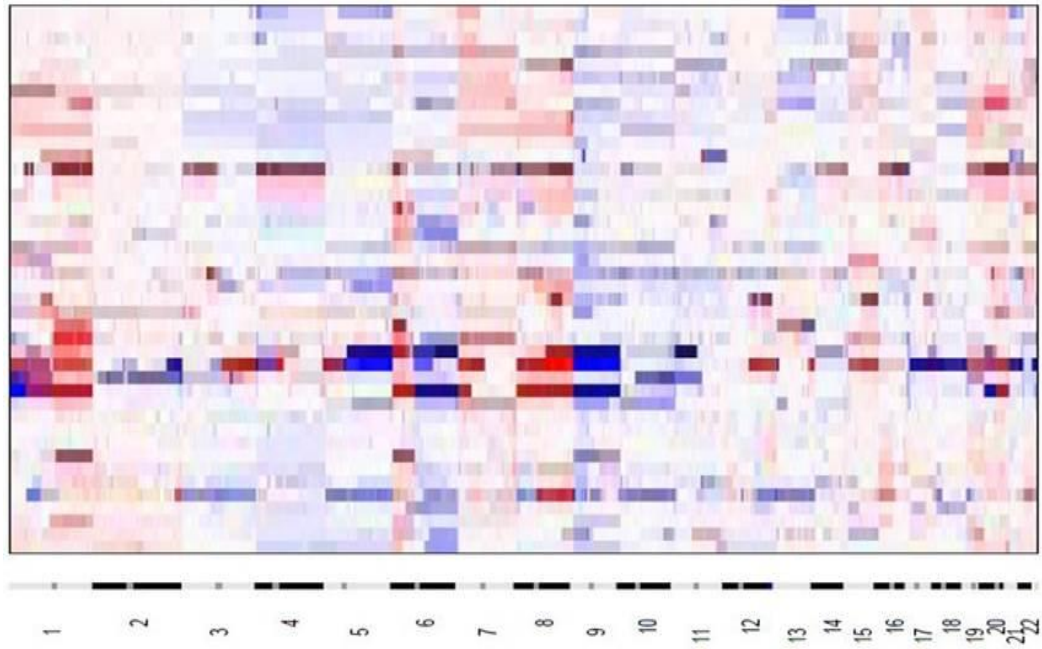


**Figure 14: Row-segmented copy number data obtained from the SNP6.0 microarray analysis of 42 melanoma samples inferred from log2 ratios by *CopyNumberInferencePipeline*. Chromosome positions indicated along the x axis. Samples are arranged horizontally from top to bottom. Red: regions of gain; blue: regions of loss.**

However, an effective way to discover key genes (drivers) that play casual roles in cancer development and progression is to study a large number of tumor samples and detect genomic regions that undergo frequent alterations across the samples. This is based on the fact that genomic regions that contain driver genes should be affected more frequently than regions contain passenger genes [37, 78-80] (Figure 15).

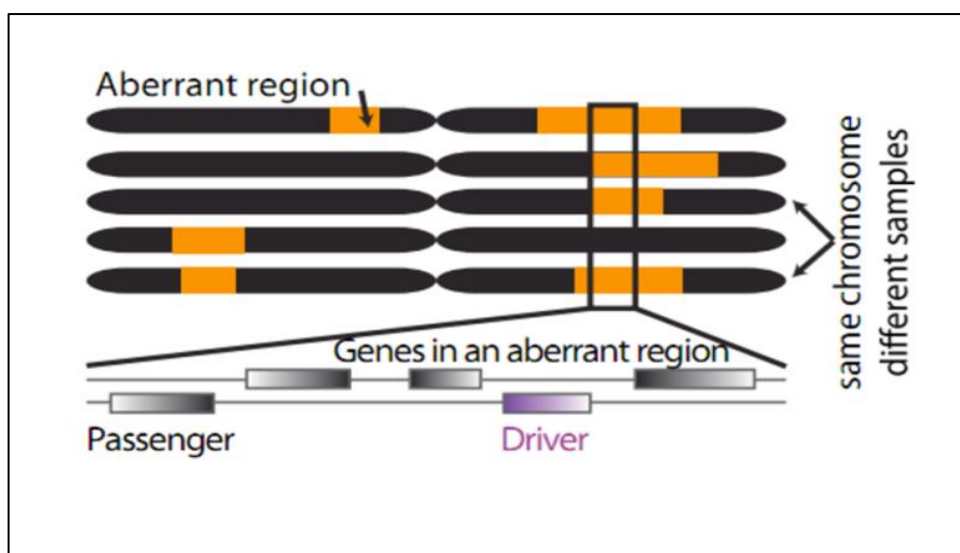


**Figure 15: A driver mutation should occur in multiple tumors more often than would be expected by chance.**

Therefore, we applied a rigorous statistical method called Genomic Identification of Significant Targets In Cancer (GISTIC) to the row copy number data obtained from our microarray analysis of 42 melanoma samples. GISTIC detects regions of aberration that are more likely to promote tumorigenesis. It does so by identifying genomic regions that are altered more often than would be expected by chance, with priority to high amplitude aberrations (for example, high level copy number amplifications or homozygous deletions) [35, 36].

GISTIC analysis of 42 melanoma samples revealed statistically significant large regions and focal peaks of chromosome gain and loss. 8 regions of significant copy number gain and 32 regions of significant copy number loss. Broad regions of amplifications were shown on 1q, 6p, and 8q; focal amplification peaks were identified on 7p12.3, 7p14.3, 10q11.21, 11q14.1, and 21.q22.1 (Figure 16).

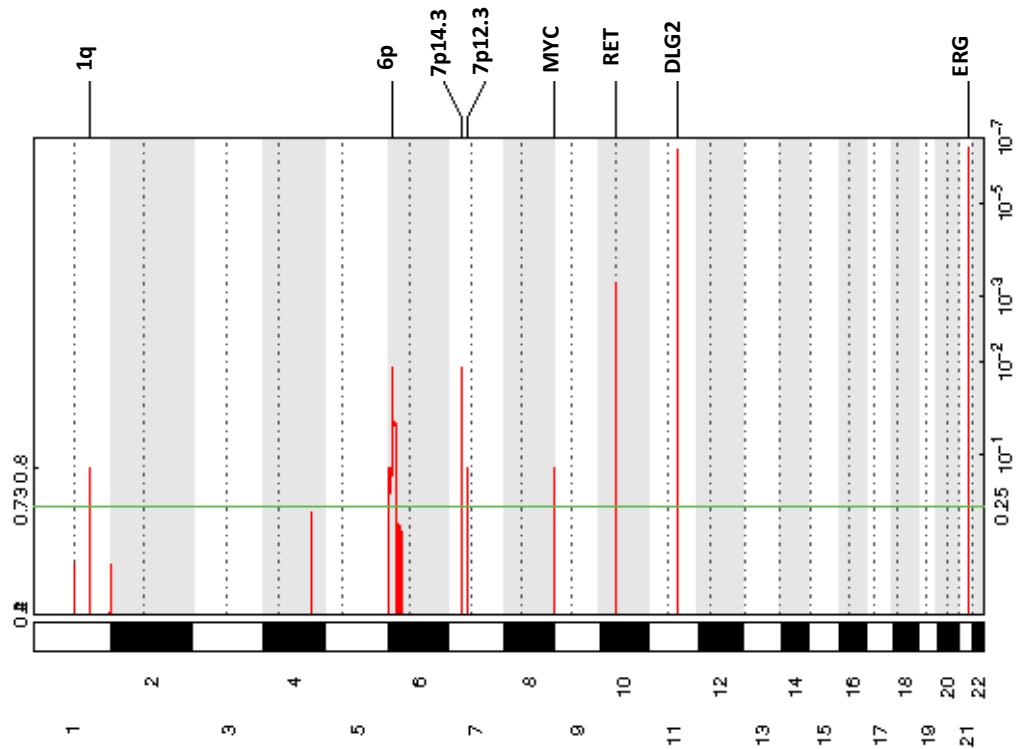


**Figure 16: Statistically significant genomic amplifications identified by GISTIC analysis.** Chromosome positions are indicated along the x axis with centromere positions indicated by dotted lines. The statistical significance of the aberration are displayed as false-discover rate q-values on the right y axis (significant for values  $<0.25$ , represented as a horizontal green line). G-score at the left y axis weights to the amplitude of aberrations and the frequency of it is occurrence across samples (see material and methods). Interesting or known genes are indicated at the top of the peaks.

Description of the regions of amplifications identified by GISTIC is in (Table 4). The importance of each peak in cancer pathogenesis and how they are correlated with previous findings in melanoma are discussed below.



**Table 4: Description of the statistically significant amplified regions Identified by GISTIC.**

Rank	Genomic Location	Peak Region	GISTIC q-value	Gene count	Known in Cancer	Known in Melanoma
1	21q22.1	chr21:39861045-39866904	2.22E-7	1	ERG	-
2	11q14.1	chr11:83358080-83366882	2.56E-7	1	DLG2	-
3	10q11.21	chr10:43622934-43623811	5.92E-4	1	RET	-
4	6p24.3	chr6:1-22748031	1.17E-2	118	NEDD9, DEK, E2F3	6p, NEDD9, RREB1, DEK
5	7p14.3	chr7:34477091-34483332	1.17E-2	1	-	7p
6	1q31.2	chr1:114755790-249250621	1.30E-1	1206	AKT3,MDM4, ABL2	1q
7	8q24.23	chr8:99387730-146364022	1.30E-1	284	MYC	MYC
8	7p12.3	chr7:46879412-46880294	1.30E-1	1	7p12	7p

- Identified peaks are listed in the table based on their significant q-value.

**Discussions regarding the importance of each peak in cancer and how they are correlated with previous findings in melanoma:-**

**21q22.1:**

This region has not been shown to be amplified in melanoma before. Only one gene was reported in this region , which is ERG. ERG "Avian v-ets erythroblastosis virus E26 oncogen" is a proto-oncogene that belongs to the ETS transcription factor gene family that plays a role in embryonic development, cell proliferation, angiogenesis, and apoptosis [81, 82]. Overexpression of ERG has been found in different cancers including Ewing sarcoma, acute myeloid leukemia, and meningiomas [81]. Moreover, the oncogenic role of ERG is prominent in the TMPRSS2-ERG fusion gene in prostate cancer[83-87]. These recent findings have declared the role of this gene in cancer. In this study, a high focal amplification targeting the ERG gene on chromosome 21 was identified. This focal amplification strongly suggests that ERG could be an important driver gene in melanoma.

### **11q14.1:**

This region has just one gene, which is DLG2. DLG2 "discs, large homolog2" is a member of membrane-associated guanylate kinases family that has important roles in tissue developments, cell-cell communications, cell polarity control, and cellular signal transductions [88]. A study found DLG2 was upregulated in renal oncocytoma, a benign tumor of the kidney, which explains its potential role as an oncogene[89]. Interestingly, this chromosomal location "11q14.1" is located close to 11q13"CCND1", an amplified region in melanoma that is used as a FISH target to distinguish between melanoma and benign nevi[7].

### **10q11.21:**

This peak represent a focal amplification of this region that spanned the RET gene. RET "Rearranged during transfection" is a proto-oncogene that encodes a transmembrane receptor tyrosine kinase [90-92]. RET has been shown to have an important role in human cancers [91, 92], and its amplification and overexpression have been reported in different types of cancers such as thyroid cancer [93], lung cancer [94], breast cancer [90], and pancreatic cancer [95]. Furthermore, RET has been shown to be involved in activation of several important signaling pathways including PI3K, Ras/MAPK, Jun N-terminal kinase "JNK" and PLC-dependent pathways [92, 96].

In melanoma, a study on human melanoma cell lines has showed a correlation between the expression of RET and melanomagenesis. Also, the study showed that inhibition of RET signaling suppressed all proliferation and invasion in melanoma [96]. Another study reported the involvement of RET in melanoma development in RET-mice and human melanoma cells [97]. These two studies besides the focal region

of amplification centered on the RET gene in our study indicate the potential importance of RET in melanoma. Therefore, our study suggest that RET could be one of the driver genes in melanoma tumorigenesis.

### **6p24.3:**

Gain of 6p is a common chromosomal imbalance in several human cancers, which indicate the importance of genes involved in this region in cancer pathogenesis [98]. In melanoma, gain of 6p is one of the most common chromosomal abnormalities that was reported in several studies [5, 6, 24, 25, 34, 98, 99]. Identifying important genes in this large gain still a challenge. In melanoma, the minimal region of 6p gain has not been characterized [99]. In our study, this peak "6p24.3" represents a partial gain of 6p (22.74 Mb). Interestingly, several important genes in melanoma were identified in this peak. NEDD9, one of the main melanoma metastasis genes [34], RREB1, one of the FISH assay targets that is used to distinguish between melanoma and benign nevi[7], and DEK, an oncogene that was reported to have a dual and selective roles in proliferation and apoptotic resistance in melanoma [99]. Another important gene in this region is E2F3 gene, an oncogene that has an important role in tumorigenesis in bladder cancer [100]. Therefore, against the large background of 6p gain that is common in melanoma, the partial gain of this part of chromosome 6p in our analysis (with known genes in melanoma located in this part) minimizes the broad gain of 6p to a smaller region that is highly associated with melanoma.

### **1q31.2:**

This peak represents gain of the entire long arm of chromosome 1 (1q). Gain of the long arm of chromosome 1 represents a common genetic alteration in melanoma [5, 6, 24, 25, 98]. A CGH study has shown that Patients with 1q and 6p gain had a lower

overall survival rate in comparison with patients without these gains, which implies that 1q and 6p gains could give a prognostic differences [101]. Several important genes in cancer, and more specifically in melanoma, are located on this genomic region. This includes AKT3 [66, 67], MDM4 [102], and ABL2 [103]. Our study confirms that gain in chromosome 1q as one of the most genetic alterations in melanoma.

### **8q24.23:**

Gain of 8q is another hallmark in melanoma that was reported in many different studies [4, 6, 24, 25, 104]. In our findings, the peak on chromosome 8 represent high amplification of a part of the long arm of chromosome 8, which is 8q24. A study has suggested that targeting this region "8q24" by FISH assays could be a useful prognostic marker in melanoma cancers[105]. Later, a recent study that sought to improve the sensitivity and specificity of FISH assay for discriminating melanoma from nevi has confirmed and included the 8q24 region as one of four FISH targets with high discriminatory power to differentiate between melanoma and benign nevi[7]. The most prominent gene in this region is MYC, a proto-oncogene that encodes a nuclear phosphoprotein transcription factor that plays a role in different cellular processes, such as proliferation, cell cycle progression, metabolism, differentiation and apoptosis[106]. MYC amplification has been shown in different cancers including prostate [107]and breast cancer [108]. In melanoma, it has been shown that melanomas with gain of 8q24 have elevated cytoplasmic and membranous expression of MYC in comparison with melanomas without gain of 8q24, where they had significantly decreased MYC expression. This elevated expression of MYC seems to play a role in the aggressive clinical behavior of melanomas [65]. This is another common genetic alteration in melanoma that is confirmed in our study.

### **7p12.3 & 7p14.3:**

Gain of the p arm of chromosome 7 is one of the most common copy number gains in melanoma [6, 24, 25, 109]. On the other hand, the q arm in melanoma is known with the activating point mutation of the BRAF oncogene [110]. Although the gain of 7p is common in melanoma, targets in this arm still undescribed [109]. Here, two focal amplifications were identified in our study, 7p12.3 and 7p14.3 regions. For the 7p12.3 region, GISTIC has reported this region with no known genes, but only one gene (TNS3) was denoted in brackets, which indicates that it is the nearest known gene to that region. Despite what gene was found here, this chromosomal region has got the attention in cancer studies. Amplification of this region has been reported in different types of cancers including amplification of 7p12.3 in pancreatic cancer[111] and rectal cancer [112]. Also amplifications in the 7p12 band has been shown in acute lymphoblastic leukemia [113] and osteosarcomas [114]. The attention to this region is mainly because that the oncogene EGFR "Epidermal growth factor receptor" is located in this band [115]. EGFR is known to play a role in metastasis, cellular proliferation, invasion, and in cancer progression in general [116]. Gain of 7p12 band has been associated with gain of EGFR gene as in the squamous cell carcinoma of the lung [117] and gastric cancer [118]. In melanoma, a study that used two different cytogenetic approaches "FISH and aCGH" has found a frequent amplification of the region "7p12.3" among melanoma samples[68]. Other studies that focused on the expression level of EGFR on 7p12.3 in melanoma have shown a correlation between high expression of EGFR and gain in copy number of this region, which might explain the role of this amplification in development of malignant melanomas [119, 120].

The other region, 7p14.3, was reported with amplification of just one gene, AAA1(NPSR1-AS1). However, these findings do not exclude the possibility that other genes located at 7p14 can be influenced by this gain of this region. An example, the gene NPSR1, a G protein coupled receptor, which is located on 7p14.3. Overexpression of this gene has been reported to activate cancer-related pathways [121].

The importance of our results lies in showing a focal amplification of 7p12-p14 region in chromosome 7p as a statically significant copy number gain, instead of showing a broad copy number change that encompasses the entire arm, which implies the importance of this region on chromosome 7p in melanoma.

Regarding the statistically significant deletions that were found by GISTIC, large regions of deletions were identified on 2q33, all of 9, 13q34, 15q26, 16p13, and 22q13; focal deletion peaks were identified on 1q21.3, 1p32.3, 2p21, 3q13.31, 3p22.1, 4p16.3, 5q35.1, 5q35.3, 5p15.33, 6q14.1, 6q26, 6p22.1, 8p23.2, 9p21.3, 10q23.2, 10p15.3, 11q13.1, 11p15.4, 12q21.31, 13q13.3, 15q26.1, 16q23.3, 17q11.2, 18p11.31 and 20q11.21 (Figure 17).

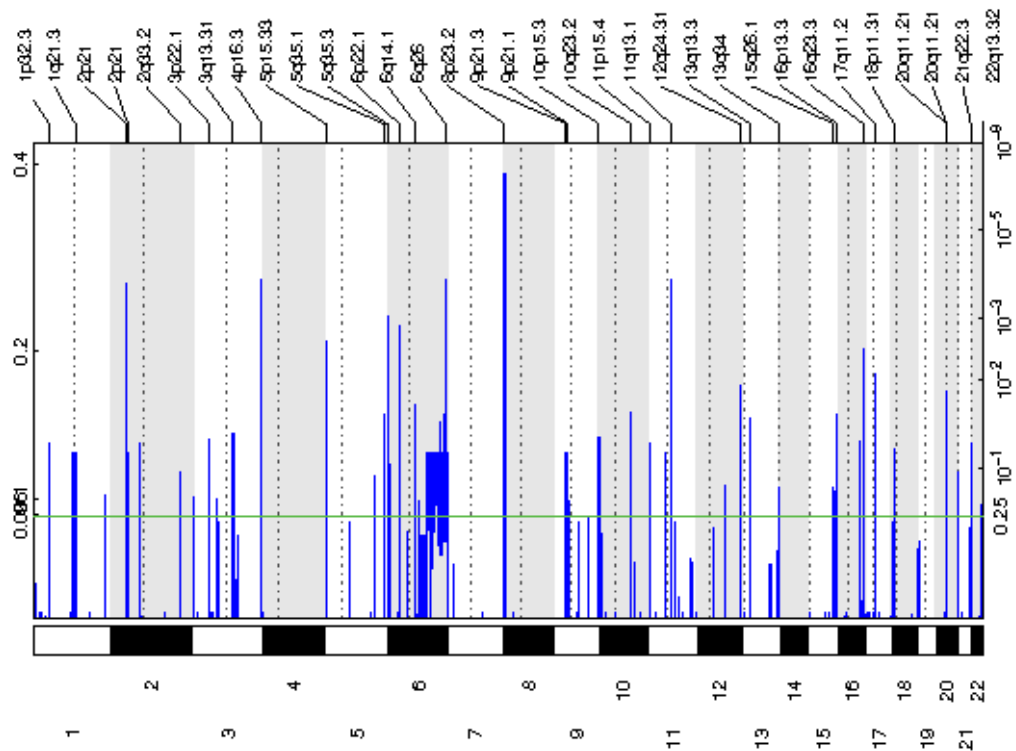


**Figure 17: Statistically significant genomic deletions identified by GISTIC analysis. Chromosome positions are indicated along the x axis with centromere positions indicated by dotted lines. The statistical significance of the aberration are displayed as false-discover rate q-values on the right y axis (significant for values  $<0.25$ , represented as a horizontal green line). G-score at the left y axis weight to the amplitude of aberrations and the frequency of it is occurrence across samples (see material and methods).**

Description of the regions of deletions identified by GISTIC is in (Table 5). The importance of each peak in cancer pathogenesis and how they are correlated with previous findings in melanoma are discussed below.

**Table 5: Description of the statistically significant deleted regions Identified by GISTIC.**

Rank	Genomic Location	Peak Region	GISTIC q-value	Gene count	Known in Cancer	Known in Melanoma
1	8p23.2	chr8:1986591-6269441	1.5489E-7	3	CSMD1	8p
2	4p16.3	chr4:1-1110173	1.74E-04	23	FGFRL1	-
3	6q26	chr6:161767520-163770210	1.74E-04	4	PARK2, PACRG	6q
4	11q13.1	chr11:63680046-63774300	1.74E-04	3	OTUB1	11q
5	2p21	chr2:42180913-42397164	2.03E-04	1	EML4	-
6	5q35.3	chr5:179219193-179388308	1.04E-03	6	SQSTM1	5q
7	6p22.1	chr6:29427138-29498496	1.36E-03	1	6p22.1	-
8	5p15.33	chr5:1-1054830	2.56E-03	18	SDHA, AHRR, NKD2	-
9	16q23.3	chr16:82658729-83542835	3.40E-03	3	CDH13	16q
10	17q11.2	chr17:29704122-29872630	7.98E-03	2	NF1	NF1
11	12q24.31	chr12:124452696-125266431	1.18E-02	4	NCOR2 (SMRT)	12q24
12	20q11.21	chr20:31830310-31946860	1.43E-02	1	BPIFB1 (LPLUNC1)	-
13	6q14.1	chr6:80412926-80513550	2.10E-02	1	SH3BGR12	6q
14	10q23.2	chr10:88278583-88520408	2.67E-02	2	WAPAL	10q
15	5q35.1	chr5:169759991-169932228	2.77E-02	1	-	5q
16	16p13.3	chr16:1-752680	2.80E-02	40	AXIN1, ARHGDIG	16p
17	13q13.3	chr13:36341439-36742905	3.05E-02	1	DCLK1	13q12-34
18	3q13.31	chr3:114054708-114463757	4.46E-02	3	ZBTB20	-
19	10p15.3	chr10:1208827-1601334	5.09E-02	2	ADARB2	-
20	3p22.1	chr3:42451413-42590432	5.27E-02	1	VIPR1	-
21	1p32.3	chr1:54870183-55085182	5.81E-02	1	ACOT11	-
22	11p15.4	chr11:3076258-3249828	5.81E-02	3	11p15.5	11p
23	21q22.3	chr21:45878481-48129895	5.81E-02	50	21q22.3	21q22.3
24	18p11.31	chr18:6929284-7231471	6.72E-02	1	LAMA1	-
25	1q21.3	chr1:154596123-154898074	7.09E-02	1	KCNN3	-
26	2p21	chr2:44460525-44590065	7.09E-02	3	PPM1B	-
27	9p21.3	chr9:20651454-25679201	7.09E-02	34	CDKN2A, CDKN2B	CDKN2A, CDKN2B
28	22q13.32	chr22:41481652-51304566	7.09E-02	154	BIK, PRR5, PANX5	-
29	2q33.2	chr2:200814810-206486163	1.10E-01	45	RAPH1, CASP8, ABI2	-
30	13q34	chr13:109280035-115169878	1.47E-01	42	ING1, COL4A1, COL4A2	-
31	15q26.1	chr15:91642272-93012556	1.51E-01	3	SLCO3A1	-
32	Chr.9	chr9:1-141213431	1.91E-01	953	Chr.9	Chr.9

- Identified peaks are listed in the table based on their significant q-value.



**Discussions regarding the importance of each peak in cancer and how they are correlated with previous findings in melanoma:-**

**8p23.2:**

This region was reported by GISTIC with the lowest q value among all other deletions. Loss or decrease in copy number in chromosome 8p has been observed in melanoma[4, 24, 25] and other cancers such as prostate cancer[122] and breast cancer[123]. Despite the frequent deletion of this chromosomal arm in melanoma, the molecular drivers of the 8p loss remain uncharacterized. Here, our study shows a minimal region of deletion within chromosome 8p. This focal deletion of 8p23.2 harbors the tumor suppressor gene CSMD1. Deletion of this minimal region with the tumor suppressor gene CSMD1 has been reported in many different cancers, including colorectal cancer [124], liver cancer [125], ovary cancer [126], and more common in the head and neck squamous cell carcinoma (HNSCC) and correlates with poor prognosis [127, 128]. In melanoma, a recent study of Tang et al " the only study that have shown the effect of CSMD1 on melanoma cell, as they claimed" has reported that CSMD1 functions as a tumor suppressor gene in melanoma cells. They found that the level of CSMD1 mRNA and protein in melanoma cells was lower than in normal skin cancer. Also, they showed that CSMD1 expression decreased proliferation and migration, and increased apoptosis and G1 arrest in A375 melanoma cells in vitro. Furthermore, the survival rate of mice with tumors expression CSMD1 was significantly higher than mice with tumors that did not express CSMD1. Moreover, the study showed that CSMD1 exhibits antitumor activity through activation of Smad pathway[129]. That study and our study provide CSMD1 as a candidate biomarker gene in melanoma.

#### **4p16.3:**

Deletion of the short arm of chromosome 4 is common in several cancers including breast cancer [130], colon cancer [131], gastric cancer [132], and lung cancer[133]. However, deletion of this chromosomal arm does not seem to be noticed in melanoma. Yet, loss of the chromosome 4 has been reported in melanoma before [4]. In this study, a novel minimal deletion of the 4p16.3 telomeric region was identified. This region spanning 1.05 Mb included 26 genes, 6 of which are zinc finger genes. An interesting gene that is also mapped to this region is the atypical fibroblast growth factor receptor (FGFRL1). Deletion or LOH of the FGFRL1 has been investigated intensively in bladder cancer, where a recent study [134] has investigated the role of FGFRL1 as a candidate tumor suppressor in cancer. The reasons that were proposed to consider FGFRL1 as a candidate tumor suppressor were that FGFRL1 acts as a decoy receptor preventing activation of conventional FGFRs due to its lack of the intracellular tyrosine-kinase domain, also it interacts with the negative regulator of the MAPK signaling pathway SPRED1, and it is ability to promote cell adhesion by promoting cell adhesion and could therefore prevent tumor development and spreading by enhancing cell-cell adhesion and inhibiting invasion and metastasis [134]. Moreover, FGFRL1 has been shown to be down regulated in ovarian tumor [135] "and to reduce cell proliferation in response to FGF2 when ectopically expressed in the osteosarcoma cell line, MG-63" [134].

#### **6q26:**

Loss of the long arm of chromosome 6 is well-known genetic alteration in melanoma[4-6, 24, 25]. Yet, few drivers have been pinpointed in this region of loss. One of the melanoma biomarkers in this chromosomal arm is MYB (6q23) that is

used in FISH assays[7]. Here, rather than detecting the broad loss of the chromosome 6q that is known in melanoma, a high significant of deletion in a narrow region was detected (in fact, the broad deletion of 6q was reported in the GISTIC figure 16, but another higher and smaller peak emerged from that broad deletion, which is 6q26, indicating that this small deletion is the most significant minimal deletion in 6q) This region 6q26 contains the tumor suppressor gene PARK2. Inactivation of PARK2 due to copy number loss has been identified in various human cancers including esophageal adenocarcinoma, glioma, non-small cell lung cancer, lung adenocarcinoma, ovarian cancer, pancreatic adenocarcinoma, and in skin cutaneous melanoma (3.5%) (reviewed in [136]). The copy number loss is the primary mode of alteration that inactivate PARK2 [137]. This gene was studied as an important tumor suppressor gene for several reasons; First, its frequent deletion in many cancer, as it was mentioned above. Second, it is involvement in many crucial cellular process and pathways, such as controlling the cell cycle progression. A study on a large group of tumors has reported the PARK2 as master regulator of G1/S cyclins, where it mediates the coordination of different classes of cyclins and therefore regulating the cell cycle. The study showed that PARK2 targets cyclin D and cyclin E for degradation, therefore inactivation of PARK2 results in the accumulation of cyclin D and acceleration of cell cycle progression[137](similar function to CDKN2A). Moreover, the mRNA and the protein expression of PARK2 have been shown to be downregulated in many different cancers, and the low mRNA expression correlates with increased lymph node metastasis, higher tumor grade, and worse overall survival in ccRCC [136].

The other gene that was reported in this narrow deletion is PACRG, which is located 670 bp upstream of PARK2 and transcribed from the opposite DNA strand. PACRG

has been shown to be downregulated in leukemias, glioblastoma, and astrocytic tumors [138]. A study on ccRCC has reported that the mRNA and protein expression of PACRG and PARK2 together was significantly downregulated compared with the nonmalignant tissue [138].

So, this focal deletion in our study, different than the large deletion of chromosome 6q that is frequently detected in melanoma, seems to be important in cancer development.

### **11q13.1:**

Deletion of chromosome 11q is commonly known in melanoma [4, 22, 24, 139] and other types of cancers such as breast cancer [140], lung cancer [141], and neuroblastoma [142]. Different studies and biological evidences support the existence of melanoma tumor suppressor genes on chromosome 11q, and deletion of this chromosome in melanoma has been reported to be associated with advanced tumor stage, younger age at presentation, poorer prognosis, and metastasis to the brain [139]. In our study, a focal deletion of ~94 kb region was defined in this chromosomal arm. This narrow region contains the ovarian tumour domain-containing Ub aldehyde-binding protein 1 (OTUB1). OTUB1 is expected to play broad functions in cells [143]. However, a recent study has shown that Otub1 is positive regulator of the tumor suppressor p53 [144]. The study showed that Otub1 plays a critical role in p53 stabilization and activation in cells in response to DNA damage, and that through suppression the MDM2-mediated p53 ubiquitination. Further, overexpression of Otub1 results in marked apoptosis and inhibition of cell proliferation in a p53-dependent manner. Also, Inhibition of Otub1 markedly impaired p53 activation

induced by DNA damage [144]. Therefore, a recent review article concluded that Otub1 may act as a tumor suppressor, and more studies are needed to determine if Otub1 is downregulated in human cancers[143].

### **2p21:**

This deletion centered on the gene PKDCC, which has a developmental role [145] but no suspected significance in cancer. It also overlaps a portion of a long noncoding RNA LOC102723824, which has not been characterized. Interestingly, this region includes the first exon of EML4. Multiple fusion products of EML4 and ALK have been characterized in non-small cell lung cancer[146-149].

### **5q35.3:**

Although several genes fall within this region, few may be of interest in cancer. SQSTM1 is an activator of NF- $\kappa$ B [150], which plays a complex role in cancer etiology. It is thought that early inhibition of NF- $\kappa$ B may help cancer cells evade the immune system, although late inhibition is known to promote cancer cell survival [151, 152].

Deletions on chromosome 5 do not seem to be a common genetic alteration in melanoma. One study has observed deletion of chromosome 5q in melanoma, but indicated that deletion of this chromosome has not been associated with harboring any putative TSGs in melanoma [32]. However, loss of this region (5q35.3) has been reported in a number of tumors such as non-small cell lung carcinoma [153], and breast tumors [154], which implies the potential importance of genes within these region in cancer development.

### **6p22.1:**

Deletion of chromosome 6p has been reported in various types of tumors [155]. Yet, this is not true in melanoma, where amplification of this Chromosomal arm is well-known, as mentioned above. However, here, a very narrow focal deletion was reported, spanning only one gene, MAS1L. This deletion does not overlap with the amplified region that was reported here (6p24.3). Interestingly, homozygous deletion at 6p22.1 has been shown in different cancers such as gliomas [155] and high frequent LOH of this region was reported in cervical cancer [156]. Although MAS1L does not seem to have a known role in tumorigenesis, frequent deletion of this region in different cancers suggest a potential importance for genes in this region.

### **5p15.33:**

As was mentioned above, deletions on chromosome 5 in melanoma is not common. However, here, a very interesting minimal region of deletion was identified on the chromosome 5p. Since deletion or LOH of 5p15 is common in different cancers [157], several studies aimed to identify the minimal deletion of this region. A study on sporadic gastric carcinomas found high frequent LOH at 5p15.33, and an obvious genotype-phenotype correlation on 5p15.33 was observed [158]. Moreover, other studies on cervical carcinoma and sporadic colorectal cancer have reported ( through detailed deletion mapping on 5p) 5p15.3 as the minimal deletion on 5p [159, 160]. Further, 5p15.3 has been proposed to contain one or more tumor suppressor genes [157]. In our study, this narrow region (1.05Mb) was reported harboring 18 genes, 3 of which are important putative tumor suppressor genes AHRR, SDHA, and NKD2.

ARHH: a study has reported AHRR as a tumor suppressor gene in multiple human cancers. This study found a consistent downregulation of AHRR mRNA in human malignant tissue from different origins including colon, breast, lung, stomach, cervix and ovary. Moreover, they found that silencing of ARHH enhances tumor growth in vitro and in vivo through deregulation in cell cycle control and protects against apoptosis and enhances angiogenic potential, migration and invasion in tumor cells. Furthermore, ectopic expression of AHRR resulted in growth inhibition and reduced angiogenic potential. The study concluded that AHRR plays an important role in suppressing tumor formation in humans[157].

SDHA: a study on paraganglioma (known with RET mutation) has reported SDHA as a tumor suppressor gene. SDHA is not well studied, but the study, through immunohistochemistry and transcriptome analysis, indicated that SDHA acts as a tumor suppressor gene through activation of pseudo-hypoxic pathway[161].

NKD2: in a very recent study on osteosarcoma (OS), NKD2 was shown to be a negative regulator of WNT signaling pathway. The study showed that decreased expression of NKD2 is associated with highly aggressive OS state. Also, overexpression of NKD2 in metastatic human and mouse OS cells significantly decreases cell proliferation, migration, and invasion ability in vitro and significantly diminishes OS tumor growth and metastasis in vivo. Therefore, the study showed NKD2 as a novel suppressor of OS tumor growth and metastasis in both mouse and human [162].

### **16q23.3:**

Loss of chromosome 16q, and particularly 16q23 has been reported in different cancers [163-165]. In melanoma, different studies have shown loss of chromosome 16q [6, 166]. Moreover, a CGH study on primary and metastatic melanoma has reported the loss of this minimal deletion of 16q23, but no gene was specified in this region [167]. In our study, chromosome 16q was reported with a focal deletion centered at the 16q23.3 band. This narrow region harbors the putative tumor suppressor gene CDH13, and two non-coding genes has-mir-3180 and MIR 3182. The involvement of CDH13 in various cancers was reviewed recently by Andreeva and Kutuzov [168]. Downregulation of CDH13 has been reported in broad range of cancers, including melanoma cell lines, and undetection of CDH13 transcript in all examined breast cancer and most other cancer cell lines supports its role as a tumor suppressor. Further, the review discussed association between downregulation of CDH13 and poor prognosis in various carcinoma. CDH13 re-expression in most cancer cell lines inhibits cell proliferation and invasiveness, increase susceptibility to apoptosis, and reduce tumor growth in vivo models. Reporting this minimal deletion containing CDH13 as the most significant loss in chromosome 16q across the melanoma samples in our analysis might imply the importance of this gene in melanoma tumorigenesis.

### **17q11.2:**

This is a well-known frequent region of deletion in different cancers, and that because it harbors the well-known tumor suppressor gene NF1 (the RAS inhibitor) [169]. NF1 is the gene that encodes RAS GTPase-activating protein, so affecting this gene by deletion or mutation affects RAS-MAPK signaling pathway [170]. NF1 has been



reported to work as a tumor suppressor in melanoma [171]. Loss of NF1 function in melanoma has been shown in several studies [170, 172]. These findings confirm the frequent inactivation of the NF1 tumor suppressor in melanoma.

#### **12q24.31:**

This is focal deletion was reported on chromosome 12q, which has been found to be amplified in melanoma [22]. Yet, this particular region of deletion (12q24) has also been reported in melanoma [167, 173], which indicated the tendency of this region to be lost in melanoma cells. In our results, this minimal deletion was reported containing NCOR2 gene. Interestingly, NCOR2 (which known as SMRT) is a tumor suppressor that has been reported in different cancers. SMRT was shown to be involved as a novel tumor suppressor in non-Hodgkin lymphomas [174]. Also, down-regulation of SMRT in multiple myeloma has been shown to jeopardize several gene functions that play an important role in apoptosis, therefore, restoration of SMRT activity might correct the overexpression of antiapoptotic genes [175]. Lastly, a recent study has reported that SMRT is an activator of p53 transcription [176].

#### **20q11.21:**

Here, a very short region of deletion in the chromosome 20q was reported. This short deletion contains just one gene called BPIFB1, Known also as LPLUNC1. Recent study has reported this gene to act as an important tumor suppressor gene in NPC (Nasopharyngeal Carcinoma) [177]. The study reported that "LPLUNC1 inhibited NPC cell proliferation in vitro and tumor formation in vivo. LPLUNC1 also delayed cell cycle progression from G1 to S phase and inhibited the expression of cyclin D1, cyclin-dependent kinase 4 (CDK4) and phosphorylated Rb. LPLUNC1 inhibited the expression of certain mitogen-activated protein (MAP) kinases (MAPK) kinases and

cell cycle-related molecules. Western blotting confirmed that the expression of MEK1, phosphorylated ERK1/2, phosphorylated JNK1/2, c-Myc and c-Jun were inhibited by LPLUNC1, suggesting that the MAPK signaling pathway is regulated by LPLUNC1 [177]. Another 2014 study reported that LPLUNC1 inhibit NPC cell proliferation through inactivation Stat3 "Induction of LPLUNC1 overexpression inhibited NPC cell proliferation, induced NPC cell arrest, promoted NPC cell apoptosis even after IL-6 stimulation and inhibited the growth of implanted NPC tumors in vivo, which were associated with decreasing cyclin D1 and Bcl-2 expression and the Janus kinase 2 (JAK2)/Stat3 activation, but enhancing Bax and p21 expression"[178].

#### **6q14.1:**

The gene SH3BGRL2 is an paralog to SH3BGRL. While the latter has been shown to contribute to Rel-mediated transformation when inactivated [179], so such role has yet been identified in the former.

#### **10q23.2:**

10q is known deletion in melanoma [4]. Loss of 10q23 is common in melanoma and loss of this region (more specifically 10q23.3) has been associated with inactivation of the tumor suppressor gene PTEN in melanoma [4, 180, 181]. The PTEN gene was not among genes reported in this peak. Yet, deletion of this region in our analysis emphasizes the tendency of this region to be deleted in melanoma.

This region also contains the last exon of WAPAL, a gene which is a component of the cohesin complex. Loss of WAPAL function potentially prevents the release of cohesin from sister chromatids [182] or interferes with DNA repair [183].

### **5q35.1:**

Only one gene was reported at this focal deletion, which is the potassium channel subfamily M regulatory beta subunit 1, KCNMB1. There is no known importance of this gene in oncogenesis. However, this region has been reported to be frequently deleted in lung cancer, indicating the presence of important genes with tumor suppression function at this region[153, 184, 185].

### **16p13.3:**

Deletion of 16p has been reported in melanoma [25, 186]. Here, a small (~752 Kb) telomeric deletion that contains 40 genes (some of them are non-protein coding genes). Here, at least two known tumor suppressors can be identified: AXIN1 and ARHGDI1.

AXIN1: is a WNT pathway tumor suppressor that is essential for beta catenin degradation, and its inactivation has been reported in various tumors[187, 188]. Furthermore, AXIN has been shown to act as a tumor suppressor through stimulating the p53 function [189].

ARHGDI1: is a metastasis suppressor that has been shown to contribute to cancer cell invasion and metastasis, and also has been shown to be involved in mouse melanoma B16 cells [190].

### **13q13.3:**

Deletion of this particular region 13q13.3 has been reported in different cancers such as breast cancer [191, 192], and lung cancer [193]. Here, this region was reported with one gene DCLK1. Some studies have reported deletion of this region with this gene

such as in testicular primary seminoma [194], and in pleomorphic sarcoma of bone [195]. A study on melanoma has reported a large deletion of 13q12-34 [166].

### **3q13.31:**

ZBTB20 is involved in NF- $\kappa$ B signaling and promotes the innate immune response [196] (cf. SQSTM1 also deleted). It is also a negative regulator of Sox9 [197]. Sox9 has been shown to induce cell cycle arrest and apoptosis in melanoma via antagonism of Sox10 [198]. Therefore, deletion of Sox9 has the potential to promote melanoma initiation and progression.

### **10p15.3:**

Loss of 10p15.3 is a common deleted region in different cancers including colorectal cancers [199] and lung cancer [184]. In melanoma, loss of 10p is common genetic alteration (with loss of 10q as well as loss of the whole chromosome) [4, 32, 200]. Microarrays studies on melanoma have reported deletion of 10p15.3 [32, 181]. In our study, this region of deletion was reported with the the RNA editing enzyme gene ADARB2. ADARB2 RNA level has been reported to be 99% decreased in brain tumors and ADARB2 reduction correlates with grade of malignancy of glioblastoma multiforme, the most aggressive form of brain tumors [201, 202].

### **3p22.1:**

This is a very narrow deletion centered at the gene VIPR1. This region of deletion is common in non- small cell lung cancer [203]. VIPR1 has been reported to be a tumor suppressor in lung adenocarcinoma, where it is significantly downregulated, and deletion of 3p22 is the mechanism that leads to it is downregulation [204].

### **1p32.3:**

This deletion encompasses the entire gene ACOT11, a lipid transfer protein. ACOT11 has been shown to be significantly methylated in bladder cancer, and the degree of methylation was associated with tumor stage [205, 206]. Any specific biological function of ACOT11 in cancer remains to be determined.

### **11p15.4:**

This region is adjacent to a domain on 11p15.5 known to play a role in Wilms and rhabdomyosarcoma [207], adrenocortical carcinoma[208], and lung[209], ovarian[210] and breast cancers [211]. Interestingly, 11p has been reported with reduced copy number in melanoma[24].

### **21q22.3:**

Loss of 21q22.3 has been shown to be associated with melanoma [212]. Within this large deletion, the transient receptor potential channel gene TRPM2 has been shown to increase the susceptibility of melanoma to apoptosis and necrosis [213]. An antisense transcript of TRPM2 is up-regulated in melanoma (ibid). Intriguingly, the related gene TRPM1 (melastatin, at 15q13.3) has been known to be downregulated in highly metastatic melanoma [214]. 21q22.3 deletion is also observed in prostate cancer [215].

### **18p11.31:**

Here, only one gene was reported, LAMA1. It is one of the genes that encode laminins, which are major proteins in the basal lamin. They influence cell differentiation, migration, and adhesion. Also they can play a role in invasive behavior of tumor cells [216]. LAMA1 has been reported to be hypermethylated and

underexpressed in pancreatic tumor samples compared to normal samples [217]. Moreover, downregulation of LAMA1 has been reported in ovarian cancer cell lines[216].

### **1q21.3:**

This deletion is almost exclusive to the gene KCNN3 (SK3). This potassium channel is better known for its role in neuron firing, but it has also been shown to play a role in the motility of breast cancer [218] and melanoma [219] cells. It was shown that KCNN3 was not expressed in normal melanocytes, but that induced expression of KCNN3 in melanoma cells increased migration. This work was done in cultured melanoma cell lines; the frequency of SK3 overexpression in melanoma is unknown *in situ*, but our data would suggest that SK3 overexpression could be an artifact of cell culture.

### **2p21:**

This deletion includes the last exon of PPM1B. PPM1B is thought to act as a phosphatase toward IKK $\beta$ , thereby attenuating the activity of NF-kB [220]. This locus as a whole is involved in 2p21 Deletion Syndrome (OMIM #606407), which is not known to contribute to an elevated prevalence of any cancers.

### **9p21.3:**

Although deletion of chromosome 9 was also reported in our result, a more focused (expected) deletion was also reported in chromosome 9 centered at 9p12.3. This region contains the well-known tumor suppressor gene CDKN2A, and other tumor suppressors such as CDKN2B, MTAP and ELAVL2. CDKN2A is the one of the highest-penetrance melanoma susceptibility gene [69, 70] and it is deletion or loss of

expression in melanoma is well-known [69, 70, 221, 222]. As it was mentioned above, other important genes are also located in this region. CDKN2B is one of the genes located at 9p21 and has been shown to be deleted in melanoma [6, 223] and other cancers such as cutaneous T-cell lymphoma [224]. Interestingly, codeletion of cluster of genes involving CDKN2A, CDKN2B, MTAP and in some cases ELAVL2 has been shown in different cancers. For instance, deletion of CDKN2A, CDKN2B, MTAP and ELAVL2 in myeloid leukemia [225] and CDKN2A, CDKN2B and MTAP in B- lineage acute lymphoblastic leukemia [226], head and neck squamous cell carcinoma [227], mesotheliomas [228] and in glioblastoma [229]. Deletion of this large 9p21 segment is a frequent genetic alteration in variety of cancers causing inactivation of critical tumor suppressor genes and therefore plays a very important role in development of many human cancers, including melanoma [230, 231]. Our result confirms the frequent involvement of 9p21 deletion in melanoma samples.

However, 9p21 is not a high discriminatory loci, where it is heterogeneous deletion can also be seen not just in melanoma but in melanocytic nevi as well. In contrast, homozygous deletion of 9p21 seems to be more associated in melanoma [49, 232]

### **22q13.32:**

This deletion encompasses over 150 annotated genes, and is frequently deleted in human breast and colon cancers [233]. Within this region are at least three genes with some demonstrated connection to cancer: BIK, PRR5, and PANX2. BIK is an important player in the activation of Bax to induce apoptosis, and has been found to be deleted in several human cancers [234]. Interestingly, overexpression of Bik induces apoptosis in melanoma cells, and BIK expression in a xenograft model delayed melanoma tumor growth [235]. PRR5 is suspected tumor suppressor gene in

breast cancer [233] and a component of mammalian target of rapamycin complex-2 (MTORC2) [233] although little is known about its function. PANX2 acts as a tumor suppressor in glioma cells [236]. The related pannexin family members PANX1 and PANX3 show reduced expression in basal and squamous cell carcinomas [237]; however, PANX1 may be a driver of melanoma [238]. Much remains to be understood about how these pore channel proteins play roles in tumorigenesis. 22q13.32 has also been found deleted in 25% of fibrolamellar hepatocellular carcinomas [239].

### **2q33.2:**

Two caspases falls into this region. CASP8 lies just downstream of death receptors in the cell-extrinsic apoptosis pathway. As such, it has been found to be mutated or lost in many cancers (reviewed in [240]). CASP10 mutation has been observed in gastric cancer [241], non-Hodgkin's lymphoma [242].

RAPH1, also found within this deletion, is also deleted in oral squamous cell carcinoma[243], head and neck squamous cell carcinoma [244], esophageal squamous cell carcinoma [245], lung cancer [246], and neuroblastoma [247]. Reduced expression is found in breast and ovarian [248].

ABI2 also found in this region. Many Studies have reported ABI2 as a tumor suppressor, where Abi2 promotes Abl-mediated phosphorylation of Cdc2 and inactivation of Cdc2 kinase activity, leading to suppression of cell growth [249, 250].

### **13q34:**

This deletion has been observed previously in several cancers, but not to our knowledge in melanoma. Notably, 13q34 is lost in 45% of cutaneous anaplastic large cell lymphoma [251], 67% of chronic lymphocytic leukemias [252], and 8% of Burkitt lymphomas [253]. It has also been noted missing in some cervical squamous



cell carcinomas [254-256], breast cancer cases showing centrosome abnormalities [257], one case of chronic lymphocytic leukemia [258], esophageal squamous cell carcinoma [259], bladder carcinoma [260], and cutaneous T-cell lymphomas [256]. Among the genes found in this region are ING1, COL4A1, and COL4A2. ING1 is downregulated or lost in several cancers [261, 262] ING1 (Inhibitor of growth 1) is a well-known tumor suppressor that is known to be involved in cell growth control, apoptosis, cell proliferation, senescence, and DNA replication and repair [262-264]. COL4A1 and COL4A2 are suspected tumor suppressor genes [260].

### **15q26.1:**

SLCO3A1, found here in its entirety, is another known regulator of NF- $\kappa$ B [265] (along with PPM1B, SQSTM1, and ZBTB20) deleted in our melanoma specimens. Overexpression of SLCO3A1 was shown to induce NF- $\kappa$ B transcriptional activity (ibid). It has also been suspected of serving to transport anticancer drugs out of the cell [266], but this has not been demonstrated to our knowledge. Deletion of SLCO3A1 has been observed in acute lymphoblastic leukemia [267].

### **Chromosome 9:**

This peak (with the highest q value) represents loss of the entire chromosome 9. The incidence of this genetic alteration is frequent in bladder cancer [268, 269]. CGH study on primary cutaneous melanoma by Bastian et al has reported the loss of chromosome 9 in melanoma samples [25]. Moreover, another study on sporadic and familial melanomas has shown the loss of entire copies of chromosome 9 [270].

Illustrating the potential of GISTIC and its propensity to detect driver events is that it is able to recognize regions of amplifications and deletions that are highly associated with melanoma and have been reported in several melanoma studies. For example, recognizing the amplification of 1q, 6p24 and 8q24 with deletion of 8p, 6q26, 11q, 12q24, 10q23.3, 21q22.3, all of 9, and 9p21.3. Furthermore, the identified regions we found contain almost all cancer genes known to be associated with melanoma. Identifying these previously known copy number changes in melanoma in our analysis as statistically significant copy number events indicates the reliability of GISTIC and its potential to reveal novel genes implicated in the pathogenesis of melanoma.

***GISTIC analysis reveals novel genes potentially involved in melanoma.***

A major advantage of GISTIC is its ability to find and report the minimal regions of change that are highly and frequently altered against the broad somatic copy number changes, which is frequent in melanoma. These statistically significant focal regions of amplifications and deletions imply the importance of genes within these regions. GISTIC analysis revealed three high significance of amplifications in very narrow regions, each region contains only one gene, and fourth region potentially contains a G-protein coupled receptor called NPSR1 (Table 6). These regions of amplification have not been reported in primary melanoma specimens before. As was discussed above, all of these genes have been found to be amplified in various cancers, which indicates their importance in cancer pathogenesis. Furthermore, GISTIC analysis revealed at least 10 regions of significant deletions that have not been characterized in melanoma

before. Some of these regions are within regions that have been reported in melanoma as broad chromosomal copy number changes (Table 6). Most of the genes involved in these focal deletions are known tumor suppressor genes in various cancers.

**Table 6: Summary of somatic copy number alterations containing novel genes.**

<b>Amplifications</b>		
<b>Genomic Location</b>	<b>Gene</b>	<b>Function</b>
7p14.3	NPSR1	G protein-coupled receptor.
10q11.21	RET	Receptor tyrosine kinase, proto-oncogene.
11q14.1	DLG2	Membrane-associated guanylate kinases.
21q22.1	ERG	Transcription Factor, proto-oncogene.
<b>Deletions</b>		
<b>Genomic Location</b>	<b>Gene</b>	<b>Function</b>
4p16.3	FGFRL1	Putative tumor suppressor in bladder cancer.
5p15.33	SDHA	Putative tumor suppressor in paraganglioma.
5p15.33	AHRR	Tumor suppressor gene in multiple human cancers
5p15.33	NKD2	negative regulator of WNT signaling pathway. Putative TS IN OS.
6q26	PARK2	Tumor suppressor gene in multiple human cancers.
6q26	PACRG	Putative tumor suppressor gene.
8p23.2	CSMD1	Tumor suppressor gene in multiple human cancers.
11q13.1	OTUB1	Positive regulator of p35, Putative tumor suppressor.
12q24.31	NCOR2	p53 transcription activator, tumor suppressor.
13q34	ING1	Tumor suppressor gene in multiple human cancers.
13q34	COL4A1	Suspected tumor suppressor gene.
13q34	COL4A2	Suspected tumor suppressor gene.
16p13.3	AXIN1	p53 activator and WNT pathway tumor suppressor.
16p13.3	ARHGDIG	Metastasis suppressor
16q23.3	CDH13	Putative tumor suppressor.
20q11.21	LPLUNC1	Tumor suppressor gene in Nasopharyngeal Carcinoma.

- References are shown in peak discussions above.

### **III. CONCLUSION AND SIGNIFICANCE.**

Thus, GISTIC provided a robust and unbiased analysis to identify somatic copy number alterations in melanoma samples. The identified regions of aberrations represent the most statistically significant differences between the clinical melanoma and benign nevi specimens. Therefore, these results can be exploited to improve current diagnostic techniques and provide more sensitive techniques to discriminate between problematic melanomas and benign nevi neoplasms. Moreover, GISTIC detected key genomic regions whose genes seem to play important role in melanoma pathogenesis. Some of these novel identified genes (especially in significant region of amplifications) are potential candidates for molecular targeted therapies. In fact, proposed therapies have been introduced targeting some of the novel genes identified in our analysis, such as targeting the RET gene with small receptor tyrosine kinase inhibitors in thyroid cancer (specifically for identified activating mutations in RET) and other cancers [271-273]. Another gene that is being targeted for cancer therapy is ERG transcription factor, the gene with the most significant copy number gain in our analysis. Several studies have reported their attempts in developing drugs that target the ERG transcription factor, mostly in prostate cancer [274, 275].

Further work is needed to validate these findings and test their potential to be implicated in current diagnostic tools. These findings were obtained from examining actual clinical specimens, which indicates the high potential of considering these results to improve current diagnostic techniques for differentiating melanoma from benign nevi.

### III. REFERENCES.

1. American Cancer Society. Skin Cancer Prevention and Early Detection [cited 2015 17 July]; Available from: <http://www.cancer.org/cancer/skincancer-melanoma/moreinformation/skincancerpreventionandearlydetection/skin-cancer-prevention-and-early-detection-what-is-skin-cancer>.
2. Olszanski, A.J., Current and future roles of targeted therapy and immunotherapy in advanced melanoma. *J Manag Care Spec Pharm*, 2014. **20**(4): p. 346-56.
3. Giblin, A.V. and J.M. Thomas, Incidence, mortality and survival in cutaneous melanoma. *J Plast Reconstr Aesthet Surg*, 2007. **60**(1): p. 32-40.
4. Jonsson, G., et al., Genomic profiling of malignant melanoma using tiling-resolution arrayCGH. *Oncogene*, 2007. **26**(32): p. 4738-48.
5. Chin, L., L.A. Garraway, and D.E. Fisher, Malignant melanoma: genetics and therapeutics in the genomic era. *Genes Dev*, 2006. **20**(16): p. 2149-82.
6. Dabas, N., et al., Diagnostic role of chromosomal instability in melanoma. *J Skin Cancer*, 2012. **2012**: p. 914267.
7. Gerami, P., et al., A highly specific and discriminatory FISH assay for distinguishing between benign and malignant melanocytic neoplasms. *Am J Surg Pathol*, 2012. **36**(6): p. 808-17.
8. Corona, R., et al., Interobserver variability on the histopathologic diagnosis of cutaneous melanoma and other pigmented skin lesions. *J Clin Oncol*, 1996. **14**(4): p. 1218-23.
9. Farmer, E.R., R. Gonin, and M.P. Hanna, Discordance in the histopathologic diagnosis of melanoma and melanocytic nevi between expert pathologists. *Hum Pathol*, 1996. **27**(6): p. 528-31.
10. Veenhuizen, K.C., et al., Quality assessment by expert opinion in melanoma pathology: experience of the pathology panel of the Dutch Melanoma Working Party. *J Pathol*, 1997. **182**(3): p. 266-72.
11. Wechsler, J., et al., Reliability of the histopathologic diagnosis of malignant melanoma in childhood. *Arch Dermatol*, 2002. **138**(5): p. 625-8.

12. McGinnis, K.S., et al., Pathology review of cases presenting to a multidisciplinary pigmented lesion clinic. *Arch Dermatol*, 2002. **138**(5): p. 617-21.
13. Barnhill, R.L., et al., Atypical Spitz nevi/tumors: lack of consensus for diagnosis, discrimination from melanoma, and prediction of outcome. *Hum Pathol*, 1999. **30**(5): p. 513-20.
14. Lodha, S., et al., Discordance in the histopathologic diagnosis of difficult melanocytic neoplasms in the clinical setting. *J Cutan Pathol*, 2008. **35**(4): p. 349-52.
15. Jing, X., C.W. Michael, and C.G. Theoharis, The use of immunocytochemical study in the cytologic diagnosis of melanoma: evaluation of three antibodies. *Diagn Cytopathol*, 2013. **41**(2): p. 126-30.
16. Dorvault, C.C., et al., Microphthalmia transcription factor: a sensitive and specific marker for malignant melanoma in cytologic specimens. *Cancer*, 2001. **93**(5): p. 337-43.
17. Orchard, G.E., Comparison of immunohistochemical labelling of melanocyte differentiation antibodies melan-A, tyrosinase and HMB 45 with NKIC3 and S100 protein in the evaluation of benign naevi and malignant melanoma. *Histochem J*, 2000. **32**(8): p. 475-81.
18. Gerami, P., et al., Fluorescence in situ hybridization (FISH) as an ancillary diagnostic tool in the diagnosis of melanoma. *Am J Surg Pathol*, 2009. **33**(8): p. 1146-56.
19. Vergier, B., et al., Fluorescence in situ hybridization, a diagnostic aid in ambiguous melanocytic tumors: European study of 113 cases. *Mod Pathol*, 2011. **24**(5): p. 613-23.
20. Gaiser, T., et al., Classifying ambiguous melanocytic lesions with FISH and correlation with clinical long-term follow up. *Mod Pathol*, 2010. **23**(3): p. 413-9.
21. Kallioniemi, A., et al., Comparative genomic hybridization for molecular cytogenetic analysis of solid tumors. *Science*, 1992. **258**(5083): p. 818-21.
22. Bastian, B.C., et al., Classifying melanocytic tumors based on DNA copy number changes. *Am J Pathol*, 2003. **163**(5): p. 1765-70.
23. Bauer, J. and B.C. Bastian, Distinguishing melanocytic nevi from melanoma by DNA copy number changes: comparative genomic hybridization as a research and diagnostic tool. *Dermatol Ther*, 2006. **19**(1): p. 40-9.
24. Curtin, J.A., et al., Distinct sets of genetic alterations in melanoma. *N Engl J Med*, 2005. **353**(20): p. 2135-47.

25. Bastian, B.C., et al., Chromosomal gains and losses in primary cutaneous melanomas detected by comparative genomic hybridization. *Cancer Res*, 1998. **58**(10): p. 2170-5.
26. Lindblad-Toh, K., et al., Loss-of-heterozygosity analysis of small-cell lung carcinomas using single-nucleotide polymorphism arrays. *Nat Biotechnol*, 2000. **18**(9): p. 1001-5.
27. Zhao, X., et al., An integrated view of copy number and allelic alterations in the cancer genome using single nucleotide polymorphism arrays. *Cancer Res*, 2004. **64**(9): p. 3060-71.
28. Bignell, G.R., et al., High-resolution analysis of DNA copy number using oligonucleotide microarrays. *Genome Res*, 2004. **14**(2): p. 287-95.
29. Zhao, X., et al., Homozygous deletions and chromosome amplifications in human lung carcinomas revealed by single nucleotide polymorphism array analysis. *Cancer Res*, 2005. **65**(13): p. 5561-70.
30. Dalmaso, C., et al., Patterns of chromosomal copy-number alterations in intrahepatic cholangiocarcinoma. *BMC Cancer*, 2015. **15**: p. 126.
31. Gast, A., et al., Somatic alterations in the melanoma genome: a high-resolution array-based comparative genomic hybridization study. *Genes Chromosomes Cancer*, 2010. **49**(8): p. 733-45.
32. Stark, M. and N. Hayward, Genome-wide loss of heterozygosity and copy number analysis in melanoma using high-density single-nucleotide polymorphism arrays. *Cancer Res*, 2007. **67**(6): p. 2632-42.
33. Garraway, L.A., et al., Integrative genomic analyses identify MITF as a lineage survival oncogene amplified in malignant melanoma. *Nature*, 2005. **436**(7047): p. 117-22.
34. Kim, M., et al., Comparative oncogenomics identifies NEDD9 as a melanoma metastasis gene. *Cell*, 2006. **125**(7): p. 1269-81.
35. Mermel, C.H., et al., GISTIC2.0 facilitates sensitive and confident localization of the targets of focal somatic copy-number alteration in human cancers. *Genome Biol*, 2011. **12**(4): p. R41.
36. Beroukhi, R., et al., Assessing the significance of chromosomal aberrations in cancer: methodology and application to glioma. *Proc Natl Acad Sci U S A*, 2007. **104**(50): p. 20007-12.
37. Beroukhi, R., et al., The landscape of somatic copy-number alteration across human cancers. *Nature*, 2010. **463**(7283): p. 899-905.
38. Bass, A.J., et al., SOX2 is an amplified lineage-survival oncogene in lung and esophageal squamous cell carcinomas. *Nat Genet*, 2009. **41**(11): p. 1238-42.

39. Chiang, D.Y., et al., Focal gains of VEGFA and molecular classification of hepatocellular carcinoma. *Cancer Res*, 2008. **68**(16): p. 6779-88.
40. Cancer Genome Atlas Research, N., Comprehensive genomic characterization defines human glioblastoma genes and core pathways. *Nature*, 2008. **455**(7216): p. 1061-8.
41. Weir, B.A., et al., Characterizing the cancer genome in lung adenocarcinoma. *Nature*, 2007. **450**(7171): p. 893-8.
42. Isola, J., et al., Analysis of changes in DNA sequence copy number by comparative genomic hybridization in archival paraffin-embedded tumor samples. *Am J Pathol*, 1994. **145**(6): p. 1301-8.
43. Siwoski, A., et al., An efficient method for the assessment of DNA quality of archival microdissected specimens. *Mod Pathol*, 2002. **15**(8): p. 889-92.
44. Reich, M., et al., GenePattern 2.0. *Nat Genet*, 2006. **38**(5): p. 500-1.
45. Gordon Saksena, B.T., Jeff Gentry, Broad Institute,. Copy Number Inference Pipeline. 2012 [cited 2015; Available from: <http://www.broadinstitute.org/cancer/software/genepattern/affymetrix-snp6-copy-number-inference-pipeline>
46. Olshen, A.B., et al., Circular binary segmentation for the analysis of array-based DNA copy number data. *Biostatistics*, 2004. **5**(4): p. 557-72.
47. Thorvaldsdottir, H., J.T. Robinson, and J.P. Mesirov, Integrative Genomics Viewer (IGV): high-performance genomics data visualization and exploration. *Brief Bioinform*, 2013. **14**(2): p. 178-92.
48. Robinson, J.T., et al., Integrative genomics viewer. *Nat Biotechnol*, 2011. **29**(1): p. 24-6.
49. Busam, K.J., Molecular pathology of melanocytic tumors. *Semin Diagn Pathol*, 2013. **30**(4): p. 362-74.
50. Ben-Ezra, J., et al., Effect of fixation on the amplification of nucleic acids from paraffin-embedded material by the polymerase chain reaction. *J Histochem Cytochem*, 1991. **39**(3): p. 351-4.
51. Srinivasan, M., D. Sedmak, and S. Jewell, Effect of fixatives and tissue processing on the content and integrity of nucleic acids. *Am J Pathol*, 2002. **161**(6): p. 1961-71.
52. Bonin, S., et al., PCR analysis in archival postmortem tissues. *Mol Pathol*, 2003. **56**(3): p. 184-6.



53. Tuefferd, M., et al., Genome-wide copy number alterations detection in fresh frozen and matched FFPE samples using SNP 6.0 arrays. *Genes Chromosomes Cancer*, 2008. **47**(11): p. 957-64.
54. Senguven, B., et al., Comparison of methods for the extraction of DNA from formalin-fixed, paraffin-embedded archival tissues. *Int J Med Sci*, 2014. **11**(5): p. 494-9.
55. Ludyga, N., et al., Nucleic acids from long-term preserved FFPE tissues are suitable for downstream analyses. *Virchows Arch*, 2012. **460**(2): p. 131-40.
56. Specht, K., et al., Quantitative gene expression analysis in microdissected archival formalin-fixed and paraffin-embedded tumor tissue. *Am J Pathol*, 2001. **158**(2): p. 419-29.
57. Potluri, K., et al., Genomic DNA extraction methods using formalin-fixed paraffin-embedded tissue. *Anal Biochem*, 2015. **486**: p. 17-23.
58. Lee, W., et al., PRC2 is recurrently inactivated through EED or SUZ12 loss in malignant peripheral nerve sheath tumors. *Nat Genet*, 2014. **46**(11): p. 1227-32.
59. Zack, T.I., et al., Pan-cancer patterns of somatic copy number alteration. *Nat Genet*, 2013. **45**(10): p. 1134-1140.
60. McCarroll, S.A., et al., Integrated detection and population-genetic analysis of SNPs and copy number variation. *Nat Genet*, 2008. **40**(10): p. 1166-74.
61. Tuefferd, M., et al., Microarray profiling of DNA extracted from FFPE tissues using SNP 6.0 Affymetrix platform. *Methods Mol Biol*, 2011. **724**: p. 147-60.
62. Chandler, W.M., et al., Differentiation of malignant melanoma from benign nevus using a novel genomic microarray with low specimen requirements. *Arch Pathol Lab Med*, 2012. **136**(8): p. 947-55.
63. Dalton, S.R., et al., Use of fluorescence in situ hybridization (FISH) to distinguish intranodal nevus from metastatic melanoma. *Am J Surg Pathol*, 2010. **34**(2): p. 231-7.
64. Gerami, P., et al., Fluorescence in situ hybridization for distinguishing nevoid melanomas from mitotically active nevi. *Am J Surg Pathol*, 2009. **33**(12): p. 1783-8.
65. Pouryazdanparast, P., et al., The role of 8q24 copy number gains and c-MYC expression in amelanotic cutaneous melanoma. *Mod Pathol*, 2012. **25**(9): p. 1221-6.
66. Robertson, G.P., Functional and therapeutic significance of Akt deregulation in malignant melanoma. *Cancer Metastasis Rev*, 2005. **24**(2): p. 273-85.

67. Stahl, J.M., et al., Deregulated Akt3 activity promotes development of malignant melanoma. *Cancer Res*, 2004. **64**(19): p. 7002-10.
68. Moore, S.R., et al., Detection of copy number alterations in metastatic melanoma by a DNA fluorescence in situ hybridization probe panel and array comparative genomic hybridization: a southwest oncology group study (S9431). *Clin Cancer Res*, 2008. **14**(10): p. 2927-35.
69. Marzuka-Alcala, A., M.J. Gabree, and H. Tsao, Melanoma susceptibility genes and risk assessment. *Methods Mol Biol*, 2014. **1102**: p. 381-93.
70. Hayward, N.K., Genetics of melanoma predisposition. *Oncogene*, 2003. **22**(20): p. 3053-62.
71. Wu, H., V. Goel, and F.G. Haluska, PTEN signaling pathways in melanoma. *Oncogene*, 2003. **22**(20): p. 3113-22.
72. Speleman, F., et al., Copy number alterations and copy number variation in cancer: close encounters of the bad kind. *Cytogenet Genome Res*, 2008. **123**(1-4): p. 176-82.
73. Stratton, M.R., P.J. Campbell, and P.A. Futreal, The cancer genome. *Nature*, 2009. **458**(7239): p. 719-24.
74. Tsao, M.S., et al., Erlotinib in lung cancer - molecular and clinical predictors of outcome. *N Engl J Med*, 2005. **353**(2): p. 133-44.
75. Lowe, S.W., et al., p53 status and the efficacy of cancer therapy in vivo. *Science*, 1994. **266**(5186): p. 807-10.
76. Cheang, M.C., et al., Ki67 index, HER2 status, and prognosis of patients with luminal B breast cancer. *J Natl Cancer Inst*, 2009. **101**(10): p. 736-50.
77. Krasnitz, A., et al., Target inference from collections of genomic intervals. *Proc Natl Acad Sci U S A*, 2013. **110**(25): p. E2271-8.
78. Bignell, G.R., et al., Signatures of mutation and selection in the cancer genome. *Nature*, 2010. **463**(7283): p. 893-8.
79. Greenman, C., et al., Patterns of somatic mutation in human cancer genomes. *Nature*, 2007. **446**(7132): p. 153-8.
80. Pleasance, E.D., et al., A comprehensive catalogue of somatic mutations from a human cancer genome. *Nature*, 2010. **463**(7278): p. 191-6.
81. Sullivan, H.C., et al., The utility of ERG, CD31 and CD34 in the cytological diagnosis of angiosarcoma: an analysis of 25 cases. *J Clin Pathol*, 2015. **68**(1): p. 44-50.
82. Sharrocks, A.D., The ETS-domain transcription factor family. *Nat Rev Mol Cell Biol*, 2001. **2**(11): p. 827-37.

83. Klezovitch, O., et al., A causal role for ERG in neoplastic transformation of prostate epithelium. *Proc Natl Acad Sci U S A*, 2008. **105**(6): p. 2105-10.
84. Furusato, B., et al., ERG oncoprotein expression in prostate cancer: clonal progression of ERG-positive tumor cells and potential for ERG-based stratification. *Prostate Cancer Prostatic Dis*, 2010. **13**(3): p. 228-37.
85. Falzarano, S.M. and C. Magi-Galluzzi, ERG protein expression as a biomarker of prostate cancer. *Biomark Med*, 2013. **7**(6): p. 851-65.
86. Zong, Y., et al., ETS family transcription factors collaborate with alternative signaling pathways to induce carcinoma from adult murine prostate cells. *Proc Natl Acad Sci U S A*, 2009. **106**(30): p. 12465-70.
87. Minner, S., et al., High level of Ets-related gene expression has high specificity for prostate cancer: a tissue microarray study of 11 483 cancers. *Histopathology*, 2012. **61**(3): p. 445-53.
88. Zhu, J., et al., Guanylate kinase domains of the MAGUK family scaffold proteins as specific phospho-protein-binding modules. *EMBO J*, 2011. **30**(24): p. 4986-97.
89. Zubakov, D., Z. Stupar, and G. Kovacs, Differential expression of a new isoform of DLG2 in renal oncocytoma. *BMC Cancer*, 2006. **6**: p. 106.
90. Morandi, A., I. Plaza-Menacho, and C.M. Isacke, RET in breast cancer: functional and therapeutic implications. *Trends Mol Med*, 2011. **17**(3): p. 149-57.
91. Santoro, M., et al., Molecular mechanisms of RET activation in human cancer. *Ann N Y Acad Sci*, 2002. **963**: p. 116-21.
92. Jhiang, S.M., The RET proto-oncogene in human cancers. *Oncogene*, 2000. **19**(49): p. 5590-7.
93. Nakashima, M., et al., RET oncogene amplification in thyroid cancer: correlations with radiation-associated and high-grade malignancy. *Hum Pathol*, 2007. **38**(4): p. 621-8.
94. Yang, H.S. and B. Horten, Gain of copy number and amplification of the RET gene in lung cancer. *Exp Mol Pathol*, 2014. **97**(3): p. 465-9.
95. Zeng, Q., et al., The relationship between overexpression of glial cell-derived neurotrophic factor and its RET receptor with progression and prognosis of human pancreatic cancer. *J Int Med Res*, 2008. **36**(4): p. 656-64.
96. Narita, N., et al., Functional RET G691S polymorphism in cutaneous malignant melanoma. *Oncogene*, 2009. **28**(34): p. 3058-68.

97. Ohshima, Y., et al., c-RET molecule in malignant melanoma from oncogenic RET-carrying transgenic mice and human cell lines. *PLoS One*, 2010. **5**(4): p. e10279.
98. Santos, G.C., et al., Chromosome 6p amplification and cancer progression. *J Clin Pathol*, 2007. **60**(1): p. 1-7.
99. Khodadoust, M.S., et al., Melanoma proliferation and chemoresistance controlled by the DEK oncogene. *Cancer Res*, 2009. **69**(16): p. 6405-13.
100. Feber, A., et al., Amplification and overexpression of E2F3 in human bladder cancer. *Oncogene*, 2004. **23**(8): p. 1627-30.
101. Namiki, T., et al., Genomic alterations in primary cutaneous melanomas detected by metaphase comparative genomic hybridization with laser capture or manual microdissection: 6p gains may predict poor outcome. *Cancer Genet Cytogenet*, 2005. **157**(1): p. 1-11.
102. Gembarska, A., et al., MDM4 is a key therapeutic target in cutaneous melanoma. *Nat Med*, 2012. **18**(8): p. 1239-47.
103. Ganguly, S.S., et al., c-Abl and Arg are activated in human primary melanomas, promote melanoma cell invasion via distinct pathways, and drive metastatic progression. *Oncogene*, 2012. **31**(14): p. 1804-16.
104. van den Bosch, T., et al., Higher percentage of FISH-determined monosomy 3 and 8q amplification in uveal melanoma cells relate to poor patient prognosis. *Invest Ophthalmol Vis Sci*, 2012. **53**(6): p. 2668-74.
105. Gerami, P., et al., Copy number gains in 11q13 and 8q24 [corrected] are highly linked to prognosis in cutaneous malignant melanoma. *J Mol Diagn*, 2011. **13**(3): p. 352-8.
106. Chen, Y. and O.I. Olopade, MYC in breast tumor progression. *Expert Rev Anticancer Ther*, 2008. **8**(10): p. 1689-98.
107. Jenkins, R.B., et al., Detection of c-myc oncogene amplification and chromosomal anomalies in metastatic prostatic carcinoma by fluorescence in situ hybridization. *Cancer Res*, 1997. **57**(3): p. 524-31.
108. Singhi, A.D., et al., MYC gene amplification is often acquired in lethal distant breast cancer metastases of unamplified primary tumors. *Mod Pathol*, 2012. **25**(3): p. 378-87.
109. Jane-Valbuena, J., et al., An oncogenic role for ETV1 in melanoma. *Cancer Res*, 2010. **70**(5): p. 2075-84.
110. Davies, H., et al., Mutations of the BRAF gene in human cancer. *Nature*, 2002. **417**(6892): p. 949-54.

111. Holzmann, K., et al., Genomic DNA-chip hybridization reveals a higher incidence of genomic amplifications in pancreatic cancer than conventional comparative genomic hybridization and leads to the identification of novel candidate genes. *Cancer Res*, 2004. **64**(13): p. 4428-33.
112. Liang, J.W., et al., Analysis of genomic aberrations associated with the clinicopathological parameters of rectal cancer by arraybased comparative genomic hybridization. *Oncol Rep*, 2013. **29**(5): p. 1827-34.
113. Papaemmanuil, E., et al., Loci on 7p12.2, 10q21.2 and 14q11.2 are associated with risk of childhood acute lymphoblastic leukemia. *Nat Genet*, 2009. **41**(9): p. 1006-10.
114. Hulsebos, T.J., et al., Malignant astrocytoma-derived region of common amplification in chromosomal band 17p12 is frequently amplified in high-grade osteosarcomas. *Genes Chromosomes Cancer*, 1997. **18**(4): p. 279-85.
115. Wang, Y., S. Minoshima, and N. Shimizu, Precise mapping of the EGF receptor gene on the human chromosome 7p12 using an improved fish technique. *Jpn J Hum Genet*, 1993. **38**(4): p. 399-406.
116. Yarden, Y. and G. Pines, The ERBB network: at last, cancer therapy meets systems biology. *Nat Rev Cancer*, 2012. **12**(8): p. 553-63.
117. Kang, J.U., et al., Gain of the EGFR gene located on 7p12 is a frequent and early event in squamous cell carcinoma of the lung. *Cancer Genet Cytogenet*, 2008. **184**(1): p. 31-7.
118. Higaki, E., et al., Gene copy number gain of EGFR is a poor prognostic biomarker in gastric cancer: evaluation of 855 patients with bright-field dual in situ hybridization (DISH) method. *Gastric Cancer*, 2014.
119. Udart, M., et al., Chromosome 7 aneusomy. A marker for metastatic melanoma? Expression of the epidermal growth factor receptor gene and chromosome 7 aneusomy in nevi, primary malignant melanomas and metastases. *Neoplasia*, 2001. **3**(3): p. 245-54.
120. Koprowski, H., et al., Expression of the receptor for epidermal growth factor correlates with increased dosage of chromosome 7 in malignant melanoma. *Somat Cell Mol Genet*, 1985. **11**(3): p. 297-302.
121. Pulkkinen, V., et al., Neuropeptide S receptor 1 (NPSR1) activates cancer-related pathways and is widely expressed in neuroendocrine tumors. *Virchows Arch*, 2014. **465**(2): p. 173-83.
122. Huang, S.F., et al., Fluorescence in situ hybridization evaluation of chromosome deletion patterns in prostate cancer. *Am J Pathol*, 1996. **149**(5): p. 1565-73.

123. Armes, J.E., et al., Candidate tumor-suppressor genes on chromosome arm 8p in early-onset and high-grade breast cancers. *Oncogene*, 2004. **23**(33): p. 5697-702.
124. Zhang, R. and C. Song, Loss of CSMD1 or 2 may contribute to the poor prognosis of colorectal cancer patients. *Tumour Biol*, 2014. **35**(5): p. 4419-23.
125. Midorikawa, Y., et al., Allelic imbalances and homozygous deletion on 8p23.2 for stepwise progression of hepatocarcinogenesis. *Hepatology*, 2009. **49**(2): p. 513-22.
126. Wright, K., et al., Frequent loss of heterozygosity and three critical regions on the short arm of chromosome 8 in ovarian adenocarcinomas. *Oncogene*, 1998. **17**(9): p. 1185-8.
127. Ma, C., et al., Characterization CSMD1 in a large set of primary lung, head and neck, breast and skin cancer tissues. *Cancer Biol Ther*, 2009. **8**(10): p. 907-16.
128. Sun, P.C., et al., Transcript map of the 8p23 putative tumor suppressor region. *Genomics*, 2001. **75**(1-3): p. 17-25.
129. Tang, M.R., et al., CSMD1 exhibits antitumor activity in A375 melanoma cells through activation of the Smad pathway. *Apoptosis*, 2012. **17**(9): p. 927-37.
130. Turner, N.C. and J.S. Reis-Filho, Basal-like breast cancer and the BRCA1 phenotype. *Oncogene*, 2006. **25**(43): p. 5846-53.
131. Brosens, R.P., et al., Deletion of chromosome 4q predicts outcome in stage II colon cancer patients. *Cell Oncol (Dordr)*, 2011. **34**(3): p. 215-23.
132. Kimura, Y., et al., Genetic alterations in 102 primary gastric cancers by comparative genomic hybridization: gain of 20q and loss of 18q are associated with tumor progression. *Mod Pathol*, 2004. **17**(11): p. 1328-37.
133. Han, J.Y., et al., Whole-genome analysis of a patient with early-stage small-cell lung cancer. *Pharmacogenomics J*, 2014. **14**(6): p. 503-8.
134. di Martino, E., et al., An integrated genomic, transcriptional and protein investigation of FGFR1 as a putative 4p16.3 deletion target in bladder cancer. *Genes Chromosomes Cancer*, 2013. **52**(9): p. 860-71.
135. Schild, C. and B. Trueb, Aberrant expression of FGFR1, a novel FGF receptor, in ovarian tumors. *Int J Mol Med*, 2005. **16**(6): p. 1169-73.
136. Xu, L., et al., An emerging role of PARK2 in cancer. *J Mol Med (Berl)*, 2014. **92**(1): p. 31-42.

137. Gong, Y., et al., Pan-cancer genetic analysis identifies PARK2 as a master regulator of G1/S cyclins. *Nat Genet*, 2014. **46**(6): p. 588-94.
138. Toma, M.I., et al., PARK2 and PACRG are commonly downregulated in clear-cell renal cell carcinoma and are associated with aggressive disease and poor clinical outcome. *Genes Chromosomes Cancer*, 2013. **52**(3): p. 265-73.
139. Goldberg, E.K., et al., Localization of multiple melanoma tumor-suppressor genes on chromosome 11 by use of homozygosity mapping-of-deletions analysis. *Am J Hum Genet*, 2000. **67**(2): p. 417-31.
140. Tomlinson, I.P., et al., Loss of heterozygosity on chromosome 11 q in breast cancer. *J Clin Pathol*, 1995. **48**(5): p. 424-8.
141. Walch, A.K., et al., Typical and atypical carcinoid tumors of the lung are characterized by 11q deletions as detected by comparative genomic hybridization. *Am J Pathol*, 1998. **153**(4): p. 1089-98.
142. Spitz, R., et al., Deletions in chromosome arms 3p and 11q are new prognostic markers in localized and 4s neuroblastoma. *Clin Cancer Res*, 2003. **9**(1): p. 52-8.
143. Sun, X.X. and M.S. Dai, Deubiquitinating enzyme regulation of the p53 pathway: A lesson from Otub1. *World J Biol Chem*, 2014. **5**(2): p. 75-84.
144. Sun, X.X., K.B. Challagundla, and M.S. Dai, Positive regulation of p53 stability and activity by the deubiquitinating enzyme Otubain 1. *EMBO J*, 2012. **31**(3): p. 576-92.
145. Imuta, Y., et al., Short limbs, cleft palate, and delayed formation of flat proliferative chondrocytes in mice with targeted disruption of a putative protein kinase gene, *Pkdcc* (AW548124). *Dev Dyn*, 2009. **238**(1): p. 210-22.
146. Martelli, M.P., et al., EML4-ALK rearrangement in non-small cell lung cancer and non-tumor lung tissues. *Am J Pathol*, 2009. **174**(2): p. 661-70.
147. Fukuyoshi, Y., et al., EML4-ALK fusion transcript is not found in gastrointestinal and breast cancers. *Br J Cancer*, 2008. **98**(9): p. 1536-9.
148. Penzel, R., P. Schirmacher, and A. Warth, A novel EML4-ALK variant: exon 6 of EML4 fused to exon 19 of ALK. *J Thorac Oncol*, 2012. **7**(7): p. 1198-9.
149. Soda, M., et al., Identification of the transforming EML4-ALK fusion gene in non-small-cell lung cancer. *Nature*, 2007. **448**(7153): p. 561-6.
150. Sanz, L., et al., The interaction of p62 with RIP links the atypical PKCs to NF-kappaB activation. *EMBO J*, 1999. **18**(11): p. 3044-53.
151. Hoesel, B. and J.A. Schmid, The complexity of NF-kappaB signaling in inflammation and cancer. *Mol Cancer*, 2013. **12**: p. 86.

152. Oswal, D.P., et al., Divergence between human and murine peroxisome proliferator-activated receptor alpha ligand specificities. *J Lipid Res*, 2013. **54**(9): p. 2354-65.
153. Mendes-da-Silva, P., et al., Frequent loss of heterozygosity on chromosome 5 in non-small cell lung carcinoma. *Mol Pathol*, 2000. **53**(4): p. 184-7.
154. Johannsdottir, H.K., et al., Chromosome 5 imbalance mapping in breast tumors from BRCA1 and BRCA2 mutation carriers and sporadic breast tumors. *Int J Cancer*, 2006. **119**(5): p. 1052-60.
155. Piao, Z., et al., Identification of novel deletion regions on chromosome arms 2q and 6p in breast carcinomas by amplotype analysis. *Genes Chromosomes Cancer*, 2001. **30**(2): p. 113-22.
156. Mazurenko, N., et al., High resolution mapping of chromosome 6 deletions in cervical cancer. *Oncol Rep*, 1999. **6**(4): p. 859-63.
157. Zudaire, E., et al., The aryl hydrocarbon receptor repressor is a putative tumor suppressor gene in multiple human cancers. *J Clin Invest*, 2008. **118**(2): p. 640-50.
158. Lu, Y., et al., Identification of a new target region by loss of heterozygosity at 5p15.33 in sporadic gastric carcinomas: genotype and phenotype related. *Cancer Lett*, 2005. **224**(2): p. 329-37.
159. Xu, S.F., et al., Refinement of heterozygosity loss on chromosome 5p15 in sporadic colorectal cancer. *World J Gastroenterol*, 2003. **9**(8): p. 1713-8.
160. Arias-Pulido, H., et al., Mapping common deleted regions on 5p15 in cervical carcinoma and their occurrence in precancerous lesions. *Mol Cancer*, 2002. **1**: p. 3.
161. Burnichon, N., et al., SDHA is a tumor suppressor gene causing paraganglioma. *Hum Mol Genet*, 2010. **19**(15): p. 3011-20.
162. Zhao, S., et al., NKD2, a negative regulator of Wnt signaling, suppresses tumor growth and metastasis in osteosarcoma. *Oncogene*, 2015.
163. Burger, H., et al., Chromosome 16q loss--a genetic key to the understanding of breast carcinogenesis. *Histol Histopathol*, 2013. **28**(3): p. 311-20.
164. Yakicier, M.C., et al., Identification of homozygous deletions at chromosome 16q23 in aflatoxin B1 exposed hepatocellular carcinoma. *Oncogene*, 2001. **20**(37): p. 5232-8.
165. Li, C., et al., Distinct deleted regions on chromosome segment 16q23-24 associated with metastases in prostate cancer. *Genes Chromosomes Cancer*, 1999. **24**(3): p. 175-82.



166. Vincek, V., S. Xu, and Y.S. Fan, Comparative genome hybridization analysis of laser-capture microdissected in situ melanoma. *J Cutan Pathol*, 2010. **37**(1): p. 3-7.
167. Balazs, M., et al., Chromosomal imbalances in primary and metastatic melanomas revealed by comparative genomic hybridization. *Cytometry*, 2001. **46**(4): p. 222-32.
168. Andreeva, A.V. and M.A. Kutuzov, Cadherin 13 in cancer. *Genes Chromosomes Cancer*, 2010. **49**(9): p. 775-90.
169. Ratner, N. and S.J. Miller, A RASopathy gene commonly mutated in cancer: the neurofibromatosis type 1 tumour suppressor. *Nat Rev Cancer*, 2015. **15**(5): p. 290-301.
170. Nissan, M.H., et al., Loss of NF1 in cutaneous melanoma is associated with RAS activation and MEK dependence. *Cancer Res*, 2014. **74**(8): p. 2340-50.
171. Andersen, L.B., et al., Mutations in the neurofibromatosis 1 gene in sporadic malignant melanoma cell lines. *Nat Genet*, 1993. **3**(2): p. 118-21.
172. Johnson, M.R., et al., Inactivation of the NF1 gene in human melanoma and neuroblastoma cell lines without impaired regulation of GTP.Ras. *Proc Natl Acad Sci U S A*, 1993. **90**(12): p. 5539-43.
173. North, J.P., S.S. Vemula, and B.C. Bastian, Chromosomal copy number analysis in melanoma diagnostics. *Methods Mol Biol*, 2014. **1102**: p. 199-226.
174. Song, L., et al., Alteration of SMRT tumor suppressor function in transformed non-Hodgkin lymphomas. *Cancer Res*, 2005. **65**(11): p. 4554-61.
175. Ghoshal, P., et al., Loss of the SMRT/NCoR2 corepressor correlates with JAG2 overexpression in multiple myeloma. *Cancer Res*, 2009. **69**(10): p. 4380-7.
176. Adikesavan, A.K., et al., Activation of p53 transcriptional activity by SMRT: a histone deacetylase 3-independent function of a transcriptional corepressor. *Mol Cell Biol*, 2014. **34**(7): p. 1246-61.
177. Yang, Y., et al., LPLUNC1 inhibits nasopharyngeal carcinoma cell growth via down-regulation of the MAP kinase and cyclin D1/E2F pathways. *PLoS One*, 2013. **8**(5): p. e62869.
178. Liao, Q., et al., LPLUNC1 suppresses IL-6-induced nasopharyngeal carcinoma cell proliferation via inhibiting the Stat3 activation. *Oncogene*, 2014. **33**(16): p. 2098-109.
179. Majid, S.M., et al., The suppression of SH3BGRL is important for v-Rel-mediated transformation. *Oncogene*, 2006. **25**(5): p. 756-68.

180. Dankort, D., et al., Braf(V600E) cooperates with Pten loss to induce metastatic melanoma. *Nat Genet*, 2009. **41**(5): p. 544-52.
181. Lin, W.M., et al., Modeling genomic diversity and tumor dependency in malignant melanoma. *Cancer Res*, 2008. **68**(3): p. 664-73.
182. Peters, J.M. and T. Nishiyama, Sister chromatid cohesion. *Cold Spring Harb Perspect Biol*, 2012. **4**(11).
183. Peters, J.M., A. Tedeschi, and J. Schmitz, The cohesin complex and its roles in chromosome biology. *Genes Dev*, 2008. **22**(22): p. 3089-114.
184. Girard, L., et al., Genome-wide allelotyping of lung cancer identifies new regions of allelic loss, differences between small cell lung cancer and non-small cell lung cancer, and loci clustering. *Cancer Res*, 2000. **60**(17): p. 4894-906.
185. Shin, J.H., et al., Identification of tumor suppressor loci on the long arm of chromosome 5 in pulmonary large cell neuroendocrine carcinoma. *Chest*, 2005. **128**(4): p. 2999-3003.
186. Treszl, A., et al., Molecular cytogenetic characterization of a novel cell line established from a superficial spreading melanoma. *Front Biosci*, 2006. **11**: p. 1844-53.
187. Noutsou, M., et al., Critical scaffolding regions of the tumor suppressor Axin1 are natively unfolded. *J Mol Biol*, 2011. **405**(3): p. 773-86.
188. Salahshor, S. and J.R. Woodgett, The links between axin and carcinogenesis. *J Clin Pathol*, 2005. **58**(3): p. 225-36.
189. Rui, Y., et al., Axin stimulates p53 functions by activation of HIPK2 kinase through multimeric complex formation. *EMBO J*, 2004. **23**(23): p. 4583-94.
190. Wang, P., et al., GM3 signals regulating TNF-alpha expression are mediated by Rictor and Arhgdib in mouse melanoma B16 cells. *Oncology*, 2007. **73**(5-6): p. 430-8.
191. Morelle, A., et al., Clinical and genetic characterization of basal cell carcinoma and breast cancer in a single patient. *Springerplus*, 2014. **3**: p. 454.
192. Rouault, A., et al., Deletion of chromosomes 13q and 14q is a common feature of tumors with BRCA2 mutations. *PLoS One*, 2012. **7**(12): p. e52079.
193. Lo, F.Y., et al., The database of chromosome imbalance regions and genes resided in lung cancer from Asian and Caucasian identified by array-comparative genomic hybridization. *BMC Cancer*, 2012. **12**: p. 235.

194. LeBron, C., et al., Genome-wide analysis of genetic alterations in testicular primary seminoma using high resolution single nucleotide polymorphism arrays. *Genomics*, 2011. **97**(6): p. 341-9.
195. Niini, T., et al., Array comparative genomic hybridization reveals frequent alterations of G1/S checkpoint genes in undifferentiated pleomorphic sarcoma of bone. *Genes Chromosomes Cancer*, 2011. **50**(5): p. 291-306.
196. Liu, X., et al., Zinc finger protein ZBTB20 promotes Toll-like receptor-triggered innate immune responses by repressing IkappaBalpha gene transcription. *Proc Natl Acad Sci U S A*, 2013. **110**(27): p. 11097-102.
197. Zhou, G., et al., Zbtb20 regulates the terminal differentiation of hypertrophic chondrocytes via repression of Sox9. *Development*, 2015. **142**(2): p. 385-93.
198. Shakhova, O., et al., Antagonistic cross-regulation between Sox9 and Sox10 controls an anti-tumorigenic program in melanoma. *PLoS Genet*, 2015. **11**(1): p. e1004877.
199. Nakao, M., et al., DNA copy number aberrations associated with the clinicopathological features of colorectal cancers: Identification of genomic biomarkers by array-based comparative genomic hybridization. *Oncol Rep*, 2011. **25**(6): p. 1603-11.
200. Kwong, L.N. and L. Chin, Chromosome 10, frequently lost in human melanoma, encodes multiple tumor-suppressive functions. *Cancer Res*, 2014. **74**(6): p. 1814-21.
201. Paz, N., et al., Altered adenosine-to-inosine RNA editing in human cancer. *Genome Res*, 2007. **17**(11): p. 1586-95.
202. Oswal, D.P., et al., Low-dose sarin exposure produces long term changes in brain neurochemistry of mice. *Neurochem Res*, 2013. **38**(1): p. 108-16.
203. Yendamuri, S., et al., 3p22.1 and 10q22.3 deletions detected by fluorescence in situ hybridization (FISH): a potential new tool for early detection of non-small cell lung Cancer (NSCLC). *J Thorac Oncol*, 2008. **3**(9): p. 979-84.
204. Mlakar, V., et al., Oligonucleotide DNA microarray profiling of lung adenocarcinoma revealed significant downregulation and deletions of vasoactive intestinal peptide receptor 1. *Cancer Invest*, 2010. **28**(5): p. 487-94.
205. Reinert, T., et al., Comprehensive genome methylation analysis in bladder cancer: identification and validation of novel methylated genes and application of these as urinary tumor markers. *Clin Cancer Res*, 2011. **17**(17): p. 5582-92.
206. Oswal, D.P., et al., A single amino acid change humanizes long-chain fatty acid binding and activation of mouse peroxisome proliferator-activated receptor alpha. *J Mol Graph Model*, 2014. **51**: p. 27-36.

207. Chen, L., et al., Clonality and evolutionary history of rhabdomyosarcoma. *PLoS Genet*, 2015. **11**(3): p. e1005075.
208. Soon, P.S., et al., Molecular markers and the pathogenesis of adrenocortical cancer. *Oncologist*, 2008. **13**(5): p. 548-61.
209. Czarnecka, K.H., et al., Allelic imbalance in 1p, 7q, 9p, 11p, 12q and 16q regions in non-small cell lung carcinoma and its clinical association: a pilot study. *Mol Biol Rep*, 2013. **40**(12): p. 6671-84.
210. Kim, S.W., et al., Analysis of chromosomal changes in serous ovarian carcinoma using high-resolution array comparative genomic hybridization: Potential predictive markers of chemoresistant disease. *Genes Chromosomes Cancer*, 2007. **46**(1): p. 1-9.
211. Wikman, H., et al., Clinical relevance of loss of 11p15 in primary and metastatic breast cancer: association with loss of PRKCDP expression in brain metastases. *PLoS One*, 2012. **7**(10): p. e47537.
212. Chiu, C.G., et al., Genome-wide characterization of circulating tumor cells identifies novel prognostic genomic alterations in systemic melanoma metastasis. *Clin Chem*, 2014. **60**(6): p. 873-85.
213. Orfanelli, U., et al., Identification of novel sense and antisense transcription at the TRPM2 locus in cancer. *Cell Res*, 2008. **18**(11): p. 1128-40.
214. Duncan, L.M., et al., Down-regulation of the novel gene melastatin correlates with potential for melanoma metastasis. *Cancer Res*, 1998. **58**(7): p. 1515-20.
215. Boyd, L.K., et al., High-resolution genome-wide copy-number analysis suggests a monoclonal origin of multifocal prostate cancer. *Genes Chromosomes Cancer*, 2012. **51**(6): p. 579-89.
216. Januchowski, R., et al., Extracellular matrix proteins expression profiling in chemoresistant variants of the A2780 ovarian cancer cell line. *Biomed Res Int*, 2014. **2014**: p. 365867.
217. Vincent, A., et al., Genome-wide analysis of promoter methylation associated with gene expression profile in pancreatic adenocarcinoma. *Clin Cancer Res*, 2011. **17**(13): p. 4341-54.
218. Potier, M., et al., Identification of SK3 channel as a new mediator of breast cancer cell migration. *Mol Cancer Ther*, 2006. **5**(11): p. 2946-53.
219. Chantome, A., et al., KCa2.3 channel-dependent hyperpolarization increases melanoma cell motility. *Exp Cell Res*, 2009. **315**(20): p. 3620-30.
220. Sun, W., et al., PPM1A and PPM1B act as IKKbeta phosphatases to terminate TNFalpha-induced IKKbeta-NF-kappaB activation. *Cell Signal*, 2009. **21**(1): p. 95-102.

221. Young, R.J., et al., Loss of CDKN2A expression is a frequent event in primary invasive melanoma and correlates with sensitivity to the CDK4/6 inhibitor PD0332991 in melanoma cell lines. *Pigment Cell Melanoma Res*, 2014. **27**(4): p. 590-600.
222. Hodis, E., et al., A landscape of driver mutations in melanoma. *Cell*, 2012. **150**(2): p. 251-63.
223. Frigerio, S., et al., A large de novo 9p21.3 deletion in a girl affected by astrocytoma and multiple melanoma. *BMC Med Genet*, 2014. **15**: p. 59.
224. Laharanne, E., et al., CDKN2A-CDKN2B deletion defines an aggressive subset of cutaneous T-cell lymphoma. *Mod Pathol*, 2010. **23**(4): p. 547-58.
225. Kamath, A., et al., Double-minute MYC amplification and deletion of MTAP, CDKN2A, CDKN2B, and ELAVL2 in an acute myeloid leukemia characterized by oligonucleotide-array comparative genomic hybridization. *Cancer Genet Cytogenet*, 2008. **183**(2): p. 117-20.
226. Mirebeau, D., et al., The prognostic significance of CDKN2A, CDKN2B and MTAP inactivation in B-lineage acute lymphoblastic leukemia of childhood. Results of the EORTC studies 58881 and 58951. *Haematologica*, 2006. **91**(7): p. 881-5.
227. Worsham, M.J., et al., Fine-mapping loss of gene architecture at the CDKN2B (p15INK4b), CDKN2A (p14ARF, p16INK4a), and MTAP genes in head and neck squamous cell carcinoma. *Arch Otolaryngol Head Neck Surg*, 2006. **132**(4): p. 409-15.
228. Illei, P.B., et al., Homozygous deletion of CDKN2A and codeletion of the methylthioadenosine phosphorylase gene in the majority of pleural mesotheliomas. *Clin Cancer Res*, 2003. **9**(6): p. 2108-13.
229. Crespo, I., et al., Detailed characterization of alterations of chromosomes 7, 9, and 10 in glioblastomas as assessed by single-nucleotide polymorphism arrays. *J Mol Diagn*, 2011. **13**(6): p. 634-47.
230. Kohno, T. and J. Yokota, Molecular processes of chromosome 9p21 deletions causing inactivation of the p16 tumor suppressor gene in human cancer: deduction from structural analysis of breakpoints for deletions. *DNA Repair (Amst)*, 2006. **5**(9-10): p. 1273-81.
231. Sasaki, S., et al., Molecular processes of chromosome 9p21 deletions in human cancers. *Oncogene*, 2003. **22**(24): p. 3792-8.
232. Shahbain, H., C. Cooper, and P. Gerami, Molecular diagnostics for ambiguous melanocytic tumors. *Semin Cutan Med Surg*, 2012. **31**(4): p. 274-8.
233. Johnstone, C.N., et al., PRR5 encodes a conserved proline-rich protein predominant in kidney: analysis of genomic organization, expression, and

- mutation status in breast and colorectal carcinomas. *Genomics*, 2005. **85**(3): p. 338-51.
234. Chinnadurai, G., S. Vijayalingam, and R. Rashmi, BIK, the founding member of the BH3-only family proteins: mechanisms of cell death and role in cancer and pathogenic processes. *Oncogene*, 2008. **27 Suppl 1**: p. S20-9.
  235. Oppermann, M., et al., Caspase-independent induction of apoptosis in human melanoma cells by the proapoptotic Bcl-2-related protein Nbk / Bik. *Oncogene*, 2005. **24**(49): p. 7369-80.
  236. Lai, C.P., J.F. Bechberger, and C.C. Naus, Pannexin2 as a novel growth regulator in C6 glioma cells. *Oncogene*, 2009. **28**(49): p. 4402-8.
  237. Cowan, K.N., et al., Pannexin1 and Pannexin3 exhibit distinct localization patterns in human skin appendages and are regulated during keratinocyte differentiation and carcinogenesis. *Cell Commun Adhes*, 2012. **19**(3-4): p. 45-53.
  238. Penuela, S., et al., Loss of pannexin 1 attenuates melanoma progression by reversion to a melanocytic phenotype. *J Biol Chem*, 2012. **287**(34): p. 29184-93.
  239. Cornella, H., et al., Unique genomic profile of fibrolamellar hepatocellular carcinoma. *Gastroenterology*, 2015. **148**(4): p. 806-818 e10.
  240. Fulda, S., Caspase-8 in cancer biology and therapy. *Cancer Lett*, 2009. **281**(2): p. 128-33.
  241. Park, W.S., et al., Inactivating mutations of the caspase-10 gene in gastric cancer. *Oncogene*, 2002. **21**(18): p. 2919-25.
  242. Shin, M.S., et al., Inactivating mutations of CASP10 gene in non-Hodgkin lymphomas. *Blood*, 2002. **99**(11): p. 4094-9.
  243. Yamamoto, N., et al., Allelic loss on chromosomes 2q, 3p and 21q: possibly a poor prognostic factor in oral squamous cell carcinoma. *Oral Oncol*, 2003. **39**(8): p. 796-805.
  244. Beder, L.B., et al., Genome-wide analyses on loss of heterozygosity in head and neck squamous cell carcinomas. *Lab Invest*, 2003. **83**(1): p. 99-105.
  245. Pack, S.D., et al., Molecular cytogenetic fingerprinting of esophageal squamous cell carcinoma by comparative genomic hybridization reveals a consistent pattern of chromosomal alterations. *Genes Chromosomes Cancer*, 1999. **25**(2): p. 160-8.
  246. Otsuka, T., et al., Deletion mapping of chromosome 2 in human lung carcinoma. *Genes Chromosomes Cancer*, 1996. **16**(2): p. 113-9.

247. Takita, J., et al., Allelic imbalance on chromosome 2q and alterations of the caspase 8 gene in neuroblastoma. *Oncogene*, 2001. **20**(32): p. 4424-32.
248. Dahl, E., et al., Systematic identification and molecular characterization of genes differentially expressed in breast and ovarian cancer. *J Pathol*, 2005. **205**(1): p. 21-8.
249. Huang, C., Roles of E3 ubiquitin ligases in cell adhesion and migration. *Cell Adh Migr*, 2010. **4**(1): p. 10-8.
250. Kano, S., et al., Tripartite motif protein 32 facilitates cell growth and migration via degradation of Abl-interactor 2. *Cancer Res*, 2008. **68**(14): p. 5572-80.
251. Szuhai, K., et al., Array-CGH analysis of cutaneous anaplastic large cell lymphoma. *Methods Mol Biol*, 2013. **973**: p. 197-212.
252. Gelmez, M.Y., et al., Analysis of activation-induced cytidine deaminase mRNA levels in patients with chronic lymphocytic leukemia with different cytogenetic status. *Leuk Lymphoma*, 2014. **55**(2): p. 326-30.
253. Nelson, M., et al., An increased frequency of 13q deletions detected by fluorescence in situ hybridization and its impact on survival in children and adolescents with Burkitt lymphoma: results from the Children's Oncology Group study CCG-5961. *Br J Haematol*, 2010. **148**(4): p. 600-10.
254. Oh, E.K., et al., Differential DNA copy number aberrations in the progression of cervical lesions to invasive cervical carcinoma. *Int J Oncol*, 2012. **41**(6): p. 2038-46.
255. Son, J.W., et al., Genome-wide combination profiling of DNA copy number and methylation for deciphering biomarkers in non-small cell lung cancer patients. *Cancer Lett*, 2011. **311**(1): p. 29-37.
256. Laharanne, E., et al., Genome-wide analysis of cutaneous T-cell lymphomas identifies three clinically relevant classes. *J Invest Dermatol*, 2010. **130**(6): p. 1707-18.
257. Gao, Y., et al., Chromosome aberrations associated with centrosome defects: a study of comparative genomic hybridization in breast cancer. *Hum Pathol*, 2011. **42**(11): p. 1693-701.
258. Antic, D., et al., Monosomy 12 and deletion of 13q34 in a case of chronic lymphocytic leukemia with concomitant lung cancer. *Vojnosanit Pregl*, 2010. **67**(10): p. 864-6.
259. Chattopadhyay, I., et al., Genome-wide analysis of chromosomal alterations in patients with esophageal squamous cell carcinoma exposed to tobacco and betel quid from high-risk area in India. *Mutat Res*, 2010. **696**(2): p. 130-8.

260. Igci, M., et al., Loss of heterozygosity of chromosome 13q33-34 region and molecular analysis of ING1 and p53 genes in bladder carcinoma. *Mol Biol Rep*, 2015. **42**(2): p. 507-16.
261. Garkavtsev, I., et al., Suppression of the novel growth inhibitor p33ING1 promotes neoplastic transformation. *Nat Genet*, 1996. **14**(4): p. 415-20.
262. Guerillon, C., N. Bigot, and R. Pedeux, The ING tumor suppressor genes: status in human tumors. *Cancer Lett*, 2014. **345**(1): p. 1-16.
263. Guerillon, C., D. Larrieu, and R. Pedeux, ING1 and ING2: multifaceted tumor suppressor genes. *Cell Mol Life Sci*, 2013. **70**(20): p. 3753-72.
264. Luo, Z.G., et al., Genetic alterations of tumor suppressor ING1 in human non-small cell lung cancer. *Oncol Rep*, 2011. **25**(4): p. 1073-81.
265. Wei, S.C., et al., SLCO3A1, A novel crohn's disease-associated gene, regulates nf-kappaB activity and associates with intestinal perforation. *PLoS One*, 2014. **9**(6): p. e100515.
266. Hays, A., U. Apte, and B. Hagenbuch, Organic anion transporting polypeptides expressed in pancreatic cancer may serve as potential diagnostic markers and therapeutic targets for early stage adenocarcinomas. *Pharm Res*, 2013. **30**(9): p. 2260-9.
267. Giguere, A. and J. Hebert, Identification of a novel fusion gene involving RUNX1 and the antisense strand of SV2B in a BCR-ABL1-positive acute leukemia. *Genes Chromosomes Cancer*, 2013. **52**(12): p. 1114-22.
268. Hoglund, M., The bladder cancer genome; chromosomal changes as prognostic makers, opportunities, and obstacles. *Urol Oncol*, 2012. **30**(4): p. 533-40.
269. Williams, S.V., et al., Molecular genetic analysis of chromosome 9 candidate tumor-suppressor loci in bladder cancer cell lines. *Genes Chromosomes Cancer*, 2002. **34**(1): p. 86-96.
270. Isshiki, K., et al., Chromosome 9 deletion in sporadic and familial melanomas in vivo. *Oncogene*, 1994. **9**(6): p. 1649-53.
271. Phay, J.E. and M.H. Shah, Targeting RET receptor tyrosine kinase activation in cancer. *Clin Cancer Res*, 2010. **16**(24): p. 5936-41.
272. Mazumdar, M., et al., Targeting RET to induce medullary thyroid cancer cell apoptosis: an antagonistic interplay between PI3K/Akt and p38MAPK/caspase-8 pathways. *Apoptosis*, 2013. **18**(5): p. 589-604.
273. Lanzi, C., et al., Targeting RET for thyroid cancer therapy. *Biochem Pharmacol*, 2009. **77**(3): p. 297-309.



274. Kissick, H.T., et al., Development of a peptide-based vaccine targeting TMPRSS2:ERG fusion-positive prostate cancer. *Cancer Immunol Immunother*, 2013. **62**(12): p. 1831-40.
275. Nhili, R., et al., Targeting the DNA-binding activity of the human ERG transcription factor using new heterocyclic dithiophene diamidines. *Nucleic Acids Res*, 2013. **41**(1): p. 125-38.